Alloy and Isotope Sputtering

By Peter Sigmund
Physics Department, Odense University
DK-5230 Odense M, Denmark
and
Physics Division, Argonne National Laboratory
Argonne, IL 60439, USA
and
Nghi Q. Lam
Materials Science Division, Argonne National Laboratory
Argonne, IL 60439, USA

Synopsis

We present a summary of our current understanding of collisional sputtering from isotopic mixtures and alloys. In view of the large number of theoretical and experimental investigations reported in the literature, we made a considerable effort to provide precise definitions of pertinent physical parameters and a unified notation. This is fairly straightforward with regard to primary processes, i.e., the atomistics of the individual sputtering event which is in general preferential. In case of secondary processes, which address all compositional changes induced by ion bombardment and their influence on sputtering, we have tried to identify the common origin of two theoretical schemes that the present authors have been utilizing in the past, and to generate a unified version that also comprises several simpler treatments that were proposed in the literature. This goal has not yet been reached completely but we have come very close to it. The scheme allows for preferential sputtering from a nonvanishing depth of origin, collisional mixing treated beyond the diffusion picture, pressure relaxation, radiation-enhanced diffusion, as well as Gibbsian and radiation-induced segregation.

Progress in the understanding of primary sputter effects is reviewed, based upon transport theory, Monte Carlo and molecular-dynamics simulation, and measurements at low and high fluences. Available knowledge on secondary processes is summarized, based in part on theoretical and experimental work not addressing sputter phenomena directly. Quantitative comparison between theoretical predictions and experimental results is most feasible with respect to isotopic mixtures. The agreement is not yet perfect, and reasons for this are discussed. Many experimental

results found on alloys under bombardment are well understood in qualitative terms, yet the number of unknown or uncertain parameters entering theoretical estimates is still too large to allow for theoretical predictions except for particularly simple systems. A list of open problems concludes the paper.

Contents

1 Introduction

The elementary event in sputtering is the emission of one or more atoms from the surface of some material, caused by the impact of an energetic particle. This elementary event is most often an intricate sequence of collision processes, i.e., a collision cascade involving a large number of target atoms. It is characteristic of the physicist's approach to science that initial studies of such a process are carried out on the simplest target materials. From a theoretician's point of view, elemental targets are simplest. Experimental studies are rarely if ever performed on truly monoatomic target materials. Real experiments deal with alloys, compounds, and mixtures with or without surface coverage because one or more of the following requirements are more or less violated: ultrapure, single-isotope starting material; clean surface; excellent vacuum in the target chamber; and self-bombardment by a high-purity, isotope-separated ion beam.

Sputter experiments on multicomponent materials show a much wider variety of processes. This increases the complexity but also allows extraction of more information in fortunate cases. For example, all reported experimental investigations on

the depth of origin of sputtered atoms involve overlayers of some material deposited on a matrix. Most important, virtually all applications of sputtering involve multicomponent targets. Thus, understanding the different sputter properties of the components making up a given material is both necessary and major challenge.

This paper addresses isotopic mixtures, alloys, and some compounds, as opposed to molecular solids, biomolecular materials, and ionic crystals. The materials considered here are expected to show a sputter behavior typical of metals where collisional sputtering dominates and where the sputtered flux is composed primarily of neutral atoms and small molecules.

The key problem to be addressed is the preferential sputtering of the species present in the target material and the way how this manifests itself in experiments. Another question, frequently asked yet of less fundamental interest is the relation between the erosion rate of an alloy and the erosion rates of the pure constituent materials. Because of a variety of processes that lead to composition changes in alloys under ion bombardment that are only remotely related to sputter emission, a broad approach needs to be taken.

Composition changes under ion bombardment were discovered many years ago (Asada & Quasebarth, 1929). Theoretical studies were initiated much later (Andersen & Sigmund, 1974). A survey of the early history of the field has been given by Betz & Wehner (1983). Their chapter also offers a compilation of experimental data available at the time. An illuminating outline of the entire complex of problems, open questions, as well as available knowledge was given by Andersen (1984). Other reviews on more specific items will be mentioned in context.

In accordance with the title of this book, fundamental processes will be studied and very little will be said about applications. However, as indicated above, *all* application areas of sputtering are more or less affected by the processes that determine the sputtering of alloys and compounds. At this point we just list keywords such as ion beam analysis involving sputtering, ion beam modification of materials, sputter deposition of thin films, sputter cleaning and polishing, and plasma-wall interaction in fusion technology. Moreover, some control over sputter processes is demanded in virtually all experiments involving particle-solid interaction.

The experimental and theoretical literature in the field is extensive, yet there has been rather little systematic comparison between experimental findings and theoretical predictions, mostly due to the restricted range of validity of available quantitative predictions. An exception is the case of isotopic mixtures which will be discussed in sect. 3.

The mutually related topics of sputtering from a multicomponent target and compositional changes during ion bombardment will be discussed in general terms in sect. 2. An attempt has been made to outline a comprehensive scheme allowing to incorporate athermal and thermally-activated processes, flexible enough to allow

for analytic or numerical input. The scheme is compatible with the seemingly different schemes used in previous work by each of the present authors, and it contains most existing phenomenological descriptions as special cases. An attempt has also been made to stick to a simple, comprehensive notation. In addition, sect. 2 summarizes simple estimates of sputter cross sections and partial sputter yields.

Section 4 addresses alloys. The processes that are thought to cause compositional changes under ion bombardment are discussed in physical terms, and simple quantitative estimates are given. The complex interplay between these processes and preferential sputtering is illustrated on a number of limiting cases, and the relation to measurable parameters is exemplified both schematically and by a survey of pertinent experiments.

A summary and outlook listing the most urgent needs for future effort concludes the chapter.

2 General Theory

2.1 General Considerations

Sputtering from a polyatomic mixture is a priori preferential: By this is meant that the behavior of a target atom with regard to sputtering is species-dependent. Therefore, measurable sputter parameters will generally not reflect the composition of the pertinent surface layer in a given material. This is a major handicap in surface analytical techniques involving sputtering; it is also a main motivation for fundamental studies of alloy sputtering.

Several factors determine preferential sputter behavior. First of all, binding forces acting on an atom at the surface or in the bulk are species-dependent. Differences may amount to an order of magnitude or more for hydrogen or noble gases in metals, to a factor of two for some metallic alloys, or perhaps a per mille for isotopic mixtures, but some difference will always exist. Secondly, in order to get sputtered, an atom must first be set in motion during the process of energy dissipation by primary radiation. The sharing of energy is species dependent through pertinent collision cross sections as well as conservation laws of momentum and energy. Finally, atoms may be ejected not only from the top surface layer of a solid or liquid but also from a shallow depth range underneath. Clearly, the ability of an atom to penetrate a number of overlayers is species dependent; this feature is well documented from the inverse process of ion implantation.

From a theoretical point of view, it is convenient to divide up the study of alloy sputtering into primary and secondary processes. Primary processes deal with the sputter behavior of a target with a given composition depth profile; they lead to nonstoichiometries in the sputtered flux even from a homogeneous target.

Secondary processes deal with changes in the target material due to a variety of effects initiated by the primary radiation.

Thus, the quantitative characterization of preferential sputter behavior is the main issue in the study of primary processes. Secondary processes are numerous, and at least five of them are important in the context of sputtering.

While a recoil cascade may give rise to sputtering only if it intersects the target surface, all recoil cascades generate disorder and transport atoms in the bulk. This causes compositional changes on several time scales. Collisional mixing proceeds concurrently with sputtering. At the end of the slowing-down cascade, major pressure gradients have normally built up which are thought to relax rapidly by collective motion of atoms from high-pressure to lower-pressure zones.

The concentration of point defects created in a cascade and surviving its cooling phase is usually higher than in equilibrium. These defects may be mobile at elevated temperatures and give rise to phenomena such as radiation-enhanced diffusion. Moreover, nonuniform production and/or annihilation of defects results in persistent defect fluxes. Preferential association of defects to particular alloy elements will couple a net flux of atoms of that component to the defect fluxes. This leads to radiation-induced segregation. In thermal equilibrium, Gibbsian segregation occurs, i.e., segregation to free surfaces and interfaces. This process reduces the free energy of an alloy system. In the absence of irradiation it would be frozen in at ambient temperature. It can be enhanced by diffusion of nonequilibrium defects during irradiation. The latter two secondary processes are preferential and may give rise to changes in target stoichiometry that are not necessarily related to sputtering.

In addition to initiating collision cascades, the implanted ion beam itself also changes the overall alloy composition. As a result, one may experience changes in chemical properties which may affect all processes described above. Finally, under certain bombardment conditions, nuclear transmutations may occur which, again, may result in chemical changes.

The study of radiation-induced compositional changes is complex and full of hidden surprises. One direct implication is the existence of several pertinent length scales. Sputter ejection and Gibbsian segregation are characterized by depth scales of the order of little more than an interatomic distance. The characteristic length in collisional mixing may be as large as the dimension of the pertinent collision cascade or subcascade, i.e., roughly the penetration depth of the incident ion beam. However, energy spectra in collision cascades are skew, with low energies and, hence, low relocation distances dominating. Activated processes may go over large distances since the target region that may be considered to be in an excited state will in general include atoms with energies that are too low to cause displacement.

An important limiting case in studies of alloy sputtering is the steady-state

limit which may be reached after prolonged bombardment. A necessary condition for such a state to be reached by an eroding target is that the composition be initially homogeneous in the bulk. Another condition is that matter may not be transported over long distances; in other words, the thickness of the altered layer must be smaller than the total target thickness. If both conditions are fulfilled, the composition of the sputtered flux in the steady state must reflect the bulk composition of the target, unless atoms change identity by nuclear transformation. This is a direct consequence of the conservation of matter and an important test on any theory of compositional changes. This, however, does not preclude observable deviations from stoichiometry in differential quantities like energy spectra and angular distributions of sputtered particles.

2.2 Primary Processes

2.2.1 Fundamental Parameters

The primary quantity characterizing sputtering of a polyatomic mixture is a set of partial sputter yields, Y_i, defined as the mean number of sputtered i-atoms per incident beam particle. In the following, we shall assume the index i to include both the components that are initially present in an n-atomic target, $i = 1, 2 \ldots n$, and the implanted species, $i = 0$. Several techniques are available to measure partial yields, such as laser fluorescence or ionization, or collection of sputtered material and subsequent quantification by surface analytical techniques. Differential partial sputter yields such as the energy spectrum or angular distribution of i-atoms may also be measured. Such measurements may be demanding: In order to provide information on primary processes, they require low bombardment fluences.

Integral quantities may be measured such as the average mass change of the target per incoming beam particle due to sputtering,

$$\Delta m = \sum_i M_i Y_i, \tag{1}$$

where M_i is the mass of an i-atom, or the surface recession

$$w = \frac{dx}{d\Phi} = \sum_i \Omega_i Y_i, \tag{2}$$

where $d\Phi$ is the fluence [number of beam particles/area] necessary to erode a layer of thickness dx, and Ω_i is the effective atomic volume occupied in the target by an i-atom.

Measurable quantities like Δm or w may be converted into dimensionless effec-

tive sputter yields

$$Y_{\text{eff}}^{(M)} = \frac{1}{\overline{M}} \sum_i M_i Y_i \tag{3}$$

or

$$Y_{\text{eff}}^{(\Omega)} = \frac{1}{\overline{\Omega}} \sum_i \Omega_i Y_i, \tag{4}$$

which allow comparison with sputter yields of elemental target materials. Here, $\overline{M}$ and $\overline{\Omega}$ are the mean mass and mean atomic volume, respectively, per bulk atom. Evidently, the two effective sputter yields may differ for a given material in both magnitude and fluence dependence. In the older literature, a total sputter yield $Y_{\text{tot}} = \sum_i Y_i$ has frequently been introduced. This quantity is not measurable directly, and it is meaningful only in case of stoichiometric sputtering, where $Y_{\text{eff}}^{(M)} = Y_{\text{eff}}^{(\Omega)} = Y_{\text{tot}}$, as is easily verified.

In relating measurable quantities to theory one usually makes reference to a semi-infinite target with a plane surface. In view of the possible presence of microscopic and macroscopic surface roughness this idealization is not necessarily justified. On the other hand, this feature is presumably no more significant for multicomponent than for monoatomic targets, where that simplification is also quite common.

The partial sputter yield may be split into contributions from different depths,

$$Y_i = \int_0^\infty dx \sigma_i(x) N_i(x), \tag{5}$$

where $N_i(x)$ is the density [average number of i-atoms/volume] at depth x and $\sigma_i(x)$ is a quantity characterizing the sputter behavior of an i-atom as a function of depth. The target surface will always be assumed to coincide with the plane $x = 0$. This is appropriate for the standard backsputtering geometry.

The function $\sigma_i(x)$ has the dimension of an area and has therefore been termed sputter cross section (Sigmund et al., 1982). It depends on the environment, i. e., all densities $N_j(x)$ $(j = 0 \ldots n)$. For a uniform incident beam of fluence $d\Phi$, the probability for ejection of a given i-atom at depth x is $\sigma_i(x) d\Phi$. In general, $\sigma_i(x)$ will drop rapidly to zero with increasing depth x, dependent on the species.

If the target can be characterized by monolayers of a unique thickness, i.e., mostly for single crystals, an alternative description in terms of a discrete layer index l may be appropriate,

$$Y_i = \sum_{l=1}^{\infty} y_i^{(l)} c_i^{(l)}, \tag{6}$$

where $l = 1$ represents the top surface layer, $c_i^{(l)}$ the fraction of i-atoms in the lth layer, and $y_i^{(l)}$ a dimensionless quantity called the component yield of species

i from layer l. The component yields represent similar physical information as the sputter cross section. This discrete description, which is a special case of eq. (5), has been utilized mainly in conjunction with the assumption that only 1 (Betz & Wehner, 1983) or 2 (Lam, 1990) layers are depleted by sputtering. It is suitable for explicit incorporation of processes dealing with migrating lattice defects (vacancies, interstitials) but does not readily allow for changes in number density as a consequence of compositional changes. For nondilute alloys, this is a limitation.

As an example of a differential quantity characterizing sputter events consider

$$Y_i(\Theta)d^2\Omega = d^2\Omega \int_0^\infty dx \sigma_i(x,\Theta)N_i(x) \tag{7}$$

which represents the partial sputter yield differential in angle [mean number of i-atoms per beam atom ejected into a solid angle $d^2\Omega$ at a polar angle Θ against the outward surface normal]. Here, $\sigma_i(x,\Theta)d^2\Omega$ is the differential sputter cross section for ejection into a solid angle $d^2\Omega$ at a polar angle Θ from depth x, averaged over the distribution in energy and angle of the particle flux at depth x. With increasing depth x, the function $\sigma_i(x,\Theta)$ will reduce to an increasingly narrow peak around $\Theta = 0$. Therefore, the angular distribution of sputtered i-atoms will depend on the depth profile $N_i(x)$ (Sigmund et al., 1982). For a species enriched near the surface, the angular distribution will be broadened relative to that of a homogeneous sample, and vice versa. Similar considerations should apply to the energy distribution of sputtered atoms but do not seem to have been explored.

2.2.2 Theoretical Tools

We present a brief survey of theoretical methods that are available to predict preferential sputter behavior.

We address collisional sputtering, i.e., sputtering via cascades of elastic or quasi-elastic collisions. Calculations have been performed for random and crystalline targets. Analytic predictions are available only for random targets.

The standard system is a semi-infinite random target with a homogeneous composition. In analytic studies, the complexity may even be further reduced by operating with an infinite medium where sputtering is synonymous with the passage of target atoms through a reference plane at depth zero. For linear cascades, i.e., at low density of deposited energy, such a system is described by a linearized Boltzmann equation (Andersen & Sigmund, 1974; Watson & Haff, 1980) or, equivalently, a standard Monte Carlo code (Eckstein & Biersack, 1985; Vicanek & Urbassek, 1988). With suitable provisions about bulk and surface binding forces, particle fluxes extracted from analytic or numerical calculations may allow conclusions about preferential sputtering behavior.

The potential of Monte Carlo simulations may be extended to also comprise inhomogeneous composition profiles (Möller & Eckstein, 1984, 1985; Möller et al., 1988), provided that free flight paths are chosen small enough to make sure that the collision statistics is compatible with the local composition at any point. Also the Boltzmann equation approach can be applied to inhomogeneous composition profiles, but neither analytic nor numeric solutions have been determined this way, as far as we are aware.

Cascades are nonlinear in case of high density of energy deposition, but no unanimous agreement exists about pertinent processes even for monoatomic targets. Amongst several theoretical approaches that have been proposed for monoatomic targets, only the thermal model for the elastic-collision spike has been invoked to predict preferential sputtering (Sigmund, 1981).

In molecular-dynamics simulations the need to distinguish between linear and nonlinear cascades does not arise (Shapiro et al., 1988). All reported molecular-dynamics simulations operate with a target of initially homogeneous composition. Such codes are suited for studying preferential sputtering from both ordered and random alloys. Achieving adequate statistics is a notorious problem in molecular-dynamics simulations which is getting solved only gradually with ever more powerful hardware (Nieminen, 1993; Robinson, 1993). Studying disordered alloys requires care in setting up targets.

A common feature of all tools described in this section is that predictions on preferential sputtering can be made to emerge simultaneously with predictions on collisional mixing on the basis of compatible input.

2.2.3 Partial Sputter Yields

Analytic predictions of partial sputter yields have been provided on the basis of the theory of linear collision cascades in an infinite medium (Andersen & Sigmund, 1974; Sigmund, 1979). Two quantities were found relevant, the recoil density and the particle flux. The recoil density reflects the energy distribution of i-recoil atoms when set in motion. The particle flux reflects the energy distribution of i-atoms under steady-state conditions, i.e., under bombardment with a constant flux of primary radiation. While the recoil density is insensitive to the slowing-down behavior of recoiling atoms, the particle flux is, roughly, inversely proportional to the stopping power of an i-atom: The smaller the stopping power, the longer the slowing-down time and hence the greater the weight with which a given atom contributes to the particle flux under steady-state conditions.

Knowledge of the particle flux provides an estimate of the number of atoms passing through the surface plane at $x = 0$, provided that this plane is sufficiently close to the center of the collision cascade to be representative. This assumption,

which also underlies conventional sputter theory for monoatomic targets (Sigmund, 1969a), has limitations. Quantitative studies of this particular aspect, both by analytic and numerical methods, have been performed for specific systems (Urbassek & Vicanek, 1988; Conrad & Urbassek, 1991).

Two more simplifications enter the theoretical treatment. Firstly, energy distributions are considered in the asymptotic limit where the ratio between particle energy and incident energy is $\ll 1$. Secondly, collisions between two target particles i, j are described by a power cross section of the form

$$d\sigma_{ij}(E,T) = C_{ij} E^{-m} T^{-1-m} dT, \tag{8}$$

where E is the energy of an i-atom before the collision, T the energy of a j- atom after the collision, m an exponent in the interval $0 < m < 1$, and C_{ij} a species-dependent constant. Both C_{ij} and m are determined by the interatomic potential that governs the collision. Moreover, the exponent m depends slightly on E. With this, the following result was obtained for the ratio of particle fluxes at energy ϵ in a binary, infinite, random medium,

$$\frac{\text{flux}_1}{\text{flux}_2} = \frac{N_1}{N_2} \frac{S_{21}(\epsilon)}{S_{12}(\epsilon)}, \tag{9}$$

where S_{ij} is the stopping cross section of an i-atom interacting with a j-atom,

$$S_{ij}(E) = \frac{1}{1-m} C_{ij} \gamma_{ij}^{1-m} E^{1-2m} \tag{10}$$

and $\gamma_{ij} = 4M_iM_j/(M_i + M_j)^2$.

Vicanek et al. (1993) derived eq. (9) without going over the power cross section (8) from a principle of detailed balance in the collision cascade where the flux of energy from the subsystem of i-atoms to the subsystem of j-atoms equals the opposite flux. That work also demonstrated that eq. (9) has certain limitations for widely different masses of the constituent atoms.

Eq. (9) shows that in this approximation, the ratio of particle fluxes is independent of the energy and the type of the incident radiation. This result hinges on the assumption that $\epsilon \ll E$.

It is also seen that the ratio of particle fluxes deviates from stoichiometry by the factor $S_{21}(\epsilon)/S_{12}(\epsilon)$ which, in the power approximation, is independent of ϵ. Since conventional screened-Coulomb interaction potentials are symmetric in i and j, the above ratio is independent of the atomic numbers, and all nonstoichiometry originates in a kinematic factor which, in the power approximation, reads

$$\frac{S_{21}(\epsilon)}{S_{12}(\epsilon)} = \left(\frac{M_2}{M_1}\right)^{2m} \tag{11}$$

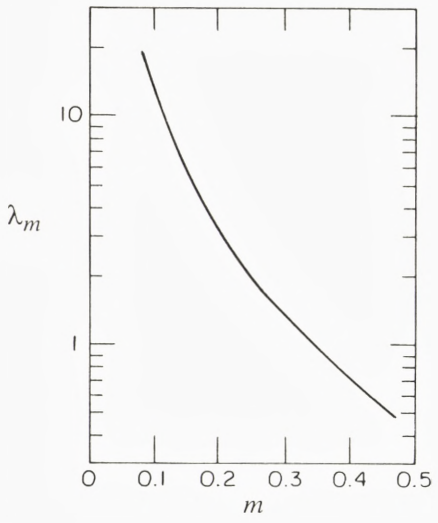

Figure 1. Numerical constant λ_m versus exponent m. The actual curve is not universal but somewhat dependent on the potential (here Born-Mayer potential). After Vicanek et al. (1989).

both for standard screened-Coulomb interaction (Lindhard et al., 1968; Ziegler et al., 1985) or for Born-Mayer-type interaction

$$C_{ij} = \frac{\pi}{2}\lambda_m a^2 \left(\frac{M_i}{M_j}\right)^m (2A_{ij})^{2m}, \tag{12}$$

which has been adopted for low-energy collisions (Sigmund, 1969a) with constants

$$A_{ij} \simeq 52eV(Z_i Z_j)^{3/4} \text{ and } a \simeq 0.219\text{Å} \tag{13}$$

according to Andersen & Sigmund (1965).

It is illuminating to analyze the physical origin of the preferential behavior expressed by eq. (9) in conjunction with (11). There are actually two intimately connected sources, each of which contributes a factor of $(M_2/M_1)^m$. Consider a j-isotope in the near-surface region, knocked on by some moving atom (another isotope or something else). The cross section for a knockon event at a given recoil energy is proportional to M_j^{-m} according to eq. (12). This accounts for one factor. Now, the fraction of recoil atoms able to leave the target is proportional to the total pathlength which a recoil is able to travel before coming to rest form a given initial energy. The stopping power of an i-atom is proportional to M_i^m according to eqs. (10,12). The pathlength is inversely proportional to the stopping power.

This accounts for the other factor. This argument is not restricted to a binary target (Sigmund, 1987a, 1993b).

The exponent m has in some applications been set equal to zero (Sigmund, 1969a). This approximation is acceptable for monoatomic targets but eliminates all collisional nonstoichiometry to first order (Watson & Haff, 1980). The value $m = 0.055$ adopted otherwise for not too light species at low energies (Sigmund, 1969a; Andersen & Sigmund, 1974) has been found to be a factor of two too small by comparison with accurate Born-Mayer scattering theory (Vicanek et al., 1989). For softer interaction potentials, m becomes even greater and can come close to $m \simeq 0.2$ (Biersack & Eckstein, 1984). The dependence of the dimensionless parameter λ_m on m is shown in fig. 1.

Not much definite information is available on potentials between atoms in solids governing collisions in the pertinent energy range (10 to 100 eV). The topic has been discussed by Robinson (1993) and Nieminen (1993) in this volume. It is conceivable that well-defined and well-analyzed measurements of preferential sputtering may provide as much information on low-energy collisions in solids as any of few other available sources.

The above equations for binary targets can be extended to polyatomic mixtures (Sigmund, 1987a; Urbassek & Conrad, 1993, Sigmund, 1993b). The particle flux in a ternary material with arbitrary mass ratios has been studied theoretically (Andersen & Sigmund, 1974). Their main result, expressed by their equations (29) and (30), can be written in the form

$$\frac{\text{flux}_1}{\text{flux}_2} = \left(\frac{N_1}{N_2}\right) \frac{N_1 S_{21} S_{31} + N_2 S_{21} S_{32} + N_3 S_{23} S_{31}}{N_1 S_{31} S_{12} + N_2 S_{32} S_{12} + N_3 S_{32} S_{13}}. \tag{14}$$

It is easily seen that for the conventional power cross section, eq. (8), numerator and denominator contain a factor that cancels out, with the result that the ratio of $\text{flux}_1/\text{flux}_2$ reduces rigorously to the prediction for the binary medium, i.e., eq. (9).

Eq. (14) was rederived by Urbassek & Conrad (1993), but allowance was made then for a species dependence of the exponent m, i.e., $m = m_{ij}$. Moreover, an analytic approach going beyond the power-law scattering cross section has been explored recently (Vicanek et al., 1993).

For a monoatomic medium, the energy-integrated particle flux is known to be $\propto U^{2m-1}$ (Sigmund, 1969a, 1981) where U is the surface binding energy, under the assumption that bulk binding energies can be ignored. This finding translates into a U_i^{2m-1}-dependence of the partial sputter yield of the i-th component in a random polyatomic target.

In summary, this form of simplified transport theory predicts the following ratio

of partial sputter yields in a binary medium (Sigmund, 1981),

$$\frac{Y_1}{Y_2} = \frac{N_1}{N_2}\left(\frac{M_2}{M_1}\right)^{2m}\left(\frac{U_2}{U_1}\right)^{1-2m}, \tag{15}$$

which has frequently served as a standard of reference.

Experience from monoatomic targets suggests that the above picture will break down at low incident energies, where the precise meaning of 'low' is not well known but clearly dependent on the ion/target mass ratio. Some limitations have been analyzed for the specific case of isotopic mixtures (Conrad & Urbassek, 1991).

2.2.4 Surface Binding

The dependence on mass and surface binding energy shown in eq. (15) predicts large yields for small target mass and small surface binding energy. Since m is small for the energy range pertinent to sputtering the yield is more sensitive to variations in surface binding energy than in mass.

Early attempts to estimate pertinent surface binding energies were based on a pair-bonding model (Swalin, 1962). In such a model, the surface binding energy can be approximated by

$$U_i = Z_S \overline{U_{ik}}^k \tag{16}$$

where Z_S is an effective surface coordination number, U_{ik} is the bond strength between an i- and a k-atom, and the average is to be taken over nearest neighbors, weighted according to the surface composition. The validity of a pair-bonding model is undoubtedly dependent on the target material and somewhat questionable for metallic targets. Moreover, the pair-bonding model implies a statistical distribution of surface binding energies governed by the actual nearest-neighbor configuration. The above expression involves average surface binding energies. Since the sputter yield Y_i depends on a negative power of U_i, the range of validity of the above estimate must be limited to small variations of the U_{ik}. Nevertheless, eq. (16) leaves no doubt that U_i will vary as a function of bombardment time due to changing surface concentration.

Experimental evidence may be drawn from comparisons of sputtered-particle energy spectra for alloys of different composition with those of the corresponding pure materials. Such comparisons invoke the assumption of a peak position $\simeq U_i/2$. This relation stems from linear cascade theory (Thompson, 1968) and is well corroborated in case of elemental targets (Gruen et al., 1982). Within the range of validity of linear cascade theory, it should be equally well justified for alloys of homogeneous composition. Caution is indicated in the spike regime: In that case, the peak position becomes sensitive to bombardment parameters like

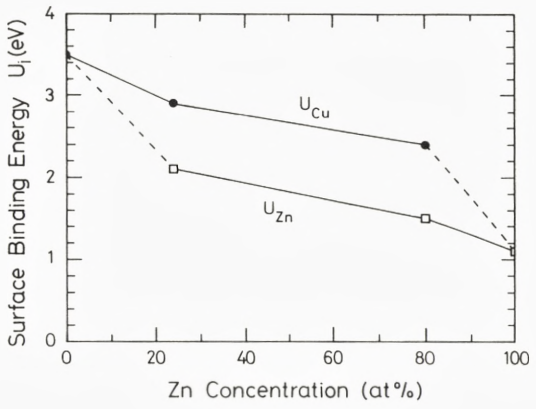

Figure 2. Compositional dependence of the surface binding energies U_{Cu} and U_{Zn} in Cu-Zn alloys. Curves drawn to guide the eye. After Szymonski (1980).

ion type and energy. Caution is also indicated after bombardment at high fluence: Here, composition gradients build up which will affect energy and angular spectra of sputtered atoms. Particularly in the presence of pronounced Gibbsian segregation, the peak position of the energy spectrum must be expected to change. Pertinent estimates are not available.

Experimental evidence suggests that surface binding energies indeed depend on alloy composition. Szymonski (1980) found U_{Zn} in Cu-Zn alloys to decrease with increasing Zn concentration toward the pure-Zn value, while U_{Cu} decreased from the pure-Cu value to a substantially smaller one (fig. 2). Similar composition dependences were observed in Au-Ag, Ni-W, and Cu-Li alloys by Szymonski et al. (1978), Oechsner & Bartella (1981), and Schorn et al. (1988), respectively. Noticeable matrix effects on the surface binding energy were also demonstrated for Cr atoms in different alloys (Husinsky et al., 1987).

Reliable values of static surface binding energies can now be calculated from standard codes on the basis of density functional and effective-medium theory for a given target configuration. Such values are implicit in molecular-dynamics simulations based on theoretical or empirical many-body potentials. For the present purpose, effective surface binding energies, valid under dynamic conditions, may be extracted from simulated energy spectra of sputtered atoms. Lam & Johannessen (1992) determined surface binding energies of Cu and Ni in a $Cu_{0.5}$-$Ni_{0.5}$ alloy dynamically and found $U_{Cu} = 3.28 \pm 0.13$ eV and $U_{Ni} = 3.97 \pm 0.17$ eV, which are lower than the heats of sublimation of pure Cu and Ni, i.e., 3.51 and 4.45 eV, respectively (Gschneidner, 1964).

Kelly (1978, 1980) related the bond strengths U_{ik} in eq. (16) to the heats of atomization of the pure components, $\Delta H_i \simeq (1/2)ZU_{ii}$, where Z is the bulk coordination number, and the heat of mixing of the alloy, ΔH_m. Since ΔH_m is usually much smaller than ΔH_i, one may approximate U_{ik} by

$$U_{ik} = \frac{1}{2}(U_{ii} + U_{kk}). \tag{17}$$

It was concluded that preferential sputtering estimated on the basis of the surface-binding-energy given by eqs. (16,17) was in most cases far smaller than experimental observations, the reason being that most measurements were affected by surface segregation (Kelly & Harrison, 1985).

2.2.5 Sputter Cross Sections

Sputter cross sections are determined via the recoil density. Let $F_i(\epsilon, \Theta, x)d\epsilon d^2\Omega dx$ be the number of i-atoms per incident particle recoiling from a layer (x, dx) with an energy $(\epsilon, d\epsilon)$ into an angular interval $d^2\Omega$ at some polar angle Θ against the surface normal. Moreover, let $P_i(\epsilon, \Theta, x)$ be the probability for such an i-atom to be ejected through the surface. Then the sputter yield reads

$$Y_i = \int_0^\infty dx \int d\epsilon \int d^2\Omega F_i(\epsilon, \Theta, x) P_i(\epsilon, \Theta, x), \tag{18}$$

from where $\sigma_i(x)$ can be extracted by comparison with eq. (5).

Recoil densities integrated over depth and direction of motion have been calculated for homogeneous polyatomic media within the approximation scheme applied to the particle flux (Andersen & Sigmund, 1974). They may be rendered differential by the assumptions of isotropy, constant energy spectrum over the pertinent depth range near the surface, and a depth distribution in accordance with the deposited energy. This yields

$$F_i(\epsilon, \Theta, x) \simeq \frac{1}{4\pi} K_i c_i' \frac{F_D}{\epsilon^2}, \tag{19}$$

where $F_D \simeq F_D(x{=}0)$ is the deposited energy per unit depth at the surface, c_i' a quantity closely related to, but not identical with an atom fraction (Andersen & Sigmund, 1974; Vicanek & Sigmund, 1994), and K_i a dimensionless factor called displacement efficiency. Actually, K_i is not identical with, but closely related to the quantity carrying the same name in conventional radiation damage theory. It is seen that K_i expresses the degree of preferentiality in the energy sharing of the collision cascade. Explicit results for the dependence of K_i on composition have been given by Andersen & Sigmund (1974). The range of validity of eq. (19) has been studied recently (Koponen, 1992).

Some discussion has been concerning the ejection probability $P_i(\epsilon, \Theta, x)$. While that discussion is not specific to polyatomic media, it deserves a comment here. Apart from the variables listed above, P_i must depend on the surface barrier as well as the cross sections for elastic and inelastic scattering. In early papers (Sigmund, 1969a; Falcone & Sigmund, 1981; Sigmund et al., 1982), P_i was determined from the continuous-slowing-down approximation, i. e., angular deflection was ignored and an atom was thought to be ejected if, after moving on a straight line toward the surface, it still had enough energy to overcome the barrier.

In subsequent work (Falcone, 1991, and earlier references quoted there), the ad hoc assumption was made that the ejection probability should be determined only by angular deflection while energy loss should be immaterial. This assumption ignores the fact that in the absence of energy loss, the ejection probability is either zero or one, dependent on whether the energy is above or below the barrier, independent of depth. In the case of dominating angular deflection and weak energy loss — which is relevant in electron emission (Sigmund, 1993a) — the pertinent escape depth becomes the geometric mean between the range and the transport mean free path Λ_t for angular deflection. This is in contrast with the claim made by Falcone (1991) that the escape depth should be identical with Λ_t. In sputtering, angular deflection is typically associated with substantial energy loss. Therefore, the limit of dominating angular deflection does not usually apply. Consequently, the dependence of the escape depth on Λ_t must be *even weaker* than $\sqrt{\Lambda_t}$.

We thus conclude, in agreement with quantitative results given by Vicanek et al. (1989), that for elemental targets, the escape function is governed primarily by energy loss while angular deflection is a perturbation which is noticeable only in accurate evaluations. The perturbation may become significant in polyatomic targets with very different masses where the light component may undergo wide-angle scattering events with only minor energy loss.

Within the continuous-slowing-down approximation, one finds

$$P = \begin{cases} 1 & \text{for } \left(1 - \dfrac{x}{R_i(\epsilon)\cos\Theta}\right)^{1/2m} > \dfrac{U_i}{\epsilon\cos^2\Theta} \\ 0 & \text{otherwise} \end{cases} \tag{20}$$

where $R_i(\epsilon)$ is the total pathlength of an i-atom of energy ϵ. This quantity can be found from the stopping power of an i-atom,

$$\left(\frac{d\epsilon}{dR}\right)_i = -\frac{1}{1-m}\sum_j N_j C_{ij}\gamma_{ij}^{1-m}\epsilon^{1-2m} = -A_i\epsilon^{1-2m}, \tag{21}$$

where the last step defines a stopping constant A_i.

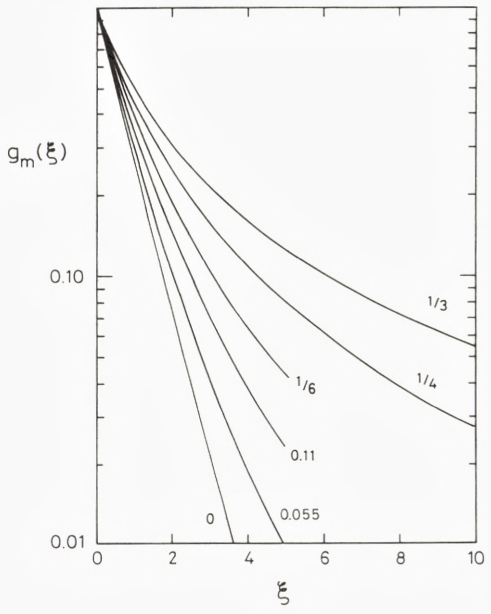

Figure 3. Depth dependence of the sputter cross section, eq. (20) for different values of the exponent m. The scale is specified by eq. (22).

Integration and comparison with eq. (18) yields (Sigmund et al. 1982)

$$\sigma_i(x) = \frac{K_i F_D}{6NU_i} g_m\left(\frac{A_i x}{U_i^{2m}}\right), \tag{22}$$

where

$$g_m(\xi) = \int_0^1 dt \frac{3t^2}{(1+2m\xi t^{4m-1})^{1/2m}}. \tag{23}$$

The functions $g_m(\xi)$ have been normalized such that $g_m(0) = 1$, and their halfwidth varies between $\xi_{1/2}$=0.5 and 0.75 for m running from 0 to 0.33 (fig. 3). Specifically, for $m = 0$, $g_0(\xi) = 3E_4(\xi)$, where $E_4(\xi)$ is an exponential integral in conventional notation (Abramowitz & Stegun, 1964).

The sputter cross section $\sigma_i(x)$ is preferential due to preferentiality of the displacement efficiency K_i and the surface binding energy U_i. The depth dependence expressed by the function $g_m(\xi)$ is also preferential in the sense that atoms with low stopping powers, i.e., low A_i, or high surface binding energy U_i, may emerge from deeper layers.

2.3 Secondary Processes

According to eq. (5), partial sputter yields of a multicomponent target are governed by sputter cross sections $\sigma_i(x)$ and densities $N_i(x)$. The physics of the sputter cross section is the subject of the theory of primary sputter processes. Secondary processes affect the behavior of densities as a function of depth and time.

In secondary processes it is appropriate to distinguish between two different time scales. For athermal processes, the rate-determing quantity is the ion fluence $d\Phi = J_0 dt$, where J_0 is the incident-ion current [number of ions/area/time] and dt a real-time interval. For thermally-activated processes, this direct correlation does not apply.

Pertinent athermal effects are 'prompt' processes in a collision cascade like sputtering, recoil mixing, and 'spike' phenomena (Sigmund, 1981). Also electronic sputtering, when present, and associated damage effects belong mostly into this category (Johnson & Schou, 1993). Moreover, pressure gradients building up in the material due to collisional rearrangement in a cascade must to some degree relax athermally on a time scale of the order of a lattice-vibrational period. This relaxation may even be affected by the energetics of Gibbsian segregation. Experimentally, athermal processes are identified by their dependence on ion fluence independent of the ion current density J_0.

Thermally activated processes like Gibbsian segregation in the conventional meaning, radiation-enhanced diffusion, and radiation-induced segregation, may be substantial during ion bombardment even at temperatures where they would be frozen in the absence of an ion beam. Once created, bombardment-induced point defects may migrate over distances that are large compared to the dimensions of an individual collision cascade. Therefore, bombardment-induced changes caused by migrating defects will depend on the density of ion current as well as on target temperature.

Thermal as well as athermal effects are governed by rate equations that are similar in structure but different in detail. The present introductory section is intended to show the gross features while specific processes will be treated in more detail in section 4.

2.3.1 Athermal Processes

In the absence of thermally activated processes, a full description of alloy sputtering must account for the compositional changes caused by primary effects of preferential sputtering, collisional mixing and ion implantation, as well as instantaneous relaxation of the target to a stable state. Numerous versions of the pertinent rate equations have been proposed. A general survey of work prior to 1981 was given by Betz & Wehner (1983). Existing treatments differ in the way how sputter-

ing, mixing, and relaxation enter into the theoretical scheme, quite apart from the numerical input. The treatment given below should comprise the essentials of different schemes.

As a starting point we use a scheme proposed initially by Hofer & Littmark (1979) for a numerical treatment of collisional mixing in depth profiling by sputtering. In the original form, that scheme assumed stoichiometric sputtering and mixing, and ion implantation was disregarded. Proper generalizations followed subsequently. The scheme was condensed into a set of nonlinear kinetic equations (Sigmund et al., 1982). Although that set of equations in its original form disregarded ion implantation, it comes fairly close to a comprehensive description that allows incorporation of most pertinent processes including thermally activated ones (Sigmund & Oliva, 1993).

The key quantity characterizing the primary processes of collisional mixing and preferential sputtering is the relocation cross section $G_i(x, x')dx'$. This is an almost universally used quantity in mixing theory although names and notation vary slightly. Let $\delta\Phi G_i(x, x')dx'$ be the probability for a given target atom of type i to be relocated from an initial depth x into a layer (x', dx') by a small ion fluence $\delta\Phi$. In the absence of competing effects, this would result in the following kinetic equation for the composition profiles $N_i = N_i(x, \Phi)$,

$$\left(\frac{\partial N_i(x,\Phi)}{\partial\Phi}\right)_{\text{unrelaxed}} = \int_0^\infty dx' N_i(x',\Phi)G_i(x',x) - N_i(x,\Phi)\int_{-\infty}^\infty dx' G_i(x,x'). \tag{24}$$

A planar target surface is assumed in $x = 0$. The first term on the right accounts for atoms relocated into depth x from some depth x' inside the target. The second term accounts for loss of atoms from depth x into some depth x' inside or outside the target.

Relocation into negative depths is synonymous with sputtering. The sputter cross section $\sigma_i(x)$ introduced in eq. (5) is related to the relocation cross section by

$$\sigma_i(x) = \int_{-\infty}^0 dx' G_i(x,x'). \tag{25}$$

It is convenient to abbreviate the right-hand side of eq. (24) by $L_i N_i$, where L_i is to be understood as an integral operator (Sigmund & Gras-Marti, 1981). The relocation cross section $G_i(x, x')dx'$ depends on the composition of the medium; hence, the relocation operator L_i will in general not be linear.

We may include the effect of ion implantation and expand eq. (24) into

$$\left(\frac{\partial N_i}{\partial\Phi}\right)_{\text{unrelaxed}} = \delta_{i0} f_0(x) + L_i N_i \tag{26}$$

with the relocation term

$$L_i N_i(x) = -N_i \sigma_i(x) + \int_0^\infty dx' [N_i(x') G_i(x', x) - N_i(x) G_i(x, x')]. \qquad (27)$$

Here, as frequently in the following, the Φ-variable has been suppressed for clarity. The index 0 denotes the implanted species, δ_{ij} is the Kronecker symbol (= 1 for $i = j$ and 0 otherwise), and $f_0(x)$ is the range profile of the primary beam normalized to $\int_{-\infty}^{\infty} dx f_0(x) = 1$. Implantation into negative depths is synonymous with ion reflection.

The integral on the right of eq. (27) represents the effect of collisional mixing, i.e., direct relocation of target atoms by beam ions ('recoil impantation') as well as relocation by cascade particles ('cascade mixing'). Due to the initial momentum of the beam particles, there is always a net transport of target atoms into the target. This leads to a pileup of matter in the region around the mean penetration depth of the beam and beyond, and a corresponding depletion in the near-surface region which adds to the loss by sputtering. The resulting pressure gradients are mechanically unstable and must relax instantaneously. In a molecular-dynamics simulation of a collision cascade, this relaxation will show up if the interatomic potential allows for a stable target configuration and if a cascade is followed over a sufficiently long time interval. Simulations of cascade processes by Monte Carlo or binary-collision codes as well as conventional analytic approaches do not incorporate this feature. Therefore it has to be superimposed separately.

A straightforward, although a bit schematic way of accounting for this relaxation is by letting the material relax homogeneously such as to satisfy a prescribed packing condition

$$\sum_{i=0}^{n} \Omega_i N_i(x) = 1, \qquad (28)$$

where Ω_i is the atomic volume of an i-atom. This criterion was adopted initially by Hofer & Littmark (1979) for a binary material with all atomic volumes being equal.

In order that eq. (28) be fulfilled, a relaxation term needs to be added on the right-hand side of eq. (26), as a result of which the rate equation reads

$$\frac{\partial N_i(x, \Phi)}{\partial \Phi} = \delta_{i0} f_0(x) + L_i N_i(x, \Phi) - \frac{\partial}{\partial x} \left(N_i(x, \Phi) \sum_{j=0}^{n} \Omega_j \int_0^x dx' [\delta_{j0} f_0(x') + L_j N_j(x', \Phi)] \right). \qquad (29)$$

It is easily verified that the packing condition (28) is obeyed at any fluence if it is fulfilled initially.

Note that it is the imposition of a packing condition which causes the target surface to recede as a result of the loss of matter by sputtering. This recession has been taken into account in the explicit derivation of eq. (29) (Sigmund et al., 1982, Collins & Sigmund, 1992) by means of a coordinate transformation that ensures the surface always to be located at $x = 0$.

The above scheme is equivalent with the seminumerical scheme applied by Littmark mostly for mixing calculations (Littmark & Hofer, 1984). In addition, numerical schemes developed by Eckstein & Möller (1985) and by Roush et al. (1981) reflect more or less the same physical content.

2.3.2 Relation to Elementary Treatments

Eq. (29) contains most earlier treatments as special cases. This will be illustrated separately for the effects of sputtering, implantation, and mixing.

Eq. (27) identifies the effect of sputtering. That contribution to eq. (29) reads

$$\left(\frac{\partial N_i}{\partial \Phi}\right)_{\text{sput}} = -\sigma_i(x)N_i(x) + \frac{\partial}{\partial x}\left(N_i(x)\sum_{j=0}^{n}\Omega_j\int_0^x dx'\sigma_j(x')N_j(x')]\right). \quad (30)$$

In many treatments, all depth dependence of sputtering is ignored, and atoms are considered to be sputtered only from the surface. Then the sputter cross section reduces to $\sigma_i(x) = \delta(x)Y_i/N_i(0)$ where $\delta(x)$ is the Dirac function, and eq. (30) to

$$\left(\frac{\partial N_i}{\partial \Phi}\right)_{\text{sput}} = -Y_i\delta(x) + w\frac{\partial N_i}{\partial x}, \quad (31)$$

where w is the surface recession due to sputtering as defined by eq. (2). The term $w\partial N_i/\partial x$ is the familiar convection term from transport theory. Note, however, that w, which is usually treated as a constant material parameter, depends on fluence via the partial sputter yields Y_i. The term containing the Dirac function is equivalent with a boundary condition, $N_i(0) = Y_i/w$, ensuring the correct sputter current of each species through the surface.

The implant term in eq. (26) is of interest mostly for the buildup of the implanted species. It can be written in the form

$$\left(\frac{\partial N_i}{\partial \Phi}\right)_{\text{impl}} = [\delta_{i0} - \Omega_0 N_i(x)]\, f_0(x) - u_0\frac{\partial N_i(x)}{\partial x}, \quad (32)$$

where

$$u_0 = \Omega_0\int_0^x dx' f_0(x') \quad (33)$$

represents the dilatation due to implanted ions. This term is frequently neglected in mixing calculations but is of central significance in estimates of ion collection efficiencies (Almén & Bruce, 1961; Titov, 1979).

The contribution from mixing is often written in the form of a diffusive term. The relation to the present notation is well established in transport theory but will be sketched here briefly. Diffusive motion implies motion in very small steps. In other words, the relocation cross section $G_i(x, x')dx'$ is nonvanishing only for x' close to x. The situation is simplest in case of translational invariance, i.e., for $G_i(x, x') = G_i(x' - x)$. Then, Tailor expansion of $N_i(x')$ around x yields

$$\left(\frac{\partial N_i}{\partial \Phi}\right)_{\text{mix,unrelaxed}} = -v_i \frac{\partial N_i(x)}{\partial x} + \hat{D}_i \frac{\partial^2 N_i(x)}{\partial x^2}. \tag{34}$$

with

$$v_i = \int_{-\infty}^{\infty} dx'(x' - x) G_i(x' - x) \tag{35}$$

and

$$\hat{D}_i = \frac{1}{2} \int_{-\infty}^{\infty} dx'(x' - x)^2 G_i(x' - x). \tag{36}$$

For a genuine random walk, the mean relocation rate v_i for species i vanishes, but in a collision cascade, the initial momentum of the beam causes preferential relocation into the beam direction and, hence, v_i to be positive. The quantity $\hat{D}_i$, as specified by eq. (36), differs from a genuine diffusion coefficient only by the conversion factor from time to fluence, i.e., $D_i = J_0 \hat{D}_i$.

While there is little doubt about the accuracy of the diffusion approximation for genuine diffusive motion, caution is indicated in case of collision cascades. Firstly, long-range relocation is possible. This implies tails at large relocation depths which the diffusion approximation can handle reasonably only in the limit of high implant fluences. Secondly, the relocation cross section will generally vary with depth over the penetration depth of the beam. This generates an ambiguity with regard to which quantity the Taylor expansion in powers of the relocation depth should be applied to. Collins & Jimenez-Rodriguez (1982) suggested an expansion in which the product of the density and the relocation cross section is assumed to vary slowly with x. Despite some success (Collins et al., 1988), it is not obvious under what circumstances this is an improvement beyond straight expansion of $N_i(x')$ (Conrad & Urbassek, 1993). Thirdly, steep composition gradients may develop near the target surface both due to sputtering and recoil implantation which require additional attention, in particular with regard to the boundary conditions to be satisfied.

Existing theoretical treatments addressing the validity of the diffusion approximation in atomic mixing addressed mostly bulk mixing and sputter profiling. Pre-

ferential sputtering was treated by means of the diffusion approximation, based on eq. (29) without the implant term, by Oliva et al. (1986).

2.3.3 The High-Fluence Limit

A useful model system for experimental and theoretical studies of alloy and isotope sputtering is a material with a homogeneous composition in the bulk. In the absence of activated processes, such a system must reach a stationary state at high fluences where all species sputter stoichiometrically.

This emerges readily from eq. (29). In the stationary state, the derivative on the left must vanish. Integration over the x-variable over the half-space yields

$$0 = \delta_{i0} t_0 - Y_i - N_i(\infty) \sum_{j=0}^{n} \Omega_j (\delta_{j0} t_0 - Y_j), \tag{37}$$

where

$$t_0 = \int_0^\infty dx f_0(x) \tag{38}$$

is the retention coefficient for incident ions. Note that

$$\int_0^\infty dx L_i N_i(x) = -Y_i \tag{39}$$

by means of eq. (27). Splitting eq. (37) into beam and target species yields

$$Y_0 = t_0 \tag{40}$$

and

$$Y_i = N_i(\infty) \sum_{j=1}^{n} \Omega_j Y_j \quad \text{for} \quad i = 1 \ldots n \tag{41}$$

in the stationary state. Eq. (40) shows that the sputter rate for implant atoms balances the retained beam flux in the stationary state as it should be. Eq. (41) shows that the partial sputter yields of the target species are all proportional to the bulk concentration, i.e., the target sputters stoichiometrically.

While these results do not imply any assumptions on the nature and magnitude of atomic mixing effects, such information does enter into the absolute magnitude of the partial sputter yields for the target species. We note that it is essentially the effective sputter yield $Y_{\text{eff}}^{(\Omega)}$, eq. (4), that enters the asymptotic formula (41).

2.3.4 Activated Processes

The theoretical scheme described above for athermal processes can readily be extended such as to comprise thermally activated processes. Two items need to be

considered. Firstly, such processes proceed in real time, i.e., fluence is insufficient as the sole time variable. Secondly, more species are involved in the transport of matter, especially point defects, i.e., vacancies and interstitials. In order to incorporate these two features, disregard relaxation for a moment and write

$$\left(\frac{\partial N_i(x,t)}{\partial t}\right)_{\text{unrelaxed}} = J_0(t)\left(\delta_{i0}f_0(x) + \sum_{\nu=n+1}^{n+z}\delta_{i\nu}F_\nu(x) + \sum_{\nu=0}^{n}\delta_{i\nu}L_\nu N_\nu(x,t)\right)$$
$$+ \Lambda_i N_i(x,t) - S_i N_i(x,t) \equiv \mathcal{Q}_i(x,t). \tag{42}$$

Here, $N_i(x,t)$ denotes the density of implanted beam atoms for $i = 0$, the density of target species for $i = 1,\ldots n$, and the density of i-type defects for $i = n+1,\cdots n+z$ if there are z different kinds of pertinent defects. The three terms in the brackets on the right-hand side of eq. (42) represent the implanted beam, the primary production of defects by the ion beam — $F_\nu(x)dx$ is the mean number of ν-defects generated per beam particle at depth (x, dx) — and primary relocation including sputtering, respectively. These processes are proportional to the beam current J_0 which may be time-dependent.

The fourth term, $\Lambda_i N_i(x,t)$, represents all transport processes which are not described by the relocation term $L_i N_i$. This term has a form analogous to eq. (27),

$$\Lambda_i N_i(x) = \int_0^\infty dx'[N_i(x')\Gamma_i(x',x) - N_i(x)\Gamma_i(x,x')] \tag{43}$$

with the difference that there is no loss term due to sputtering. The relocation function $\Gamma(x,x')$ will in general be a functional of several of the pertinent densities, especially defect densities. On the other hand, the applicability of the diffusion approximation applied to $\Lambda_i N_i(x,t)$ will most often be granted. In sect. 4.5.1 this term will be written in a form that allows for linear coupling between different species. The above notation is meant to incorporate this feature symbolically.

Finally, the last term in eq. (42) represents most of all the loss of defects by annihilation, either via interaction with other migrating defect species or at stationary sinks such as dislocations, grain boundaries, and surfaces. However, also the loss of volatile atoms from the target surface may be included here. Again, the loss operator S_i may be a functional of several other densities. This will be made explicit in sect. 4.3.

Eq. (42) does not automatically obey a stability criterion. We now generalize the packing condition (28) such as to include not only beam and target particles but also defects so that a fixed volume Ω_ν is assigned to every ν-type defect,

$$\sum_{i=0}^{n+z}\Omega_i N_i(x) = 1. \tag{44}$$

With this, the comprehensive equation governing compositional changes reads

$$\frac{\partial N_i(x,t)}{\partial t} = \mathcal{Q}_i(x,t) - \frac{\partial}{\partial x}\left(N_i(x,t) \sum_{j=0}^{n+z} \Omega_j \int_0^x dx' \mathcal{Q}_j(x',t) \right), \tag{45}$$

$\mathcal{Q}_i(x)$ being defined by eq. (42). For constant atomic volume, this equation fulfills the packing condition at all times if it is fulfilled initially. The option of a composition-dependent atomic volume has been considered recently (Sigmund & Oliva, 1993).

In the following, an alternative version of eq. (45) will occasionally be used, which is easily verified by means of the packing condition (44),

$$\frac{\partial N_i}{\partial t} = \sum_{j=0}^{n+z} \Omega_j [N_j \mathcal{Q}_i - N_i \mathcal{Q}_j] - \frac{\partial N_i}{\partial x} \sum_{j=0}^{n+z} \Omega_j \int_0^x dx' \mathcal{Q}_j(x',t). \tag{46}$$

In the absence of concentration gradients — as may be the case at small irradiated fluences — this reduces to the simple expression

$$\frac{\partial N_1}{\partial t} = \Omega_2 [N_2 \mathcal{Q}_1 - N_1 \mathcal{Q}_2] \tag{47}$$

if only two species are present. This illuminates the importance of the relaxation term: If relaxation were neglected, the right-hand side would just read $\mathcal{Q}_1$.

The main weakness of this description is its limitation to planar geometry. The real situation is unquestionably three-dimensional, at least in principle and most often in practice: An initially planar target surface does usually not retain its planar shape. The development of surface topography under sputtering has been an active area of investigation (Carter et al., 1983). It is also well documented that topography is sensitive to surface contamination. Despite this, the problem has apparently not been treated in conjunction with specific aspects of alloy sputtering.

2.3.5 The Stationary State

Several conditions must be expected to be fulfilled for a stationary state to develop in the presence of activated processes. An eroding target can reach a steady-state profile only if it has initially a homogeneous composition at least at great depths. The ion current J_0 must be reasonably constant. All pertinent sputter yields must be nonvanishing. All transport of matter must be limited to a finite depth range. If either of the two latter conditions is not fulfilled, one or more component will continue to be enriched or depleted, respectively.

While we are not sure whether a combination of these conditions makes up a sufficient criterion for the existence of a stationary state, we wish to briefly

demonstrate the implications for sputtering when such a state does exist. Following the procedure applied in sect. 2.3.3, we set the left-hand side of eq. (45) equal to zero and integrate over all x. This yields

$$0 = \int_0^\infty dx \mathcal{Q}_i(x) - N_i(\infty) \sum_{j=0}^{n+z} \Omega_j \int_0^\infty dx \mathcal{Q}_j(x). \tag{48}$$

The integral $\int_0^\infty dx \mathcal{Q}_i(x)$ receives five contributions according to eq. (42): The first and third one have been evaluated in sect. 2.3.3. The second and fifth contribution vanish for $i = 0, 1, \ldots n$, i.e., for i running over the target species and the beam particles. The fourth contribution is readily seen to vanish for arbitrary $G_i(x, x')$ by means of eq. (43). Therefore, we retain eq. (40) as was to be expected, and even eq. (41) remains strictly valid with the bounds on i and j as given: Again, sputtering proceeds stoichiometrically, independent of the quantitative input on either thermal or athermal processes. Again, the proportionality constant determining the absolute values does depend on that input.

2.3.6 Solving Equations

So far, no fully analytic solution of eq. (45) has been reported for any system. Selected numerical results will be given in sect. 4. Here a few schemes will be discussed briefly that allow to evaluate important limiting cases. While the choice of initial conditions is arbitrary within the limitations set by the packing condition (44), it is convenient – but of course not necessary – for calculations in the low-fluence limit to refer to a standard case where

$$N_i(x, 0) = \mathcal{N}_i \tag{49}$$

and the $\mathcal{N}_i$ are the initial concentrations of atoms and defects in the material, taken as independent of depth and satisfying $\sum_{i=0}^{n+z} \Omega_i \mathcal{N}_i = 1$. This allows for an initial (equilibrium) defect concentration but ignores an initial (equilibrium) segregation.

With this, we find the low-fluence behavior

$$\left(\frac{\partial N_i(x,t)}{\partial t} \right)_{t=0} = \sum_{j=0}^{n+z} \Omega_j \left[\mathcal{N}_j \mathcal{Q}_i(x,0) - \mathcal{N}_i \mathcal{Q}_j(x,0) \right]. \tag{50}$$

The initial concentration of beam particles, $\mathcal{N}_0$, will frequently be vanishing, and for many applications it is justified to ignore the initial, thermal defect concentrations $\mathcal{N}_{n+1} \ldots \mathcal{N}_{n+z}$ altogether. An additional term containing gradients of $\mathcal{N}_i$ would remain if the initial (equilibrium) segregation could not be neglected.

As did eq. (47), eq. (50) documents that the relaxation term cannot be ignored even at the lowest fluences. Indeed, in a binary material, a small ion fluence causes

one component to be depleted and the other enriched near the surface due to sputtering. If relaxation were neglected, both components would appear depleted.

Next, consider the stationary state, assuming that all pertinent conditions be fulfilled for such a state to exist. In this case, the presence of an initial equilibrium segregation is immaterial. Dropping all time dependence and integrating over x from 0 to x and from x to ∞, respectively, leads to the following identities (Sigmund & Oliva, 1993),

$$N_i(x) = \frac{\int_0^x dx' \mathcal{Q}_i(x')}{\sum_j \Omega_j \int_0^x dx' \mathcal{Q}_j(x')} \tag{51}$$

and

$$N_i(x) = \mathcal{N}_i + \frac{\sum_j \Omega_j \int_x^\infty dx' [N_i(x)\mathcal{Q}_j(x') - N_j(x)\mathcal{Q}_i(x')]}{\sum_j \Omega_j \int_0^x dx' \mathcal{Q}_j(x')}. \tag{52}$$

Here, eq. (51) is useful to explore the analytic behavior of $N_i(x)$ in the vicinity of the surface. Eq. (52) can serve as the basis of an iteration scheme determining the stationary profile without computation at intermediate fluences. This scheme involves $\mathcal{Q}_i(x)$ expressed by $N_i(x)$ through the definition, eq. (42), and an initial trial function for which eq. (49) is adequate.

Time-dependent solutions have been determined approximately by linearization of eq. (45) in terms of weak preferentiality (Sigmund et al., 1982; Jimenez-Rodriguez et al., 1992, Conrad & Urbassek, 1993). Here the assumption enters that profiles do not deviate significantly from the initial profile eq. (49), so that relocation operators can be expanded around a suitably chosen mean value. While the scheme turns out to deliver accurate profiles in the athermal case when the implanted species is left out of consideration, artefacts appear in the immediate vicinity of the surface (Sigmund & Oliva, 1993) that warrant caution in applications to sputtering.

Fully-numerical solutions have been provided by Falcone & Oliva (1984) and, more recently, by Wadsworth et al. (1990).

3 Isotopic Mixtures

3.1 General Considerations

Different isotopes of an element sputter preferentially. For solid hydrogen, under conditions of dominating electronic sputtering, large isotope effects have been found experimentally (Schou, 1992; Johnson & Schou, 1993). Under conditions of dominating collisional sputtering, measurements and theory suggest isotope effects to be small. While there has been discussion about the actual magnitude, there is little doubt that they do not exceed $\simeq \Delta M/2M$, where ΔM is the mass difference

and M the mean mass. For a typical isotopic system with $\Delta M/M \leq 0.1$, this implies an effect of the order of 5% or less. This smallness requires high standards on the accuracy of sputter experiments even when only relative yields or spectra are asked for. It also implies stringent requirements regarding systematic and statistical errors in computer simulations undertaken to study isotope effects in sputtering. Conversely, analytical estimates benefit from the smallness of the effect because of the possibility of series expansion of pertinent physical quantities in terms of the relative mass difference. The main challenge there is the necessity to consider several small effects that might contribute to the overall picture.

Measurements of preferential sputtering from isotopic mixtures have been performed at high and low fluences. At high fluences the components sputter stoichiometrically, but their angular emission patterns need not be identical and, therefore, allow conclusions on preferential sputtering. At low fluences, partial sputter yields provide a direct measure of preferential sputtering.

It may be appropriate to discuss qualitatively a number of effects that compete with the mass dependence of the partial sputter yields discussed in sect. 2.2.3.

Firstly, according to eq. (15), the ratio of partial sputter yields is sensitive to differences in binding energy. Even though it may be justified to neglect a possible difference in the binding potential which keeps the atoms to their lattice sites, a difference in the effective binding energy arises due to the mass dependence of the zero-point energy. Hence, we may take

$$\frac{\Delta U}{U} \simeq \frac{3}{2}\frac{\hbar\omega_D}{U}\frac{\Delta M}{2M} \tag{53}$$

as a first approximation, where ω_D is a Debye frequency and $3\hbar\omega_D/2$ the zero-point energy. This implies that the lightest isotope has the smallest binding energy. In the absence of other effects, this gives rise to preferential sputtering of light isotopes according to

$$\frac{\Delta Y}{Y} \simeq -(1-2m)\frac{3}{2}\frac{\hbar\omega_D}{U}\frac{\Delta M}{2M} \tag{54}$$

in accordance with the dependence on surface binding in eq. (15).

Secondly, Gibbsian segregation has generally been ignored for isotopic systems. A small isotope effect must, however, occur essentially for the same reason as in case of the surface binding energy, i.e., the vibrational contribution to the free energy of an atom. If the surface modes are softer, the surface free energy will be smaller than the bulk free energy, and the $M_i^{-1/2}$-dependence of the vibration frequency will result in a negative segregation energy for the lighter isotopes (Foiles, 1992). Enrichment of the lighter species appears to be favored in thermal equilibrium.

Thirdly, there is a well-known isotope effect in diffusion (Peterson et al., 1973; Peterson, 1975). The relative difference in diffusivity between two isotopes results

from the mass dependence of the jump frequency, i.e.,

$$\frac{\Delta D}{D} = -f \Delta K \frac{\Delta M}{2M}, \tag{55}$$

where f is the pertinent correlation factor (i.e., a geometric factor dependent only on the crystal structure and the atomic jump process) and ΔK an energy sharing factor. Eq. (55) implies that the isotope with the smallest mass diffuses most rapidly. This may give rise to a preferential coupling between the currents of radiation-produced defects (e.g., interstitials, at ambient temperature) and the lighter isotopes and may induce a surface enrichment of these isotopes during sputtering. Measurements of near-surface concentration profiles for different isotopes would be of interest.

Finally, light isotopes are recoil-implanted preferentially from the surface into deeper layers. It depends on the experimental technique whether this effect can be separated from that of preferential sputtering.

3.2 Theoretical Estimates: Primary Effects

Four groups of authors have been engaged in the theoretical study of isotope effects in sputtering. Since these groups worked rather independently we first discuss their contributions separately and subsequently try to summarize the current status.

3.2.1 Estimates of Sigmund and coworkers

The sharing of energy in linear collision cascades generated by high-energy primary ions in a homogeneous, infinite, polyatomic medium was studied by Andersen & Sigmund (1974) . The ratio between particle fluxes of two components 1, 2 was found to be given by eq. (9). For the specific case of power scattering, eq. (10), this reduces to eq. (11). The physical origin of this mass dependence has been described in sect. 2.2.3. Note in particular that eqs. (9) and (11) remain valid also between any two components of a medium containing more than two isotopes, and even in the presence of other elements.

Eq. (9) represents an asymptotic solution for the case of $E \gg \epsilon$. It is well established that anisotropy corrections need to be allowed for at moderate to low ratios of E/ϵ (Sigmund, 1981). For isotopic systems, such corrections have been explored recently (Sigmund & Sckerl, 1993).

According to conventional sputter theory, the composition of the sputtered-particle flux reflects the flux of atoms in the bulk, and the magnitude is determined by the depth distribution of deposited energy (Sigmund, 1969a). Within this picture, eqs. (9) and (11) represent an estimate of the ratio of partial sputter yields. This conclusion was implicit in the work of Andersen & Sigmund (1974)

but was drawn only with considerable caution. The reason for this caution was the awareness of concentration gradients produced by preferential sputtering. Those gradients were assumed to be very pronounced at those fluences where measurements were available, since the feeding effect of collisional mixing was not yet established at the time.

A more explicit discussion of preferential sputtering, both for isotopic mixtures and alloys, based on the above results was presented subsequently (Sigmund, 1980, 1981). Here, eq. (11) was asserted to characterize the *primary* effect of preferential sputtering, at least in the limit of high ion energy. In that limit, the composition of the sputtered flux should be independent of ion type and energy.

Within this scheme, the key parameter governing preferential sputtering is the exponent m in the power cross section, eq. (10). That quantity was discussed briefly in sect. 2.2.3. The parameter depends on ejection energy and, somewhat, on M, but it may safely be set equal for all isotopes of a given element. The value of $m = 1/3$ valid for Thomas-Fermi interaction (Lindhard et al., 1963) is undoubtedly too large, and the value $m = 0.055$ adopted originally for Born-Mayer interaction (Sigmund, 1969a) turned up to be too small by comparison with an accurate numerical evaluation of the cross section and should have been set to $m = 0.11$ (Vicanek et al., 1989). Potentials utilized at present to describe repulsive interactions between atoms in the energy range in question include the Molière and Lenz-Jensen potential as well as the so-called KrC potential. Characteristic values of m lie around $0.15 - 0.20$ for those potentials.

Allowing for uncertainties in the interatomic potential, one concludes that on the basis of bulk energy sharing and slowing-down, the deviation from stoichiometric sputtering is expected to be given by

$$\frac{\Delta Y}{Y} \simeq -k\frac{\Delta M}{M} \tag{56}$$

in the limit of high ion energy, with $k \sim 0.2 - 0.4$. The minus sign indicates that it is the low-mass component that sputters preferentially.

The leading correction term in an asymptotic expansion in terms of the ratio E/ϵ introduces a slight anisotropy into the particle flux and it modifies the magnitude of the enrichment factor. For heavy-ion bombardment at keV energies, the magnitude of that correction appears quite small (Sigmund & Sckerl, 1993).

3.2.2 Estimates of Haff, Tombrello, Shapiro and coworkers

A massive theoretical effort in the area was presented by collaborations inspired by Tombrello and colleagues.

In an early paper addressing binary compounds (Haff & Switkowski, 1976), energy sharing was treated by intuitive arguments. Sputtering was predicted to be

stoichiometric in the absence of differences in surface binding energy, 'as observed experimentally'. In a related paper (Haff, 1977), a mass effect of the order of $(M_2/M_1)^{1/4}$ was predicted on the basis of arguments involving mean free paths and energy equilibration. Neither of these two papers addressed the item of isotope effects explicitly, but the arguments applied should be valid for those systems.

In a subsequent theoretical paper (Watson & Haff, 1980), energy dissipation was treated on the basis of transport equations equivalent to those analyzed by Andersen & Sigmund (1974). The cross section adopted for those calculations was simplified to the point where no preferentiality was allowed for, corresponding to $m = 0$ in eq. (8). A small isotope effect, quadratic in the mass difference, remained since the authors chose to analyze the recoil density instead of the particle flux. In agreement with a prediction on mass effects by Kelly (1978) but in contrast to all other earlier or later work, this isotope effect was predicted to be composition-dependent.

The conclusions of Watson & Haff (1980) formed the basis of extensive tabulations and predictions of isotope fractionation in minerals addressing the planetary-science community (Haff et al., 1981) and were utilized in the analysis of a most impressive set of experimental data (Russell et al., 1980). The predictions of Andersen & Sigmund (1974) — which clearly conflicted with that picture — were not mentioned.

Although the conclusions of Watson & Haff (1980) and Haff et al. (1981) were never withdrawn, it was apparently deemed necessary to reinvestigate the problem from the beginning by means of computer simulations (Shapiro et al., 1985, 1988; Lo et al., 1989) addressing elemental copper. The main challenge in the investigation of a small effect like preferential sputtering of isotopes by molecular dynamics is statistics. In order to achieve a tolerable signal-to-noise ratio, the authors worked with 'pseudo copper', i.e., targets containing isotopes with mass differences enhanced beyond those present in natural copper. While computational capacity was insufficient initially to provide adequate statistics, a reasonably clear picture has emerged subsequently.

Isotope effects were found to be linear in the mass difference and independent of concentration. Moreover, light isotopes were found to sputter preferentially. These features are in agreement with Andersen & Sigmund (1974) and in contrast to Watson & Haff (1980). Primary sputter effects turned out to depend on the emission angle and to differ for backward and forward sputtering. Moreover, the absolute magnitude of preferential sputtering was found to be fairly large in some simulations, corresponding to values of m in eq. (15) up to $\simeq 0.3$ (Shapiro et al., 1988).

However, caution is indicated in drawing fargoing conclusions from direct comparison between these results to either analytic predictions or experimental data:

Most simulations were done on single crystals (Shapiro et al., 1985, 1988) with the incident beam aligned along a low-index crystal direction. This has two important implications. Firstly, the angular emission characteristics are affected by formation of Wehner spots (Wehner, 1955). While questions regarding the mutual interference of spot formation and preferential sputtering have barely been asked, all existing knowledge of energy and angular spectra in elemental targets (Hofer, 1991) suggests that major or minor interferences exist. In the absence of at least a qualitative analysis, conclusions based on angular patterns of preferential sputtering from single crystals require considerable caution. Secondly, bombardment along low-index directions leads to substantial reductions in sputter yields due to the dominance of near-surface events in generating sputtering (Onderdelinden, 1968). Very little is known on how energy and angular distributions of sputtered atoms are affected even for monoisotope targets. It is evident, however, that these bombardment conditions are not representative for a polycrystal.

The above ambiguities were avoided in molecular-dynamics simulations on liquid copper (Lo et al., 1989). Here a two-isotope copper target with a mass difference of 25 atomic mass units, bombarded by 5 keV Ar, led to a 12.7 % difference in backward sputter yields, corresponding to $m = 0.16$ in eq. (11). The effect in the forward direction was found smaller by more than a factor of two. Thus, there does not seem to be a discrepancy in the magnitude of the predicted preferential sputter effects. This has been documented by a more detailed comparison (Sigmund & Sckerl, 1993).

A particular point in these simulations that deserves to be mentioned is the question of target setup. In the absence of segregation and ordering, the distribution of isotopes on the existing lattice sites must be taken as random, i.e., governed by Poisson's law. This assumption enters into cascade theory (Andersen & Sigmund, 1974) and into Monte Carlo simulations to be discussed below (Eckstein & Biersack, 1985). The assumption also entered initially into molecular-dynamics simulations by Shapiro et al. (1985). However, in the latter, one and the same initial target configuration was utilized in numerous runs. As a consequence, the total number of different target configurations was so small that concern arose as to whether the spectrum of isotopic compositions was representative. Therefore, the degree of preferential sputtering was evaluated not by comparison with the average target composition but with the actual composition. The validity of this correction was questioned (Sigmund, 1987a).

A straightforward response to the criticism would have been not to apply such a correction. After all, the situation encountered here accurately reflects the one that is met in an experiment: The number of i-atoms participating in any given collision cascade will, by necessity, be a fluctuating quantity, and in the absence of order, that number will be Poisson-distributed. Certainly, each ion meets its indi-

vidual target configuration. Nevertheless, sputter yields will have to be recorded relative to the average composition. However, Shapiro et al. (1985) responded to the criticism by a modification of the algorithm so that the number of atoms of each species in a given target always reflected the nominal stoichiometry (Shapiro et al. 1988). This procedure is presumably justified in isotopic targets that exhibit long-range order but appears peculiar when applied to liquid targets (Lo et al., 1989). The associated numerical error is not known.

3.2.3 Estimates of Eckstein and Biersack

Monte Carlo simulations on isotopic mixtures of ^{10}B and ^{11}B were performed by Eckstein & Biersack (1985) in conjunction with a more comprehensive study of the sputtering of multicomponent targets. The physical picture underlying a Monte Carlo simulation resembles that of linear collision cascade theory. This is particularly true with regard to target setup and binary-collision dynamics. A distinct feature of the particular code used in these simulations is the assumption of a fixed free path as opposed to the common exponential distribution that follows from Poisson's law. This causes some peculiarities in the slowing-down of low-energy atoms (Sigmund et al., 1989) which give rise to results that differ from those of conventional Monte Carlo simulations but may in fortunate cases come closer to reality. The potential employed was the so-called KrC potential which leads to a low-energy cross section with $m \simeq 1/6$.

Most of the simulations performed in this work refer to genuine low-energy sputtering at an ion energy of 100 eV, where sputter phenomena are governed by single or double collisions (Winters & Sigmund, 1974). The significance of single-scattering events may even have been increased by carrying out most bombardments at an angle of incidence of 60^0. Typically, this results in preferential-sputtering phenomena that are governed by the 'mass mismatch' between ion and target (Taglauer & Heiland, 1978; Taglauer, 1982; Baretzky & Taglauer, 1985).

For heavy ions ($Z_0 = 10$, 18, 36, and 54) at an initial energy of 1 keV, preferential sputtering of the light isotope with a yield enhancement of 3.14 % was observed. This is in agreement with eq. (11) for $m = 1/6$. Much larger enhancements were found for He bombardment at E = 1 keV. Analytical estimates applying to this regime are not available.

3.2.4 Estimates of Urbassek and coworkers

Monte Carlo simulations of sputtering from an isotopic mixture of ^{92}Mo and ^{100}Mo were performed by Conrad & Urbassek (1991) with a code designed to accurately simulate the same physics on the basis of similar input as analytic transport theory. The validity of eq. (9) for the integrated particle flux in an infinite medium, inte-

grated over all space and all directions of motion, was confirmed, and for the case of a semi-infinite medium only a minor correction was found. Simulations of an actual sputter event were carried out for bombardment with 5 keV Ar, stimulated by experimental results reported by Gnaser & Oechsner (1989, 1990).

The results of the simulation show an enrichment in the low-energy sputtered-particle flux of a magnitude very close to the one predicted by eq. (11). No substantial dependence on emission angle was found. A dramatically higher enrichment was observed in the upper parts of the energy spectrum. This enrichment exceeded what could be expected from the smooth dependence of the exponent m on ejection energy (Vicanek et al., 1989). The effect starts to be pronounced for atoms ejected at energies exceeding $\sim$ 100 eV. Such atoms do not contribute significantly to the sputter yield. Therefore, the overall enrichment of the sputter yield is only slightly larger than the value predicted by eq. (11).

In a subsequent paper (Urbassek & Conrad, 1992), these authors studied preferential sputtering for a wider class of cross sections where the exponent m in eq. (8) was allowed to be species-dependent, i.e., $m = m_{ij}$. This work extends the variety of solutions to the transport equations solved previously. However, new features emerge only for alloys of widely different masses. The impact of this work on isotopic mixtures is very minor.

A most important implication of this work is the confirmation of a significant dependence of the enrichment on the energy of ejected sputtered particles. Measurements on isotope sputtering do not necessarily record the total sputtered flux but may utilize an energy window (in addition to other windows such as ejection angle and charge state). In comparisons between theoretical predictions and experimental data, the adopted value of m needs to be the one applying to the energy window rather than the one representative for the overall energy spectrum of sputtered particles (Sigmund & Sckerl, 1993).

3.2.5 Summary

In an attempt to sum up a variety of theoretical predictions, it appears appropriate to follow the conventional scheme of classification into three regimes of sputtering by elastic collisions (Sigmund, 1981): the single-knockon regime, the linear-cascade regime, and the spike regime.

Several sets of experimental data sort under the heading of single-knockon regime (see below), while on the theoretical side, only Monte Carlo simulations have been performed (Eckstein & Biersack, 1985). Preferential sputtering may be caused by ion/target mass mismatch, i.e., light ions tend to cause preferential sputtering of the light component, and vice versa. At very low energies — of the order of $\sim$ 100 eV or less — surface processes of the type discussed by Winters &

Sigmund (1974) and invoked by Wehner (1977) may become important. In particular, preferential sputtering of the lighter component may be caused by direct knockon events where a light surface atom bounces off from a heavy atom in the second layer. The reverse process is impossible for kinematic reasons. Such events become exceedingly rare at keV energies (Winters & Sigmund, 1974). Moreover, recoil implantation is a very strong effect at low ion energy, in particular for heavy ions like Hg^+, and may introduce density gradients that could well account for the observed angular variations in the composition of the sputtered flux (Sigmund, 1987a).

In the linear-cascade regime, a very clear and consistent picture emerges from the work of all four groups mentioned above. For disordered media, the light species is sputtered preferentially, the deviation from stoichiometry depends insignificantly on composition and is almost independent of the angle of emission at the energies in question. It is well approximated by eq. (11), with the exponent m governed by the interaction potential. Some uncertainty prevails concerning the appropriate value of this exponent.

In arriving at this coherent picture, we have chosen to discard all claims made by Haff & Switkowski (1976), Haff (1977), Watson & Haff (1980), and Haff et al. (1981): There is a clear conflict between the first two references, and in the two latter studies, no preferentiality of the cross section was allowed for. Simulations on single crystals bombarded under channeling conditions (Shapiro et al., 1985, 1988) have also been disregarded. While such studies carry considerable intrinsic interest, the differences between the results and those for liquid targets under otherwise identical conditions (Lo et al., 1989) are very pronounced, both with regard to the magnitude of preferential sputtering and the sign of the angular variation. Although polycrystalline materials are not amorphous, there is usually a good correspondence between sputter parameters for the two groups of materials. Whether this is true for a given set of experimental data depends on the role of texture, i.e., the way how targets have been prepared.

In passing on, we recall that a minor preferential-sputtering effect is caused by the difference in surface binding energies, eq. (54).

Finally, for the spike regime, we recapitulate a result derived by Sigmund (1981)

$$\frac{Y_1}{Y_2} = \frac{N_1}{N_2}\sqrt{\frac{M_2}{M_1}}\exp\left(\frac{U_2 - U_1}{kT}\right), \tag{57}$$

where T denotes an effective spike temperature (Sigmund & Claussen, 1981), and

$$U_2 - U_1 = \frac{3}{2}\hbar(\omega_{D1} - \omega_{D2}) \tag{58}$$

in accordance with eq. (53). Eq. (57) can be said to reflect an effective m-value of

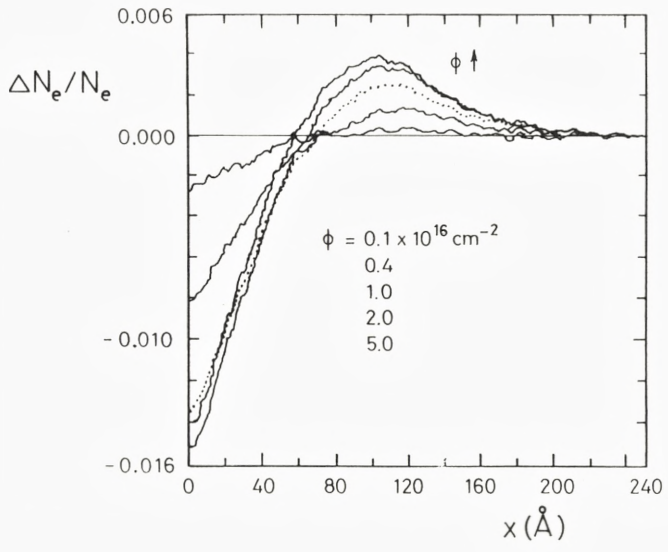

Figure 4. Calculated evolution of the concentration of a mixture of two Germanium isotopes under 5 keV argon bombardment. From Conrad & Urbassek (1992).

$m_{\text{eff}} = 0.25$ in eq. (15), but the dependence on surface binding energies is different when important.

3.3 Theoretical Estimates: Fluence Dependence and Stationary State

Theoretical results on the fluence dependence of preferential sputtering have become available recently (Jiménez-Rodríguez et al., 1992, Conrad & Urbassek, 1992). Numerical solution of eq. (29) in the limit of weak preferentiality yields predicted depth profiles of target stoichiometry *versus* ion fluence (fig. 4) as governed by collisional mixing and preferential sputtering on the basis of feasible input. In both studies it was found that the sputtered flux approaches stoichiometric composition only after an ion fluence of $\sim 10^{16}/\text{cm}^2$, i.e., after sputtering of many atomic layers. This is in accordance with experimental observations summarized below, and caused mainly by collisional mixing.

The two sets of profiles differ in the detailed behavior near the surface: The profiles calculated by Jiménez-Rodríguez et al. (1992) show a behavior that is reminiscent of segregation. This effect is caused by the flux of recoil atoms that are not energetic enough to overcome the surface barrier and hence get reflected. While

the fate of such atoms needs to be considered, it appears questionable whether the description offered by Jiménez-Rodríguez et al. is adequate (Conrad & Urbassek, 1992).

Reliable profiles should provide pertinent input for theoretical predictions of angular emission patterns as well as energy spectra of sputtered species in the stationary state.

3.4 Experiments

Existing experimental data have been determined mainly by measurement of the composition of the sputtered flux, either by deposition on a collector and subsequent analysis or by means of secondary-ion (SIMS) or sputtered-neutral mass spectroscopy (SNMS). Measurements on the target have come up recently. While the energy resolution of conventional Auger spectroscopy may be insufficient for this, the potential of ion scattering spectroscopy has been pointed out (Ackermans et al., 1990a,b). Such data may be less affected by matrix effects of the type that SIMS or SNMS data suffer from.

Targets investigated include pure metals, with the natural composition or enriched with particular isotopes, or minerals. In the latter case, we recall that theoretical predictions for binary isotopic mixtures may readily be applied to polyatomic materials.

The presence of other components in the target than the isotopes under consideration will be disregarded in the following, in accordance with the conclusions of sect. 2.2.3.

3.4.1 Analysis of Collected Material

In one class of experiments, sputtered material is collected and subsequently analyzed by mass spectrometric techniques (Fluit et al., 1961; Wehner, 1977; Olson et al., 1979; Russell et al., 1980; Weathers et al., 1993). With the exception of the latest data (Weathers et al., 1993), these measurements required generously high bombardment fluences where the sputtered-particle current approached stoichiometry. Hence, reported deviations from stoichiometric sputtering, expressed in terms of yield ratios, must be suspected to underestimate the actual (low-fluence) effect. However, deviations from stoichiometric sputtering propagate into the angular distributions with increasing fluence, and those deviations survive into the stationary state. In the absence of segregation, this allows to extract a rough estimate of sputter preferentiality even from a high-fluence experiment.

Fluit et al. (1961) reported a 1.7 % enrichment of ^{6}Li over ^{7}Li in the sputter deposit after bombardment with 5 - 20 keV Ar^+ ions, corresponding to an m-value

of 0.055 if this were a low-fluence result. Bombarding-ion fluences were not given explicitly, but it is evident that several monolayers must have been sputtered. For a light element like Li, a feasible value of m must be significantly greater than 0.11. Hence, these data do not contradict the theoretical prediction.

Wehner (1977) and Olson et al. (1979) observed very pronounced angular variations in the composition of the sputtered-particle current, up to 6 % for bombardment of Cu, Mo, W, and U with 60 - 100 eV Hg^+ ions. These variations may be caused by surface scattering events and/or recoil implantation as mentioned in sect. 3.2.5. Either explanation is consistent with the observation of much less pronounced variations (≤ 0.6 %) when the bombarding energy is raised to 300 eV. Quantitative theoretical estimates, either analytic or simulational, are missing.

Russell et al. (1980) found a 1.5 % angular variation of the isotopic ratio of ^{40}Ca over ^{44}Ca for high-energy (130 keV N^+ or 100 keV N_2^+) bombardment of Ca-containing minerals. Eq. (11) predicts an initial enrichment of 2.2 % for $m = 0.11$ or 3.3 % for $m = 1/6$. While the magnitude of the angular variation is not expected to be identical with the initial enrichment, there appears a sufficient margin to allow the conclusion that these data do not indicate more pronounced isotope effects than what can be accounted for theoretically. The same conclusion can be drawn from the fact that enrichments in the total deposit amount to up to 2 % for the lowest bombarding-ion fluences.

More recent data were reported by Weathers et al. (1993) for sputtering of Mo targets with 5 - 10 keV Ar^+ or Xe^+ ions. In the low-fluence limit, initial enrichments were large ($\sim 3 - 5\%$), corresponding to $m \sim 0.2 - 0.3$. Moreover, pronounced angular dependences were reported for part of the low-fluence data. Neither of these findings can be readily accounted for by existing theory. Since the sputtered material was analyzed by SIMS analysis of collectors, these measurements may be affected by preferential sputtering from the collector (Sigmund, 1993b). The significance of target texture has not been discussed in this context.

3.4.2 Analysis of the Secondary-Ion or Sputtered-Neutral Current

Measurements of the secondary-ion current show a pronounced isotope effect due to the dependence of the ionization probability of a sputtered particle on velocity rather than energy. Notwithstanding this, SIMS measurements may provide information on preferential sputtering if the current is measured as a function of fluence. At high fluence, the sputtered-particle current must be stoichiometric according to eq. (41). Hence, any nonstoichiometry in SIMS signals must be caused by different ionization probabilities. If the ionization probability does not change with fluence, any yield enhancement above the asymptotic value may be ascribed to preferential sputtering. While the behavior of the ionization probability was subjected to

considerable scrutiny (Baumel et al., 1988), the point is central, and objections on purely experimental grounds are hard to reject totally.

Another point to be considered is the angular window in relative measurements. The fact that concentration gradients built up at high bombardment fluences introduce an enrichment in the heavy isotope of the sputtered-particle flux at oblique angles suggests that the relative variation in the enrichment factor *versus* fluence exceeds the average at oblique ejection and should be less than average at normal ejection (Weathers, 1993; Sigmund & Sckerl, 1993). Similar effects of the energy window may exist but have not been analyzed, and complete information on experimental geometry is rarely given in experimental papers because such artefacts may not have been expected.

Shimizu and Hart (1982) found a 0.6 % initial enrichment of ^{63}Cu over ^{65}Cu during bombardment with 13.2 keV O^- ions. While they did not ascribe this effect to preferential sputtering we note that an enrichment of 0.7 % would be predicted for $m = 0.11$.

Okano et al. (1985) reported an initial enrichment of the heavier species in measurements involving a series of metallic targets bombarded with 12 keV O_2^+ ions. While these effects were assigned tentatively to recoil implantation, the measurements clearly contradict all other existing experience. An independent attempt to reproduce these results has apparently not been reported.

Gnaser and Hutcheon (1988) observed enrichments for Li, Ti, Ga, and Mo isotopes under bombardment with 14.5 keV O^- ions which, when described in terms of eq. (11), require values of $m = 0.17$, 0.38 – 0.45, 0.21, and 0.29, respectively. While the values for Li and Ga appear compatible with those characterizing feasible collision cross sections, those for Ti are outside the feasibility range. The value for Mo appears high but not excessive.

Measurements on B by Ar^+ and Ne^+ bombardment at 100 keV yielded enrichment of ^{10}B over ^{11}B by 4.6 to 5.2 % (Baumel et al., 1988), corresponding to an m-value of ~ 0.26 which is feasible for a light element.

Recent SNMS data, obtained by postionization of neutral atoms sputtered from Ge and Mo targets by 5 keV Ar^+ ions at low fluences (Gnaser & Oechsner, 1989, 1990), also showed large enrichments of the lighter isotopes (~ 5 %) corresponding to $m \sim 0.3 - 0.4$. These data are in good agreement with the collection data by Weathers et al. (1993) and in reasonable agreement with the SIMS measurements of Gnaser & Hutcheon (1988).

In a Monte Carlo simulation of preferential sputtering from a ^{70}Ge-^{76}Ge mixture, Conrad and Urbassek (1992) found that, by assuming a minor compositional gradient near the the surface, i.e., an 1.4 % increase in the ^{70}Ge concentration and a corresponding decrease in ^{76}Ge, the calculated magnitude and fluence dependence of the enrichment factor are in perfect agreement with these measurements.

Such a change in concentration, in order to be real, must be caused by equilibrium segregation. While direct evidence for the presence of segregation appears to be missing, Weathers et al. (1993) pointed out that the preferentiality in angular distributions of sputtered species, measured at low fluences, would have to have the opposite sign of what is found experimentally in Mo if segregation were the cause of discrepancy.

The above results indicate fair agreement with the linear-cascade prediction for Li, B, and Ga. The results for Mo and Ge can hardly be accounted for by this prediction alone, but a moderate spike component appears feasible for those heavy materials. According to eq. (57), evaporation from spikes predicts a more pronounced isotope effect. This could show up as a higher effective m-value. That assertion, however, does not apply to Ti which is too light to allow for a significant spike component (Sigmund, 1974; Cheng, 1990). It should be of interest to check the prevalence of this apparently most pronounced isotope effect by an independent measurement. In view of possible effects of target crystallinity, it appears to be crucial to check samples for texture in future experiments.

The present comparison between experimental findings and theoretical predictions is much more fargoing than what is currently possible in case of alloys. The reader is reminded, however, that the experimental yield ratios have not been measured directly but have been extracted from relative measurements, and thus are affected by secondary effects such as recoil implantation and alike (Sigmund, 1979; Sigmund & Sckerl, 1993).

4 Alloys

4.1 General Considerations

Eqs. (15) and (57) describe the preferential sputter behavior of a random alloy in the linear-cascade and spike regimes, respectively. In the former regime, the composition of the sputtered flux is insensitive to the bombarding-beam characteristics, i.e., the type, energy, and angle of incidence of the incoming ions. This prediction results from the assumption that cascades are fully developed and that the recoil velocity distribution within the cascades is well randomized. Measurements of 'true' preferential sputtering in alloys require quite low fluences and have been performed mainly by ions of fairly high energy (Andersen, 1984). The situation is different in the spike regime because the spike temperature depends on both beam and target parameters. Neither does eq. (15) apply to the energy range near the sputter threshold. Here the sputter preferentiality depends heavily on the type, energy, and angle of incidence of the bombarding ion (Taglauer & Heiland, 1978; Varga & Taglauer, 1981; Taglauer, 1982; Baretzky et al., 1987).

Molecular-dynamics simulations on the basis of realistic interatomic potentials provide another useful source of information on primary sputter properties. Preferential sputtering of Cu-Ni alloys was simulated by Lam & Johannessen (1992) on the basis of embedded-atom potentials given by Foiles (1985). Differential sputter parameters were calculated as functions of Ar^+ ion energy, alloy composition, and temperature. The sputtered flux was found to be slightly preferential in Cu, with a yield ratio $\sim$1.2 depending weakly on ion energy and alloy composition. From the energy spectra of sputtered atoms, effective surface binding energies of the alloy components as well as an effective value of m were extracted. Simulations aiming at the same kind of information have been performed some time ago on the basis of Monte Carlo and binary-collision codes (Rosen & Bassel, 1984; Eckstein & Biersack, 1985; Eckstein & Möller, 1985). The relative merits of different types of simulation codes have been discussed in another contribution to this volume (Robinson, 1993).

In addition to preferential sputtering, several kinetic and thermodynamic processes, including collisional mixing, radiation-enhanced diffusion, Gibbsian segregation, and radiation-induced segregation can affect the near-surface composition of a material exposed to ion beams (Andersen, 1980, 1984; Betz & Wehner, 1983; Wiedersich, 1983, 1985; Lam & Wiedersich, 1981, 1987; Lam, 1990). These secondary processes have been investigated individually, experimentally and theoretically, at various levels of sophistication, often under conditions where sputtering was not an issue. Therefore, a reasonable understanding of several component processes including their dependences on irradiation and material variables has been achieved.

Conceptually, the phenomenon of bombardment-induced compositional changes is simplest when only athermal processes, i.e. preferential sputtering and collisional mixing, are operative. Then the thickness of the resulting altered layer is approximately equal to the ion range. However, very often at least one thermally-activated process is acting. In particular Gibbsian segregation, which can be accelerated by irradiation, is capable of causing substantial changes in the near-surface composition of an alloy during ion bombardment even in the absence of competing processes. Any component that segregates to the uppermost surface layer will be preferentially removed by sputtering, simply because more of it is located within the sputter depth. Thus, 'true' preferential sputtering may be hard to distinguish experimentally from Gibbsian segregation in the low-fluence limit. Radiation-enhanced diffusion may cause the altered layer to extend considerably beyond the penetration depth of the beam at elevated temperatures. Radiation-induced segregation, which is driven by gradients in the defect concentration, tends to drive the alloy system away from thermodynamic equilibrium and may cause significant redistribution. This process is quite effective in spreading changes in the

alloy composition to large depths. It is the extension of the concentration gradient beyond the depth of origin of sputtered atoms that causes the long transients in the dependence of sputtered-flux composition on ion fluence.

We shall start by briefly characterizing pertinent individual processes. Firstly, sources and sinks will be specified, i.e., implant profiles and defect production as well as defect annihilation and entrapment. The discussion of collisional mixing will follow the conventional classification into cascade mixing and recoil implantation. Radiation-enhanced diffusion is a feeding mechanism with similar effects as cascade mixing except for the temperature dependence. Both tend to flatten concentration gradients. Gibbsian segregation acts only at the surface and thus interferes directly with preferential sputtering. Radiation-induced segregation is preferential, as is recoil implantation. The former gives rise to steep concentration gradients whereever there are persistent defect fluxes, e.g. near the bombarded surface. The latter leads to concentration changes of opposite sign at the near and far end of the damage depth. Consequently, both lead to a buildup of concentration gradients in the bulk. The relative importance of these processes depends on bombardment conditions and target parameters.

4.2 Diffusive Currents

Several of the processes to be discussed below may be characterized by diffusive currents. This section serves to compile a few relationships that are common to such processes.

Consider some transport process 'α' which contributes a term

$$\mathcal{Q}_i^{(\alpha)} = \Lambda_i^{(\alpha)} N_i(x,t) \tag{59}$$

to the primary evolution of $N_i(x,t)$ according to eq. (42), with Λ_i to be specified by some expression of the type of eq. (43). Within the assumptions underlying the diffusion approximation (34), we may write $\mathcal{Q}_i^{(\alpha)}$ in the form

$$\mathcal{Q}_i^{(\alpha)} = \frac{\partial^2}{\partial x^2}\left(D_i^{(\alpha)} N_i\right) \tag{60}$$

with

$$D_i^{(\alpha)} = \frac{1}{2}\int_{-\infty}^{\infty} dx'(x'-x)^2 \Gamma_i^{(\alpha)}(x,x') \tag{61}$$

if the drift term vanishes. Allowance has been made here for depth-dependent diffusion coefficients. Such a dependence must be expected because of the finite penetration depth of the ion beam and many associated phenomena like primary defect production and collisional mixing.

The conventional diffusion picture, which was applied here, assumes small individual step size and requires bounds in the relocation integrals to be replaced by boundary conditions on the solution of the resulting differential equation.

Insertion of (60) into eq. (42) leads to

$$\left(\frac{\partial N_i(x,t)}{\partial t}\right)^{(\alpha)} = -\frac{\partial}{\partial x} J_i^{(\alpha)} \tag{62}$$

with

$$J_i^{(\alpha)} = -\frac{\partial}{\partial x}(D_i^{(\alpha)} N_i) + N_i \sum_j \left(\frac{\partial}{\partial x}(D_j^{(\alpha)} N_j) - \left[\frac{\partial}{\partial x}(D_j^{(\alpha)} N_j)\right]_{x=0}\right). \tag{63}$$

Here the first term is a diffusion current of the common form (Manning, 1968). The second term represents a relaxation or Kirkendall current. Each current ($i = 0 \ldots n+z$) obeys certain boundary conditions that are determined by the physical situation. For example, for a nonvolatile material, $J_i^{(\alpha)}$ has to vanish at the surface for $i = 1 \ldots n$. This boundary condition implies that the second term in the brackets on the right-hand side of of eq. (63) drops out. By means of the packing condition, eq. (44), we may then write down eq. (63) in the more symmetric form

$$J_i^{(\alpha)} = \sum_j \Omega_j \left(-N_j \frac{\partial}{\partial x}\left(D_i^{(\alpha)} N_i\right) + N_i \frac{\partial}{\partial x}\left(D_j^{(\alpha)} N_j\right)\right). \tag{64}$$

4.3 Sources and Sinks

For the purpose of theoretical modelling, either numerically or analytically, several pieces of input are needed which are more or less accessible. The present discussion is very brief and schematic.

Following the classification in eq. (42) we first need the penetration profile $f_0(x)$ of the ion beam. In principle, this is an intricate functional of the inhomogeneous composition profile in a polyatomic medium. The capability to follow this profile as a function of time is one of the strength points of the Monte Carlo technique (Roush et al., 1982; Möller & Eckstein, 1984). However, unless there are excessive compositional changes with increasing fluence throughout the penetration depth it will be justified to assume a constant penetration profile, evaluated for a homogeneous medium on the basis of standard range theory or tables with proper allowance for the multicomponent character of the medium. Caution is indicated with regard to the popular use of average atomic numbers and masses to approximate the target: The parameters governing energy loss and, in particular, angular scattering do not depend linearly on Z_2 and M_2. Therefore, straight interpolation between data for elemental targets is justified only in case of similar masses and

atomic numbers. The shape of a penetration profile may often be approximated as a gaussian (Lindhard et al., 1963).

Similar considerations apply to the relocation operator L_i, in particular to the part covering deeply penetrating target atoms with high recoil energies. A recent study (Conrad & Urbassek, 1993) reports quantitative comparisons between mixing profiles evaluated on the basis of constant relocation cross sections (determined from the initial, homogeneous composition profile of the material) and cross sections that were continuously adjusted for compositional changes. Although the system (LuFe) exhibits pronouncedly nonstoichiometric behavior with regard to mixing and sputtering, calculated composition profiles were found to be insensitive to induced nonlinearities at all fluences.

Another piece of input is the rate of defect production $F_\nu(x)$ per unit depth. The spatial aspect of this quantity is closely related to the penetration profile (Winterbon et al., 1970). Most of the comments made on the latter apply correspondingly, with the exception that damage profiles are more pronouncedly nongaussian. The sharing of energy between the components of a polyatomic medium has been analyzed by the formalism describing preferential sputtering (Andersen & Sigmund, 1974). The most problematic part is the conversion between deposited energy and defect production. Conventional estimates may be based on the so-called modified Kinchin-Pease equation (Sigmund, 1969b,c), but major discrepancies are observed that depend on the material. This aspect will be touched upon in sect. 4.4.1. Providing feasible predictions in this area is one of the strengths of the molecular-dynamics technique.

Separate sections will be devoted to input on relocation cross sections and rates, i.e., operators L_i and Λ_i appearing in eq. (42).

Finally we need to specify sinks. Recombination between defects (e.g., vacancies and interstitials) is governed by the law of mass action,

$$\left(\frac{\partial N_\nu}{\partial t}\right)_{\text{loss}} = -\sum_{\mu=n+1}^{n+z} K_{\nu\mu} N_\nu N_\mu;\ \nu = n+1 \ldots n+z \tag{65}$$

where $K_{\nu\mu}$ is a matrix of recombination rate constants with vanishing diagonal elements. Conversely, fixed sinks (dislocations, voids, etc.) lead to first-order annihilation kinetics of migrating defects, i.e., loss terms of the type of

$$\left(\frac{\partial N_\nu}{\partial t}\right)_{\text{loss}} = -K_\nu N_\nu N_s;\ \nu = n+1 \ldots n+z \tag{66}$$

where K_ν is a rate constant and N_s the density of unsaturable sinks at depth x. The difference is important in the analysis of the time dependence of the approach to equilibrium.

The simple kinetic equations are valid if the mean separation between defects is larger than the mean distance between sinks. Interstitials and vacancies diffuse by random walk, the former significantly faster than the latter. Annihilation occurs instantaneously whenever the interstitial is sufficiently close to a vacancy, i.e., within the recombination volume.

The central recombination rate constant is defined by (Waite, 1957)

$$K_{\mathrm{IV}} = 4\pi r_{\mathrm{IV}}(D_{\mathrm{I}} + D_{\mathrm{V}}), \tag{67}$$

where r_{IV} is the recombination radius. Since the recombination volume is $\sim 10^2\Omega$ (Wollenberger, 1970), r_{IV} is of the order of two lattice constants. Defects that are eliminated by this reaction do not contribute to atomic diffusion. As a result, the rate of defect production used in the rate equations should correspond to the production of "free" defects that survive the recombination stage.

The loss term in eq. (66) implies that only one effective type of sink is present for each defect and that the sinks are inexhaustible and immobile. The annihilation rate constants are given by (Waite, 1957)

$$K_{\nu} = 4\pi r_{\nu} D_{\nu}, \tag{68}$$

where r_{ν} is the effective sink capture radius for a ν-type defect. The sink annihilation volume is generally $\sim 20\Omega$. Hence, r_{ν} is of the order of a lattice constant. For details, the reader is referred to Dienes & Vineyard (1957), Sharp (1969), and Lam et al. (1974).

The spatial and temporal dependence of the internal sink concentration during ion bombardment may also have to be considered. Steep gradients exist in both the defect and sink concentration distributions and the sink structure may evolve continously in the bombarded zone. To a first approximation, the spatial distribution of radiation-induced sinks may be assumed to be identical to that of the damage rate, and the peak density is allowed to build up linearly with time, reaching a saturation level depending on irradiation temperature (Lam & Leaf, 1986; Lam & Hoff, 1988).

For high concentrations, defects anneal by diffusion to extended sinks, in addition to mutual recombination and homogeneous sink annihilation, and hence the pertinent rate equations containing defect diffusion terms must be applied locally to each sink. Similarly, in the surface region, the diffusion of defects must also be taken into account explicitly. Then, the solution of these equations requires appropriate boundary conditions for the defect concentrations at the sink surface.

4.4 Collisional Mixing

4.4.1 Cascade Mixing

Moving atoms in a collision cascade do not only cause sputtering and defect production but also collisional mixing, i.e., compositional changes. The three effects are closely related but there are important quantitative differences which have been recognized only gradually. Collisional mixing can be roughly classified into recoil implantation and cascade mixing (Littmark & Hofer, 1980; Sigmund & Gras-Marti, 1981). The term 'recoil implantation' has been reserved for ion-impurity knockon events. This process is anisotropic and has a substantial preferential component because of potentially high recoil energies. Relocation by secondary and higher recoils is termed 'cascade mixing'. Although secondary recoils may have high energies and, therefore, may exhibit some anisotropy, the dominating events are low-energy recoils which are directed more or less isotropically. Theoretical aspects of collisional mixing have been reviewed by Littmark and Hofer (1984), and summaries of experimental studies on ion beam mixing are available (Matteson & Nicolet, 1983; Mayer & Lau, 1983; Averback, 1986; Cheng, 1990).

Cascade mixing has been studied as a contributing process in the generation of metastable material phases by ion bombardment (Mayer & Lau, 1983) and as a disturbing factor in sputter profiling (Andersen, 1979; Littmark & Hofer, 1980, 1984). In either case, experimental information can be drawn from measurements of the intermixing of adjacent layers of pure materials as a function of ion fluence or from the spreading of a thin marker layer in an otherwise homogeneous material. Accurate mixing rates may be determined experimentally by Rutherford backscattering analysis, provided that bombarding-beam energies are high enough to ensure penetration depths far in excess of the broadening of a marker layer. Information about mixing at lower energies needs to be drawn from sputter profiles. Because of the complexity of the phenomenon and the interference with surface and chemical effects (Fine et al., 1983; Marton et al., 1988,1989; Cheng et al., 1988; Wittmaack, 1991) that information is more indirect.

An estimate of the broadening of a marker layer may be found from eq. (19) which predicts the following mean square spreading per marker atom (Hofer & Littmark, 1979; Sigmund & Gras-Marti, 1980, 1981)

$$< \Delta x^2 >= \Delta\Phi \frac{1}{3} K_i \frac{F_D(x)}{N} \int \frac{d\epsilon}{\epsilon^2} \overline{R_i^2(\epsilon)} \tag{69}$$

at depth x for a fluence increment $\Delta\Phi$. Here, $R_i(\epsilon)$ is the range of a recoil atom of energy ϵ. This estimate ignores relaxation.

The factor $1/\epsilon^2$ in eq. (69) demonstrates that cascade mixing is heavily dominated by low-energy events. It is also seen that cascade mixing is preferential.

While the preferentiality in the energy sharing, as expressed by K_i, is weak except for pronounced mass differences, the preferentiality implicit in R_i may be substantial. In view of the dominance of small relocation distances and the proportionality with fluence, eq. (69) is equivalent with a random walk characterized by a diffusion coefficient (Andersen, 1979; Matteson et al., 1981)

$$D_i = \frac{1}{6} < r_i^2 > \nu_i, \tag{70}$$

where $< r_i^2 >$ is the variance of the individual jump distance and ν_i an effective site-exchange frequency.

Measured mixing rates tend to be greater than those predicted from eq. (69), even for generous choices of the relocation distance $R_i(\epsilon)$ which is rather uncertain at low energies (Paine & Nicolet, 1983; Paine & Averback, 1985). This underestimate appears striking when compared with the observation in damage production, where a proper modification of eq. (19) was long ago found to overestimate the observed defect production. Several studies were devoted to tracing the origin of this discrepancy. Those cases where large discrepancies were observed — an order of magnitude or more — seem to be governed by replacement chains, as well as relocations in the cooling phase of a collision spike. While the former could be readily included in eq. (69) by suitable definition of the range (Andersen, 1979), the latter are clearly excluded. Roughly spoken, processes in the cooling phase of a collision spike cause annihilation of defects but increase disorder.

Illuminating observations on the behavior of collision cascades at low recoil energy were made in molecular-dynamics simulations on metallic targets under self-bombardment. At low primary energies (< 1 keV), most displacements were found to occur through sequences of near-neighbor atom replacements which create a vacancy at the origin of the chain and deposit an interstitial at the end. Long, linear replacement chains are rare, and frequently-observed sequences are short segments along different close-packed atomic rows; many of them close upon themselves with no net defect production. As a result, the number of atoms changing sites is significantly larger than that of Frenkel pairs created in a displacement event (Gibson et al., 1961, King & Benedek, 1983; Zhu et al., 1992; Gao & Bacon, 1993).

In more energetic cascades, extensive mixing occurs as a consequence of local structural disorder. Diaz de la Rubia et al. (1987) simulated a 5 keV displacement cascade and found that mixing takes place mostly in the region of the melt and during the cooling phase. Only a small fraction of the observed mixing effect took place in the collisional phase. Furthermore, structural disorder in the cascade center has an important effect on defect generation. The majority of defects are annihilated in the core of the cascade; only those interstitials that escape this region via replacement sequences survive mutual recombination. Consequently,

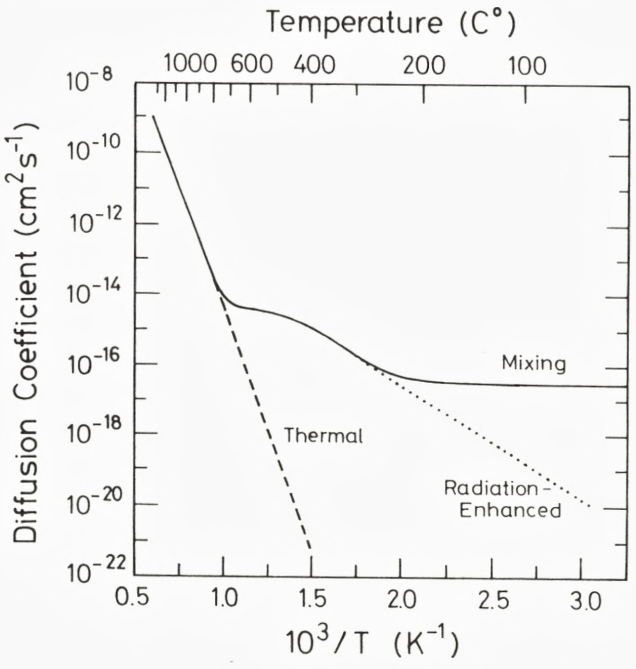

Figure 5. Temperature dependence of the steady-state diffusion coefficient calculated with physical parameters appropriate for Ni during bombardment at a typical displacement rate K = 10^{-3} dpa/s. The contributions from displacement mixing, calculated from $D = \frac{1}{6}b^2\eta K$, radiation-enhanced diffusion, determined by eq. (76), assuming a moderate sink density, and thermal diffusion, are indicated.

the defect-production efficiency is quite low, typically ≤ 0.2 (Rehn & Okamoto, 1987) relative to the modified Kinchin-Pease estimate (Sigmund, 1969b,c).

In view of this state of affairs, parameters characterizing cascade mixing in the theory of compositional changes have been chosen semi-empirically, either on the basis of measured mixing rates in the low-temperature limit (Kim et al., 1985; Averback, 1986), simulation results for the effective number of replacements per displacement (King & Benedek, 1983; Zhu et al., 1992), or measured disordering rates in ordered alloys (Kirk & Blewitt, 1982; Zee et al., 1983). Alternatively, the effect of cascade mixing on sputter parameters has been studied by sampling different mixing rates over a range of feasible values (Sigmund & Oliva, 1993).

Specific estimates reported below have been performed on the basis of a diffusion coefficient of the form $D = b^2\eta K/6$ (Lam & Wiedersich, 1981, 1987), where b is the nearest-neighbor distance, K a defect production rate [number of displacements per

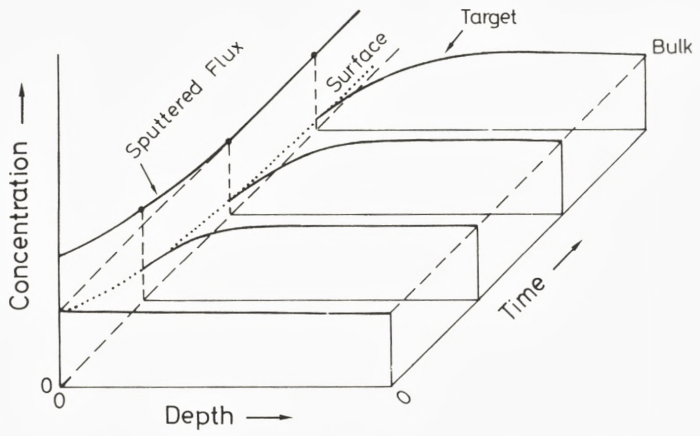

Figure 6. Schematic description of the effect of preferential sputtering on the development of the concentration profile and temporal evolution of the sputtered flux. The altered surface layer spreads into the target interior by displacement mixing and radiation-enhanced diffusion.

atom per time], and η an empirical parameter of the order of 10^2 - 10^3 representing the number of atomic replacements per displacement. By comparison with eq. (69), one notices that K must follow the depth dependence of F_D. In the presence of a significant spike component, a dependence like F_D^2 might be more appropriate (Cheng, 1990). All preferentiality has been excluded. Regardless of the specific model, cascade mixing is taken as temperature-independent.

Induced defect migration and recombination that take place during the cooling phase ($> 10^{-12}$ s) may be influenced by thermodynamic forces. Such 'quasi-thermal' diffusional processes within cascades may result in observed chemical effects in low-temperature ion-beam mixing. Thus, quantities like the heat of mixing and/or the chemical affinity can affect the intermixing rate (Cheng et al., 1984; d'Heurle et al., 1985; Averback et al., 1986; Peiner & Kopitzki, 1988; Cheng et al., 1992). Pertinent phenomenological theories have been proposed by Cheng et al. (1984), Kelly (1989a), Ma (1991), Kelly & Miotello (1991, 1992), and Koponen and Hautala (1992).

Cascade mixing is the dominant mechanism of atom transport during bombardment at low temperatures where vacancies are immobile, i.e., below $\sim 0.2\,T_m$ (T_m being the melting temperature). A typical estimate of D is given in fig. 5. This process can spread compositional changes induced in the uppermost atom layers to larger depths. Such spreading is confined to a region commensurate with the penetration depth of the ion beam.

The simultaneous effect of preferential sputtering and cascade mixing — which

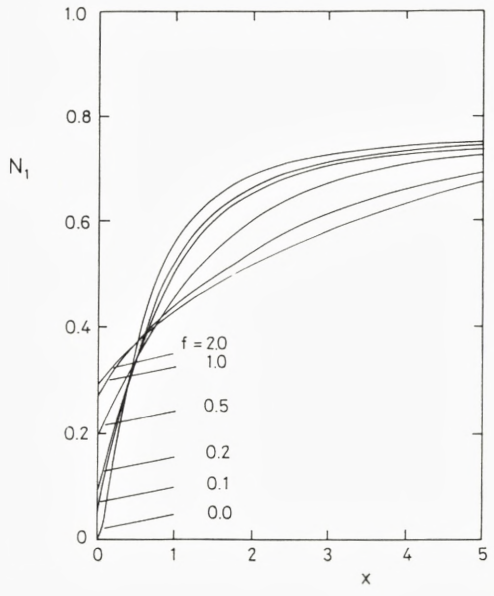

Figure 7. Calculated composition profile of a binary alloy under the action of preferential sputtering and preferential cascade mixing. The parameter f is a relative measure of the rate of cascade mixing at a fixed sputter rate. Schematic input. The length unit is the mean sputter depth. From Sigmund & Oliva (1993).

could also include the effect of radiation-enhanced diffusion to be discussed below — on the temporal evolution of the composition of the sputtered flux and the concentration profile in a binary alloy is illustrated schematically in fig. 6. The sputtered flux is initially enriched in 1-atoms. Gradually, the surface concentration decreases toward steady state, and the sputtered flux reflects the bulk composition. Under the action of displacement mixing and/or radiation-enhanced diffusion, compositional changes produced at the surface propagate into the bulk and form a relatively thick altered layer.

Fig. 7 shows steady-state profiles for different rates of atomic mixing. Here mixing is assumed preferential, in accordance with eq. (19). In this special case, the ratio of mixing rates is identical with the ratio of sputter cross sections. It is seen that the composition gradient is very steep in the absence of feeding by cascade mixing but flattens with increasing rate of mixing.

Andersen (1980, 1984) argued against cascade mixing as an effective feeding mechanism for preferential sputtering. His argument was based on the fact that both sputtering and cascade mixing are governed by eq. (19) and identical range-

energy relations. In view of the very small depth of emergence of sputtered atoms, it was thought that this could not be consistent with an altered-layer depth of the order of an ion range or more, as found experimentally. This argument ignores the magnitude of the composition gradients involved. Even if the fact that eq. (19) underestimates the mixing rate while predicting correct sputter rates is ignored, fig. 4 demonstrates that characteristic fluences may come out right if only preferential sputtering and collisional mixing are taken into account.

4.4.2 Recoil Implantation

Unlike cascade mixing, recoil implantation is by and large a single-collision phenomenon. On a relative scale, the effect tends to be particularly important at low ion energies where cross sections get large. This is particularly true at energies close to the sputter threshold where significant disordering may take place within an ordered layer that erodes only very slowly (Sigmund, 1987a). This is also the regime where 'negative recoil implantation', i.e., sputter events induced by direct ion-atom interaction, becomes significant (Winters & Sigmund, 1974; Kelly, 1978).

Recoil implantation depends significantly on ion and target masses and is thus heavily preferential. Its role in the understanding of preferential sputtering has been recognized early (Kelly & Sanders, 1976a,b; Sigmund, 1979), although achieving a unified picture has shown up to be more complex a task than anticipated originally. Roughly, the cross section for generation of a primary recoiling target atom of some given energy increases with decreasing mass/atomic number of a hit target atom; the total pathlength travelled by a target recoil of a given energy increases with decreasing mass/atomic number of that atom; the maximum energy transfer from an ion to a target atom depends on the mass mismatch; finally, the penetration depth of a light target atom in a substrate containing heavy components is substantially smaller than its pathlength because of angular scattering. All this results in a fairly complicated situation, where different computer codes simulating nominally the same physical situation were able to produce predictions of recoil implant profiles that even differed in sign (Möller & Eckstein, 1984; Roush et al., 1982, 1983; Goktepe et al., 1986). The origin of these discrepancies has been traced to angular scattering (Sigmund, 1988), but even the most recent results indicate a surprising sensitivity of predictions on recoil implantation to details of the input regarding interatomic potentials, cutoff radii, binding energies, and alike (Konoplev & Gras-Marti, 1993; Conrad & Urbassek, 1993).

Recoil implantation tends to shift the centroid of a thin, planar marker layer in the beam direction or opposite to it, depending on the mass/atomic number of marker and matrix. Motion opposite to the beam is expected when matrix atoms are implanted more efficiently than marker atoms (Andersen, 1979; Sigmund &

Gras-Marti, 1981). Matrix relocation is an effect that cannot be accounted for unless a relaxation term is included in the basic rate equation, cf. the low-fluence solution eq. (47). So far, predicted absolute marker shifts have been found to be in better agreement with theory than the broadening predicted for cascade mixing. Broadening by recoil implantation is also predicted but affects mostly the deeply penetrating tails that may be observed at low implant fluences.

The fact that recoil implantation is both anisotropic and preferential implies a depletion of the preferentially-implanted species in the surface region which may be mistaken for being caused by sputter depletion (Sigmund, 1979). This feature is well established in the related field of monolayer desorption (Winters & Taglauer, 1987). A similar degree of understanding in alloy sputtering has been halted by lacking command over the sign of recoil implantation, but the qualitative significance of the effect at not too high ion energies is unquestioned.

4.5 Processes Assisted by Defect Migration

4.5.1 General Considerations

Eq. (64) represents diffusional currents in the absence of thermodynamic forces. In order to incorporate the latter, we need to go backward for a moment and characterize diffusion currents by gradients in a chemical potential rather than composition gradients. This is necessary to properly characterize Gibbsian segregation as well as preferential coupling of certain species to certain types of defects. This section serves to provide the necessary general background. Specific migrational processes wil be discussed subsequently.

Existing notation in the field (Lam & Wiedersich, 1981) is adapted to alloys where atomic rearrangement does not cause noticeable local density changes. Therefore, atomic volumes enter mainly to straighten up dimensions, and the conserved quantity is the number of lattice sites. Presently we aim at a unified description of collisional and migrational phenomena, and the alloys considered are not generally dilute. For both reasons we shall keep to the notation adopted above, i.e., try to fulfill the requirement of volume conservation also in the description of migrational phenomena. This implies that conservation of lattice sites is not an issue. We note, however, that all existing quantitative calculations ignore the effects of different atomic volumes of the species present.

A general starting point to describe diffusional motion in the presence of forces may be taken to be Darken's equations (Shewmon, 1963; Manning, 1968)

$$J_i = -\sum_j \mathcal{M}_{ij} X_j;\ i,j = 0 \ldots n+z, \tag{71}$$

where the $X_j = -\partial\mu_j/\partial x$ are thermodynamic forces and the μ_j are chemical

potentials. The coefficients $\mathcal{M}_{ij}$ have to obey the Onsager relations

$$\mathcal{M}_{ij} = \mathcal{M}_{ji}, \tag{72}$$

and the total volume current must vanish in the absence of a change in coordinate system due to sputter erosion, i.e., $\sum_i \Omega_i J_i = 0$. For the latter to be satisfied independent of the specific chemical potential chosen, we must have

$$\sum_i \Omega_i \mathcal{M}_{ij} = 0. \tag{73}$$

This relation is fulfilled automatically if $\mathcal{M}_{ij}$ is written in the form

$$\mathcal{M}_{ij} = \mathcal{M}^*_{ij} - N_i \sum_k \Omega_k \mathcal{M}^*_{kj} \equiv \sum_k \Omega_k (N_k \mathcal{M}^*_{ij} - N_i \mathcal{M}^*_{kj}), \tag{74}$$

where the second term represents the Kirkendall current and the coefficients $\mathcal{M}^*_{ij}$ describe the 'direct' coupling between the different species. Eqs. (72,73) reduce the number of independent coefficients $\mathcal{M}_{ij}$ or $\mathcal{M}^*_{ij}$ from $(n+z+1)^2$ to $\frac{1}{2}(n+z)(n+z+1)$.

While it is conceivable to calculate *all* parameters $\mathcal{M}_{ij}$, whether independent or not, from first principles, it is more common to determine some of them by fitting experimental data. For that purpose, further reduction of the number of free parameters is desirable. A reasonable simplification is to neglect the coupling between different types of atomic species and the coupling between different types of defect, i.e.,

$$\mathcal{M}^*_{ij} = 0 \text{ for } i \neq j = 0 \ldots n \text{ and for } i \neq j = n+1 \ldots n+z. \tag{75}$$

With this, the number of free parameters reduces to $(n+1)z$. If vacancies are the only defect present, this implies that there is one independent diffusion coefficient for each atomic species. If there are two categories of defect (vacancies and interstitials), there are two independent diffusion coefficients per species, etc.

4.5.2 Radiation-Enhanced Diffusion

At sufficiently elevated temperatures, point defects become mobile. Free defects that escape homogeneous annihilation diffuse toward extended sinks such as grain boundaries and surfaces. Between ~ 0.2 and $\sim 0.6T_m$, their concentrations can exceed those present in thermodynamic equilibrium by many orders of magnitude. Therefore, diffusion is strongly enhanced by irradiation.

The simplest model for radiation-enhanced diffusion is a 3-species system consisting of one atomic species, vacancies, and interstitials. If the coupling between

vacancies and interstitials is neglected, there are only two free parameters to describe the motion of all three species, and the diffusion coefficient for atoms will be determined by the parameters governing the motion of defects, i.e.,

$$D = \frac{1}{6} b^2 Z(\nu_{\mathrm{I}} c_{\mathrm{I}} + \nu_{\mathrm{V}} c_{\mathrm{V}}), \tag{76}$$

where $c_\nu = \Omega_\nu N_\nu$, ν_ν are jump frequencies, indices $\nu = \mathrm{V}, \mathrm{I}$ refer to vacancies and interstitials, respectively, and b is the nearest-neighbor distance. Moreover,

$$\nu_\nu = \nu_\nu^0 \exp\left(-H_\nu^m / kT\right), \ \nu = \mathrm{V}, \mathrm{I} \tag{77}$$

where ν_ν^0 is the attempt frequency and H_ν^m the defect migration enthalpy.

In early theoretical studies of radiation effects (Lomer, 1954; Dienes & Damask, 1958; Damask & Dienes, 1963; Sharp, 1969; Wiedersich, 1972), defect concentrations were calculated under the assumption that defect diffusion to extended sinks was negligible and, hence, that defect distributions were uniform throughout the irradiated solid. In subsequent work (Foreman, 1972; Rothman et al., 1973; Lam et al., 1974; Seeger, 1975), defect flow to a surface was included. Steady-state defect diffusion profiles in a semi-infinite solid can be estimated analytically (Lam et al., 1974; Seeger, 1975).

A typical temperature dependence of D for radiation-enhanced diffusion is included in fig. 5. In the absence of defect sinks or in the lower end of the pertinent temperature range, the concentrations of excess point defects are mainly limited by mutual recombination. Then the diffusion coefficient is proportional to the square root of the ion current J_0, and the slope of the Arrhenius plot corresponds to $H_{\mathrm{V}}^m/2$. Annihilation of defects at sinks gains importance at higher temperatures, and D becomes temperature independent and directly proportional to J_0. The characteristics of radiation-enhanced diffusion have been summarized by Adda et al. (1975), Lam & Rothman (1976), Sizmann (1978), and Rothman (1983).

Diffusion in a binary alloy is characterized by a minimum of four independent parameters. As a matter of convention, the preferential part of radiation-enhanced diffusion will be treated separately under the heading of radiation-induced segregation, and the parameters entering eq. (76) will be taken to be suitable averages.

At higher temperatures, above $\sim 0.6\, T_m$, the equilibrium concentration of thermal vacancies is larger than that of radiation-induced defects, and consequently, thermal diffusion is dominant. The contribution from interstitials to the diffusion coefficient according to eq. (76) can be ignored, and c_{V} becomes the equilibrium concentration of vacancies.

Eq. (76) only provides a simple account of radiation-enhanced self-diffusion within the 'Lomer' model. In real alloy systems, the diffusion kinetics can be influenced by many factors (Sizmann, 1978; Rothman, 1983; Wollenberger, 1987), including defect aggregation, defect-impurity binding, defect concentration gradients,

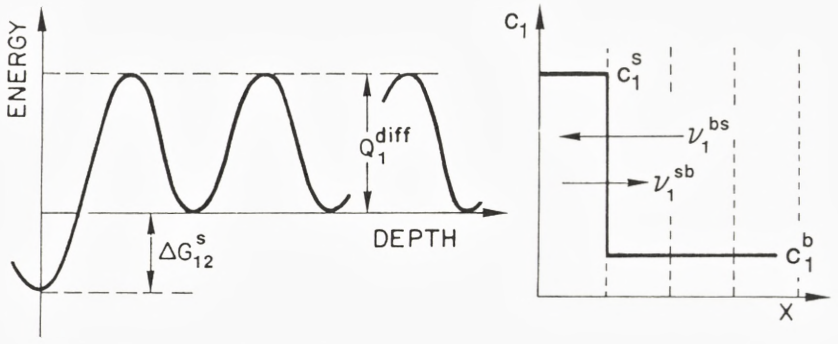

Figure 8. Schematic description of the energetics of Gibbsian segregation and its effect on near-surface concentration of 1-atoms. Pertinent jump frequencies are indicated.

and chemical effects like atomic ordering and clustering, heat of mixing, mutual solid solubility, and precipitation. The contribution of, e.g., mobile vacancy clusters to radiation-enhanced diffusion can destroy the symmetry between interstitial and vacancy, and affect the simple time and temperature dependence of D (Lam, 1975). The presence of an impurity atom changes the defect mobility in its proximity to an extent which depends on the strength of the defect-impurity interaction and the geometry of the lattice (Manning, 1968; Robrock, 1983). Strong defect-solute binding is also the physical origin of impurity segregation. A comprehensive treatment of atomic diffusion in defect gradients was given by Manning (1968, 1981). The defect concentration gradients provide additional driving forces for diffusion which must be included in eq. (71). In addition, the effects of limited mutual solubility or immiscibility should be accounted for in the analysis of the temperature dependence of intermixing and radiation-enhanced diffusion (Averback, 1986; Rehn & Lam, 1987; Marton et al. 1988). Atomic clustering and precipitation create compositional inhomogeneitites and interfaces which, if incoherent in nature, can serve as extended sinks for points defects.

The development of compositional profiles as a result of preferential sputtering and radiation-enhanced diffusion has been treated theoretically by Pickering (1976), Ho (1978), and Collins (1978). The qualitative behavior is very similar to what was shown for cascade mixing in fig. 6.

4.5.3 Gibbsian Segregation

Gibbsian segregation tends to modify concentrations of alloy components at surfaces and interfaces such as to minimize the surface free energy. As a rough rule, it

is the weakly-bound species that segregate, and those also tend to sputter preferentially. Thus, the effects of sputtering and segregation most often go into opposite directions. It is important, therefore, to study the interplay of the two effects.

In a very simple layer model, the equilibrium configuration in the absence of bombardment can be characterized by atom fractions c_i^{b} in the bulk and c_i^{s} in the top surface layer so that (Wynblatt & Ku, 1979; Hofmann, 1990; du Plessis, 1990)

$$\frac{c_i^{\mathrm{s}}}{c_j^{\mathrm{s}}} = \frac{c_i^{\mathrm{b}}}{c_j^{\mathrm{b}}} \exp\left(-\frac{\Delta G_{ij}^{\mathrm{s}}}{kT}\right), \tag{78}$$

where $\Delta G_{ij}^{\mathrm{s}}$ is a segregation free energy (fig. 8).

For the purpose of studying compositional changes under ion bombardment, a model is needed that describes the kinetics of Gibbsian segregation. This is by itself a topic under active investigation (Hofmann, 1990; du Plessis, 1990). A few ad hoc models have been designed for use in sputtering studies, all of which may appear somewhat schematic.

Lam & Wiedersich (1981) used the following ansatz to characterize the net current of 1-atoms from the bulk to the surface in a binary alloy,

$$\frac{\Omega}{\zeta} J_1 = \nu_1^{\mathrm{bs}} c_1^{\mathrm{b}} c_2^{s} - \nu_1^{\mathrm{sb}} c_1^{s} c_2^{\mathrm{b}} , \tag{79}$$

where Ω and ζ are an effective atomic volume and atomic layer thickness, respectively, and ν_1^{bs} and ν_1^{sb} are the jump frequencies of 1-atoms from the bulk into the surface layer and vice versa (fig. 8). With this, equilibrium is achieved in accordance with eq. (78) if the jump frequencies are defined in accordance with the relation

$$\nu_1^{\mathrm{sb}} = \nu_1^{\mathrm{bs}} \exp\left(\frac{\Delta G_{12}^{\mathrm{s}}}{kT}\right) \tag{80}$$

for a binary system. Eq. (79) — which has been generalized to ternary alloys (Yacout et al., 1989) — hinges on a well-defined separation of the material into a surface layer and the bulk. This is consistent with a model of a solid composed of discrete atom layers, and it provokes the occurrence of the parameter ζ which would otherwise not be needed.

Products of atom fractions appear in eq. (79) since the probability for, e.g., a 1-atom from the bulk to replace a 2-atom in the surface layer depends on both the bulk concentration of 1-atoms and the surface concentration of 2-atoms.

The key parameter determining the segregation rate is the jump frequency ν_1^{bs}. It depends on the bulk concentrations and jump frequencies of defects. Therefore, Gibbsian segregation can be strongly enhanced by irradiation in the temperature regime where point defects are mobile.

At low irradiation temperatures where thermally-activated diffusion processes are insignificant, atomic motion occurring within displacement cascades may also contribute to Gibbsian segregation (Andersen et al., 1982, 1983; Li et al., 1982, 1983). This process, which will be called 'bombardment-enhanced Gibbsian segregation', may be taken into account by inclusion of a temperature-independent term representing the mixing-induced jump frequency (of the order of ηK) on the right-hand side of eq. (80).

Alternative schemes have been proposed. Swartzfager et al. (1981) and du Plessis et al. (1989a,b) used standard theory of diffusion in a force field where the diffusion current is given by

$$J_i = -\mathcal{M}_i N_i \frac{\partial \mu_i}{\partial x}, \tag{81}$$

with mobilities $\mathcal{M}_i$ and chemical potentials μ_i. Numerical calculations were carried out in layer models similar to the one used by Lam & Wiedersich (1981). Sigmund & Oliva (1993) applied an *ansatz*

$$(J_i)_{\text{unrelaxed}} = -\frac{\partial}{\partial x}\left[N_i D_i(x)\right], \tag{82}$$

with

$$D_i(x) = \tilde{D}_i \exp\left(\frac{V_i(x)}{kT}\right). \tag{83}$$

This provides both an ordinary diffusion term and a segregation term of the type of eq. (81), governed by some segregation potential $V_i(x)$.

The latter three models are not bound to a layer model of the solid and can be incorporated into a more comprehensive description by adoption of an appropriate segregation potential.

However, relaxation effects need to be accounted for. In eq. (79), atom jumps come in pairs. Therefore, within the assumption of a species-independent atomic volume, target stability will not be affected by segregation currents. Conversely, eq. (82) was employed in connection with eq. (29) which incorporates relaxation.

A distribution of jump distances, and consequently a more flexible segregation model, can be accounted for by adoption of a suitable transport kernel $\Gamma_i(x, x')$ in eqs. (42,43) such as

$$\Gamma_i(x, x') = \exp\left(\frac{V_i(x)}{kT}\right) \Gamma_i(|x' - x|) \tag{84}$$

which induces segregation solely via a position-dependent jump frequency. The same is true, mutatis mutandis, for eq. (80). In conjunction with the diffusion

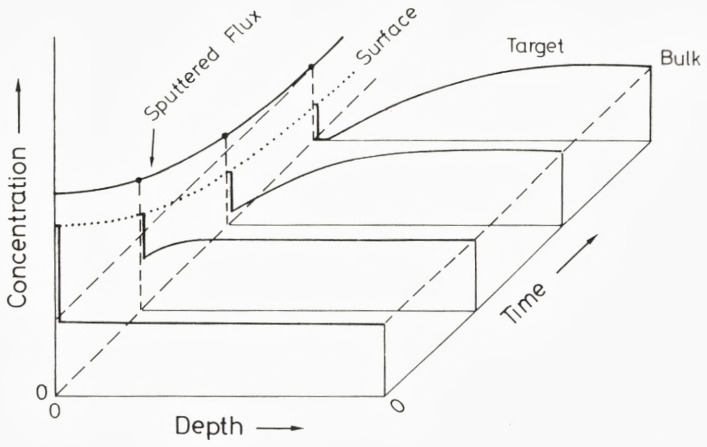

Figure 9. Schematic representation of the simultaneous effects of Gibbsian segregation and preferential sputtering on the development of the concentration profile and the time evolution of the composition of the sputtered flux.

approximation (60), eq. (84) leads to a segregation current of the form (82) with

$$\tilde{D}_i = \frac{1}{2} \int dx'(x' - x)^2 \Gamma_i(|x' - x|). \tag{85}$$

This current needs to be corrected for relaxation by means of eq. (29). As a result, one finds

$$J_i = \sum_j \Omega_j N_i N_j \left(\frac{\partial D_j}{\partial x} - \frac{\partial D_i}{\partial x} \right) + \sum_j \Omega_j \left(N_i D_j \frac{\partial N_j}{\partial x} - N_j D_i \frac{\partial N_i}{\partial x} \right), \tag{86}$$

where

$$D_i = \tilde{D}_i \exp\left(\frac{V_i(x)}{kT} \right) \tag{87}$$

Here, the first term on the right-hand side is the segregation current which is a generalized form of eq. (79). The second term is governed by concentration gradients. It is nonvanishing even in the absence of a segregation potential, as follows already from the *ansatz* eq. (82). This term could be included in the ordinary diffusion current.

The interplay of Gibbsian segregation and preferential sputtering in affecting the concentration profiles in a binary alloy and the sputtered-atom flux is shown schematically, based on the two-layer description eq. (79), in fig. 9. Here it is assumed that 1-atoms are sputtered preferentially and that all sputtered atoms

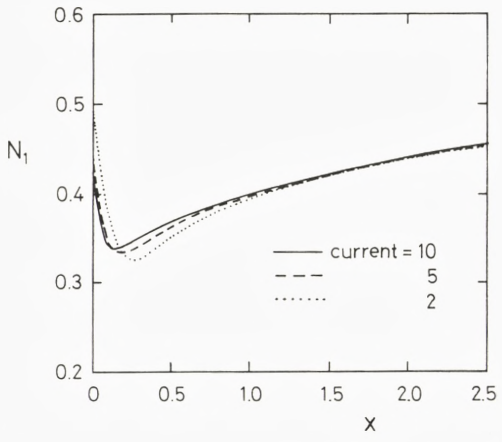

Figure 10. Stationary depth profile illustrating segregation due to preferential sputtering and Gibbsian segregation of component 1. Schematic input. The length unit is the average sputter depth. From Sigmund & Oliva (1993).

originate from the outermost atom layer. Furthermore, in the presence of Gibbsian segregation, the starting concentration of 1-atoms in the surface layer is larger than its bulk value, $c_1^{(1)} > c_1^{\mathrm{b}}$. This initial condition gives rise to initially-enhanced preferential sputtering of 1-atoms. With increasing fluence, the sputtered flux and the concentration profiles approach their steady-state values.

Fig. 10 shows stationary composition profiles under the influence of preferential sputtering and Gibbsian segregation, calculated in the continuum model based on eq. (82). This graph illustrates how the effect of segregation decreases with increasing ion current density.

Figs. 9 and 10 both demonstrate that the deviation of the surface composition from the equilibrium value, caused by preferential loss of 1-atoms, results in a reduction in the concentration of these atoms in subsurface layers as the alloy system attempts to approach equilibrium. At elevated temperatures, the steady-state subsurface depletion of the surface-segregating component can be quite severe. An example is given in fig. 11 for a Pd-20 at % Au alloy bombarded by 2 keV Ne^+ ions at several temperatures (Swartzfager et al., 1981). A gold spike is formed at the surface as a result of Gibbsian segregation, and the near-surface depleted layer extends deeper into the sample interior with increasing temperature.

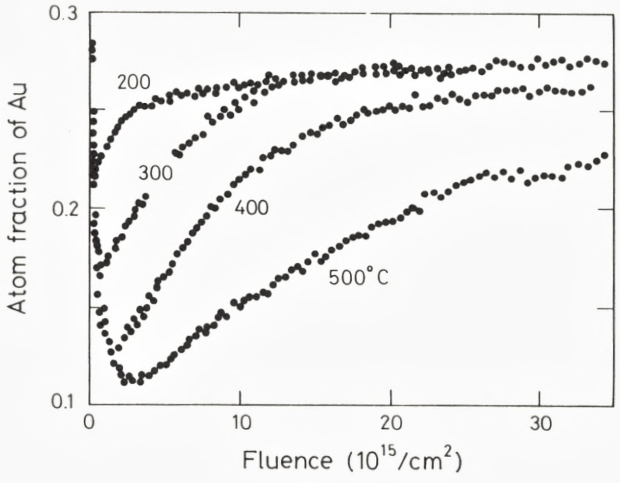

Figure 11. Depth profiles of altered layers produced in a Pd-20 at % Au alloy by sputtering with 2 keV Ne^+ at various temperatures. The bulk concentration of Au is seen to be larger than 20 at % because of preferential sputtering of Pd during the ion scattering analysis. From Swartzfager et al. (1981).

4.5.4 Radiation-induced Segregation

Among the processes that alter the stability of alloy phases during irradiation, radiation-induced segregation was found to have the most profound effect. In contrast to radiation-enhanced diffusion, which accelerates the approach to thermodynamic equilibrium, radiation-induced segregation tends to destabilize and to produce concentration gradients. This process results from two combined effects: persistent defect fluxes into or out of certain spatial regions and a preferential coupling between particular alloy components and these fluxes (Johnson & Lam, 1976; Wiedersich et al., 1979; Wiedersich & Lam, 1983; Martin et al., 1983).

Elimination of point defects at extended sinks such as grain boundaries and free surfaces is a common cause of persistent defect fluxes. Spatial nonuniformity in the defect production is another one that is particularly important in ion bombardment. Since the defect flow is always associated with fluxes of atoms, any preferential association of defects with a particular alloy component, and/or preferential participation of a component in defect diffusion will couple a net flux of the alloying element to the defect fluxes. If the defect fluxes persist in time, then this preferential defect-solute coupling leads to changing composition profiles within an initially uniform alloy phase. Theoretical descriptions of radiation-induced segregation in dilute alloys (Johnson & Lam, 1976, 1978), concentrated binary (Wiedersich

et al, 1979; Wiedersich & Lam, 1983) and ternary (Lam et al., 1982) alloys are available as well as summaries of experimental observations (Okamoto & Rehn, 1979; Rehn, 1982; Rehn & Okamoto; 1983; Ardell & Janghorban, 1983). A generalized treatment of the phenomenon in multicomponent systems was proposed by Chen (1983).

A simple formalism for non-dilute alloys was developed by Wiedersich et al. (1979). Following eq. (71), total defect fluxes consist of partial fluxes that occur by exchange with different alloy components, and similarly the total atom fluxes can be partitioned into those taking place via vacancies and interstitials. In their notation,

$$J_{\mathrm{V}} = \alpha N_{\mathrm{V}} \sum_{j=1}^{n} \mathcal{M}_{j\mathrm{V}} \frac{\partial N_j}{\partial x} - D_{\mathrm{V}} \frac{\partial N_{\mathrm{V}}}{\partial x} , \tag{88}$$

$$J_{\mathrm{I}} = -\alpha N_{\mathrm{I}} \sum_{j=1}^{n} \mathcal{M}_{j\mathrm{I}} \frac{\partial N_j}{\partial x} - D_{\mathrm{I}} \frac{\partial N_{\mathrm{I}}}{\partial x} , \tag{89}$$

$$J_i = -N_i \mathcal{M}_{i\mathrm{I}} \frac{\partial N_{\mathrm{I}}}{\partial x} + N_i \mathcal{M}_{i\mathrm{V}} \frac{\partial N_{\mathrm{V}}}{\partial x} - \alpha D_i \frac{\partial N_i}{\partial x}, \; i = 1 \ldots n, \tag{90}$$

where α is a thermodynamic factor which differs from unity for a non-ideal alloy, and $\mathcal{M}_{i\mathrm{I}}$ and $\mathcal{M}_{i\mathrm{V}}$ are diffusive coupling coefficients introduced above, satisfying Onsager's relations (72). Defect fluxes are thus driven by gradients in atom and defect concentration, and atom fluxes are induced by the gradients in defect concentration and chemical potential. The sums on the right-hand side of eqs. (88) and (89) represent the Kirkendall currents from vacancy and interstitial diffusion in accordance with eq. (74). They have opposite signs because the vacancy flux generates a flux of atoms in the opposite direction.

Eqs. (88 - 90) allow predictions of trends in segregation in a quasi-steady state. Since attainable defect concentrations are lower than concentrations of component atoms by many orders of magnitude, diffusion coefficients of alloying elements are significantly smaller than those of defects. Hence, the defect profile reaches a quasi-steady state much more quickly during irradiation than the composition profile of the alloy components. Under this condition (i.e., $J_{\mathrm{V}} = J_{\mathrm{I}}$), the following expression can be derived for the total flux of 1-atoms in a binary alloy (Wiedersich & Lam, 1983)

$$J_1 = -D' \frac{\partial}{\partial x} N_1 - D^* \left(\frac{\mathcal{M}_{1\mathrm{I}}}{\mathcal{M}_{2\mathrm{I}}} - \frac{\mathcal{M}_{1\mathrm{V}}}{\mathcal{M}_{2\mathrm{V}}} \right) \frac{\partial}{\partial x} N_{\mathrm{I}} , \tag{91}$$

with

$$D' = \frac{\mathcal{M}_{1\mathrm{V}} N_1 D_2 + \mathcal{M}_{2\mathrm{V}} N_2 D_1}{\mathcal{M}_{1\mathrm{V}} N_1 + \mathcal{M}_{2\mathrm{V}} N_2} \tag{92}$$

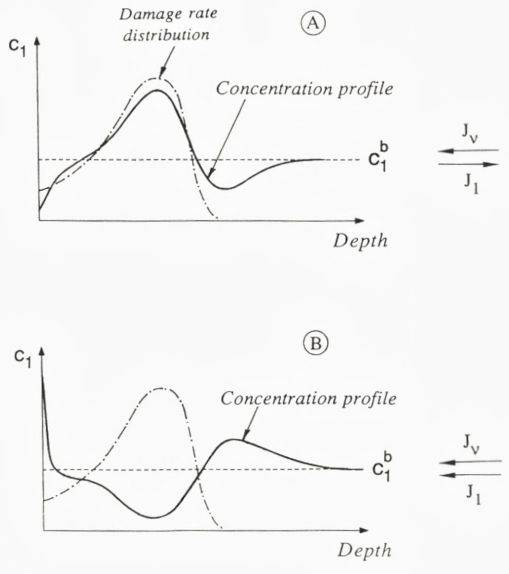

Figure 12. Schematic description of the solute concentration profile resulting from radiation-induced segregation via vacancy (A) and interstitialcy (B) mechanisms during ion bombardment.

$$D^* = \frac{\mathcal{M}_{2V}\mathcal{M}_{2I}N_1D_2}{\mathcal{M}_{1V}N_1 + \mathcal{M}_{2V}N_2} . \tag{93}$$

At low fluence, $\partial N_1/\partial x$ in an initially homogeneous alloy is small; therefore, the direction and magnitude of J_1 are controlled by the last terms in eq. (91). If $\mathcal{M}_{1I}/\mathcal{M}_{2I} > \mathcal{M}_{1V}/\mathcal{M}_{2V}$ or $\nu_{1I}/\nu_{2I} > \nu_{1V}/\nu_{2V}$, the flux of 1-atoms will be in the same direction as the defect fluxes, and the 1-component will be enriched in any region where there exists an influx of defects. Conversely, if $\nu_{1I}/\nu_{2I} < \nu_{1V}/\nu_{2V}$, the net 1-atom flux will go opposite to the defect fluxes, and the 1-component will be depleted at defect sinks. The current J_1 has its maximum when 1-atoms migrate exclusively via an interstitial mechanism and 2-atoms via vacancies.

The shapes of the solute concentration profiles that develop during ion bombardment at elevated temperature are more complex because of additional effects of defect flows from the peak-damage region (Lam et al., 1978a; Marwick et al., 1979). This is shown schematically in fig. 12. For segregation via vacancy diffusion, solute enrichment in the peak-damage region is observed at the expense of solute depletion on both sides of the peak, in addition to strong solute depletion near the bombarded surface. The opposite effect will be measured for segregation via interstitialcy diffusion. Furthermore, if vacancies interact strongly with a particular alloy component, forming tightly-bound but mobile atom-vacancy complexes, atom

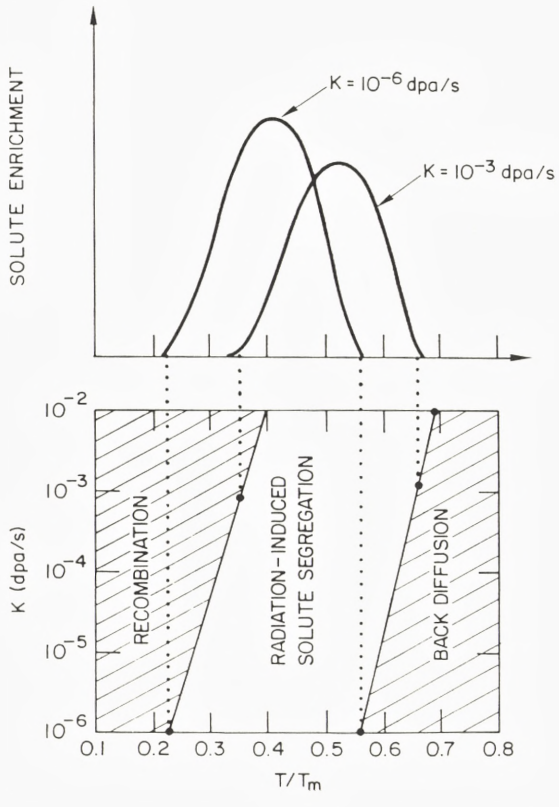

Figure 13. Schematic representation of the damage-rate and temperature dependence of radiation-induced segregation.

and defect fluxes will go in the same direction (Lam et al., 1978b; Gupta & Lam, 1979). As enrichment or depletion of the 1-component occurs, a concentration gradient will be set up which will oppose further influx of 1-atoms. Eventually, a steady-state composition profile will be reached.

At a given displacement rate, radiation-induced segregation is significant only at intermediate temperatures where sink annihilation dominates. This is shown schematically in fig. 13. At lower temperatures, high concentration and low mobility of point defects favor mutual recombination, suppressing long-range migration. Segregation is then unimportant. At high temperatures, on the other hand, concentrations and mobilities of thermal vacancies are high and effective solute back-diffusion prevents the buildup of concentration gradients. Therefore, radiation-induced segregation is small again.

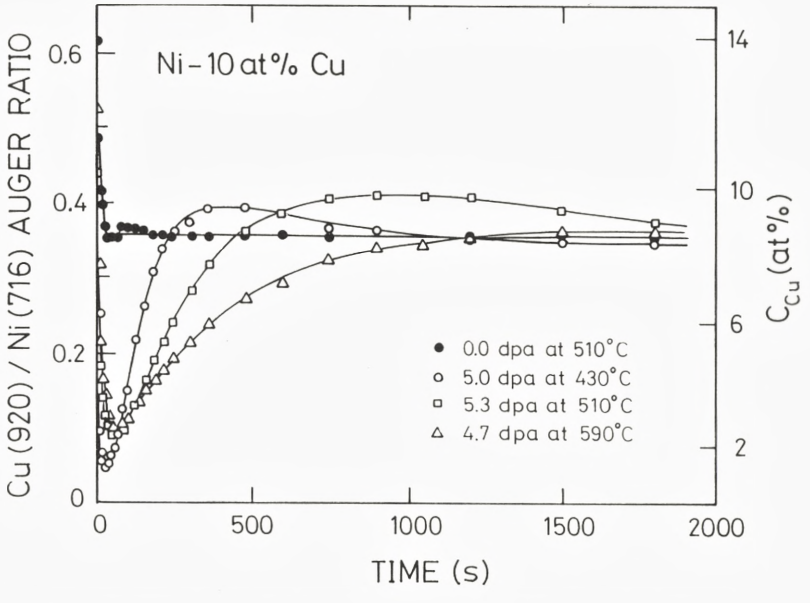

Figure 14. Depth profiles of the Cu concentration in a Ni-10 at % Cu alloy bombarded with 3 MeV Ni^+ ions to a dose of ~5 dpa at various temperatures, along with the depth profile of an unirradiated control specimen. Since Auger electrons of the transitions used for the analysis have a mean escape depth of ~1.5 nm, the compositions indicated on the right-hand ordinate represent an average over several atom layers. Consequently, a steady-state Auger ratio representing ~8.5 at % Cu was obtained for the bulk concentration in a Ni-10 at % Cu alloy. From Wagner et al. (1983).

Radiation-induced segregation and Gibbsian segregation may or may not occur in the same direction, depending on the alloy. In Ni-Si alloys, Si enrichment at the surface can result from either Gibbsian segregation (Lam & Hoff, 1988) or radiation-induced segregation (Lam et al., 1978a; Piller & Marwick, 1978; Wagner et al., 1982; Rehn, 1982; Rehn & Okamoto, 1983), whereas in Ni-Cu alloys, Gibbsian segregation gives rise to Cu enrichment at the surface (Brongersma et al., 1978; Ng et al., 1979, Lam et al., 1985b; Rehn et al., 1986), but radiation-induced segregation causes surface and subsurface Cu depletion (Wagner et al., 1983). Measurements of Cu profiles in a Ni-10 at % Cu alloy are shown in fig. 14. Upon heating of the alloy to an elevated temperature prior to irradiation, a thin Cu-rich layer was produced at the surface. Conversely, bombardment of the alloy by 3 MeV Ni^+ ions at the same temperature resulted in a severe Cu depletion. In general, the thickness of the layer affected by radiation-induced segregation is

considerably (possibly orders of magnitude) larger than the layer affected by Gibbsian segregation. Moreover, radiation-induced segregation can be more effective than radiation-enhanced diffusion in altering the alloy composition at large depths during sputtering (Rehn et al., 1985).

4.6 Sputter Depth

Pronounced changes of the alloy composition in the near-surface region can affect the differential properties of alloy sputtering. Hence we need to have an idea about the depth of origin of sputtered atoms, or sputter depth, which received considerable attention some time ago. The quantity is of special interest in connection with the depth resolution of sputter-based surface-sensitive analytical techniques.

The sputter depth x_i of an i-atom needs to be distinguished from the saturation depth which is a minimum target thickness for which the sputter yield attains its infinite-thickness value, i.e., the depth in which those collision events take place which eventually may lead to sputtering (Sigmund 1969a). While x_i should depend mainly on target parameters, the saturation depth depends also on bombarding conditions and is in general a sizable fraction of the penetration depth of the beam. Failure to recognize this difference resulted in excessively large estimates of x_i given in the older literature (Onderdelinden, 1968).

Most theoretical estimates of x_i refer to elemental targets while experiments aiming at x_i were all performed on multicomponent systems.

The fact that the energy spectrum of sputtered atoms exhibits a maximum at energies of a few eV ($\sim 0.5U_i$) implies that most sputtered atoms originate from a rather shallow depth. Conversely, there is no doubt that some fraction of the emitted atoms making up the high-energy tail must come from great depths. Fig. 3 indicates an approximately exponential decay of the sputter cross section with increasing depth. Hence, for a homogeneous target, x_i is close to the decay length characterizing the sputter cross section, cf. eq. (5). This suggests that

$$x_i \simeq U_i^{2m}/A_i \sim (1-m)\frac{U_i^{2m}}{\sum_j N_j C_{ij} \gamma_{ij}^{1-m}}, \tag{94}$$

which implies x_i to be preferential. For elemental copper, the magnitude of the sputter depth was given as 4.8 Å (Sigmund, 1969a) for $m = 0$. The exponential decay of the sputter cross section was found later (Falcone & Sigmund, 1981).

While the above value of the sputter depth was smaller than any available estimate in the literature at the time it was published, subsequent work showed that it was about a factor of two too large. Information was drawn from binary collision (Robinson, 1983; Rosen et al., 1983; Rosen & Bassel, 1984) and molecular-dynamics (Harrison, 1983; Shapiro et al., 1985) simulations which all indicated that

a very large fraction of sputtered atoms originate in the topmost two monolayers. The main reason for this difference was found much later to lie in an underestimate of the Born-Mayer scattering cross section at low energies (Vicanek et al., 1989).

Kelly & Oliva (1986a) extracted a value of the mean sputter depth of 0.8 ± 0.1 atom layers by inspection of published experimental and simulation data on a variety of materials. In response to this astonishingly small error margin, major differences were pointed out between the predictions of various simulation codes regarding the sputter depth, some of which predicted values that considerably exceeded the analytic estimate (Sigmund, 1987b). A round-robin computer simulation of a specific ejection probability was undertaken for the purpose of a direct comparison between the predictions of different codes (Sigmund et al., 1989). Six molecular-dynamics codes, four binary-collision lattice simulation codes, and eight Monte Carlo codes were applied to simulate the ejection of a low-energy Cu recoil ($5 \leq E \leq 50$ eV) from a certain depth interval ($0 \leq x \leq 5$ nm) within a Cu target. After elimination of obvious errors in some of the codes, substantial differences remained which were due first of all to different assumptions on surface binding and the statistics of free-flight paths, and secondly to sources of discrepancy like different assumptions concerning interaction potentials, cutoff radii, and electronic stopping. All molecular-dynamics and binary-collision simulations indicated that, for an intact crystalline Cu target, atoms with an initial energy up to 50 eV are sputtered largely from the outermost two layers. Monte Carlo simulations showed deeper tails.

Measurements were performed on a number of alloys. Dumke et al. (1983) reported 85 % and 70 % of the sputtered species as originating from the first atom layer during 15 keV and 25 keV Ar^+ bombardment, respectively, of a liquid Ga-In eutectic alloy. This sensitivity of the sputter fraction to the ion energy was unexpected. Repeating this experiment over a wider energy range (25 - 250 keV), Hubbard et al. (1989a,b) found ~87 % of the sputtered-atom flux to originate in the first layer, independent of the projectile energy within the range indicated. At 3 keV, the fraction was observed to increase to 94 %. This is expected to occur at low penetration depths of the ion beam (Harrison, 1983; Robinson, 1983; Biersack, 1987; Yamamura & Muraoka, 1989; Lam & Johannessen, 1992).

Less direct evidence was drawn from the temperature dependence of the surface composition of alloys in the steady state. ~65 % of the sputtered atoms were reported to originate from the outermost layer in 3 keV Ne^+ bombarded Ni-Cu (Lam et al. 1985b), ~50-65 % in Ni-Au (Lam et al. 1985a), ~55 % in Ni-Ge (Hoff and Lam 1988), ~70 % in Ni-Pd (Tang and Lam 1989), and ~95-100 % in Ni-Si alloys (Lam and Hoff 1988).

Measurements of Burnett et al. (1988) indicated that ~66 % of the sputtered-atom flux stems from the first layer in the Cu-Ru system. In addition, experimental

observations of sputtering from overlayered targets, including C/Ni (Morita et al., 1983, 1984), Li/Cu (Krauss et al., 1984a), and O/Ti (Pellin et al., 1985), all suggested that the majority of sputtered atoms originated from the outermost atomic layer.

No information has been deduced from existing experimental data on the preferentiality of the sputter depth.

4.7 Angular Distributions of Sputtered Atoms

Compositional gradients within the depth of origin of sputtered atoms affect the angular distributions of the individual sputtered species (Sigmund et al., 1982). As a rough rule, the emission pattern narrows for those species for which a relatively large fraction of sputtered particles originates from greater depth. This implies that in a binary alloy, the species that is enriched at the surface will have a flatter angular distribution than the depleted one. The situation is more complex when composition profiles are governed by both sputtering and segregation, acting on similar length scales.

An angular variation of the composition of the sputtered flux was first observed by Olson et al. (1977, 1979). They found that sputtering of Ag-Au, Cu-Ni, and Fe-Ni alloy targets by Hg^+ or Ar^+ ions at energies below 300 eV caused the lighter elements to be preferentially ejected in the direction normal to the surface. These authors suggested that sputtering of surface atoms bouncing back from subsurface atoms played a role in this phenomenon. It is well established that such events are significant in monolayer desorption studies at low beam energies (Winters & Sigmund, 1974). With increasing ion energy, the observed enrichment decreased rapidly. At 1 keV, preferential ejection of Au from Ag-Au and Ni from both Cu-Ni and Fe-Ni alloys along the surface normal was observed. The observed behavior of the angular distribution is readily understood on the basis of steep compositional gradients at the surface. In fact, Ag, Cu and Fe are known to be enriched at the surface of these respective alloys by Gibbsian segregation (Mazurowski & Dowben, 1990).

Similar effects were reported for Cu-Pt alloys under Ar^+ bombardment by Andersen et al. (1982). At ion energies above 20 keV, they found preferential ejection of Pt in the forward direction, and they interpreted this in terms of surface-directed segregation of Cu. The effect was independent of temperature over the range from -196 to 300 C. Above 300 C, the composition of the sputtered flux was significantly enriched in Cu and independent of emission angle. These measurements were performed before a steady state had been attained. The time to reach steady state is longer at high temperatures (Andersen et al., 1984a). In other experiments carried out on AgAu, Cu_3Au, Ni_5Pd, and NiPt, the weaker-bound

component was found to segregate to the surface even at 77 K (Andersen et al., 1983).

The effect of segregation on angular distributions of atoms sputtered from Cu-Ni, Co-Ni and Fe-Ni alloys under 3-keV Ar^+ bombardment at room temperature and 300 C was investigated by Ichimura et al. (1984). Preferential ejection of Ni in near-normal directions was observed during sputtering of Cu-Ni alloys at both temperatures. In Co-Ni alloys, Co atoms were ejected preferentially in the forward direction only at 300 C. For Fe-Ni, no difference in the angular distributions of the two components was discerned. The latter result differs from the behavior at lower energies observed by Olson et al. (1979).

Kang et al. (1983) measured angular distributions of Au and Cu sputtered from a Au-Cu alloy under 3 keV Ar^+ bombardment at room temperature. They found practically no difference in these distributions, although their ISS measurements (Kang et al., 1982) revealed that ion bombardment caused a strong Au enrichment in the outermost atom layer and depletion in the subsurface region. Gold segregates at the surface of Au-Cu alloys (Wynblatt & Ku, 1979; Li, 1988). An attempt to check the reproducibility of this result has not been reported.

Dumke et al. (1983) and Hubbard et al. (1989a,b) measured the angular distribution of sputtered atoms from a liquid Ga-In eutectic alloy. In this system, Gibbsian segregation gives rise to an outermost atom layer that is virtually pure In. Their data for Ar^+ sputtering showed that In atoms sputtered from the first surface layer had a nearly-normal $\cos^\chi \theta$ distribution with $\chi = 1.8 \pm 0.1$ independent of ion energy. The angular distribution of Ga atoms was significantly sharper with $\chi = 3.2 \pm 0.2$ at energies ranging from 15 to 250 keV and $\chi = 4.9 \pm 0.3$ at 3 keV. The increase in the value of χ at this low energy was accompanied by an increase in the contribution of the uppermost atomic layer to the sputtered-atom flux as a result of a decrease in the energy of higher-order recoil atoms (Hubbard et al. 1989a).

Angular distributions of atoms sputtered from Co-Au, Cu-Be, Cu-Zn, and W-Si alloys during Ar^+ bombardment at 0.25 and 2 keV were investigated by Wucher & Reuter (1988). For low bombarding energy, the two distributions differed significantly; this difference, which was most pronounced for Cu-Be, seemed to scale with the atomic mass in the way that the lighter particles were sputtered preferentially along the surface normal. For 2 keV, however, all angular distributions looked alike, following essentially a $\cos^3 \theta$ law. Forward-peaked distributions were observed for Co atoms sputtered from Co-Au alloys, Cu from Cu-Zn, Be from Cu-Be, and W from W-Si. No information on the properties of Gibbsian segregation in these alloys has been reported in the literature. However, the light, undersized solute Be is known to segregate to the surface of Cu-Be alloys during irradiation (Rehn & Okamoto, 1983). In this case the observed preferential ejection of Be

along the surface normal appears to be inconsistent with the general prediction. It should be of interest to repeat the measurement on Cu-Be alloys in an independent experiment.

In summary, the angular distributions of species sputtered from an alloy can provide useful information about compositional gradients within the first few surface layers. In fact, this information was used to demonstrate the presence of a segregated layer (Andersen et al., 1982, 1983, 1984a) as well as to identify the surface-segregating element in an alloy (Andersen et al. 1984b, Sarholt-Kristensen et al., 1992).

4.8 Theoretical Estimates

While the system of nonlinear rate equations, eq. (45), accomodates all effects that are thought to govern partial sputter rates and composition profiles versus time, temperature, and ion current density, no comprehensive solution, analytic or numerical, is available at this time for any system. One good reason for this is the fact that the equation in the present form was only found during the writing of this review. Quite apart from this, a considerable amount of reliable input is needed. Moreover, finding reliable and accurate solutions for a given input may not be a trivial matter. The present subsection serves to present a brief survey of calculations that have been performed on systems that have been simplified in one way or another and to study the interplay and synergistics of some of the important effects. The following section, dealing with measurements, will serve a very similar purpose.

Early models by Pickering (1976), Haff (1977), Ho (1978), Collins (1978), Webb et al. (1978), and Chou & Shafer (1980) considered the effects of preferential sputtering and radiation-enhanced diffusion. The analytical model of Ho (1978), in particular, has been frequently applied to analyze depth profiles in bombarded alloys. All these models operate with linear differential equations since matter transport is characterized by diffusion coefficients and sputtering by boundary conditions at the target surface. In the work of Lam et al. (1980), the interplay of preferential sputtering and radiation-induced segregation was investigated. The interplay between preferential sputtering from a nonvanishing sputter depth and collisional mixing was studied on the basis of eq. (29) (Sigmund et al., 1982, and references given below). Measurements of sputtering at elevated temperatures by Rehn et al. (1979) indicated the need to include Gibbsian segregation as an effective mechanism for feeding atoms of certain alloy components into the surface layer. Theoretical models of Swartzfager et al. (1981), Itoh & Morita (1984), Kelly (1985), Kelly & Oliva (1986b), and Koshikawa & Goto (1987) included the simultaneous effects of preferential sputtering, radiation-enhanced diffusion and Gibbsian segregation on

concentration profiles. The model of Lam & Wiedersich (1981, 1982a,b, 1987) included also radiation-induced segregation and cascade mixing. Although this model is the most comprehensive one evaluated up till now, it treats collisional mixing by means of a stoichiometric diffusion current and ignores long-range events. Sputtering is modelled by a two-layer model.

The simplest nontrivial case is that of preferential sputtering in the presence of a nonpreferential diffusive current and a vanishing sputter depth. Here, eqs. (29,31,34) lead to

$$\frac{\partial N_i}{\partial \Phi} = w \frac{\partial N_i}{\partial x} + \bar{D} \frac{\partial^2 N_i}{\partial x^2} \tag{95}$$

as well as the boundary condition

$$w N_i + \bar{D} \frac{\partial N_i}{\partial x} = Y_i \text{ at } x = 0 \tag{96}$$

and the initial condition $N_i = \mathcal{N}_i$ for $\Phi = 0$. These are the equations underlying the treatment of Ho (1978).

It is seen from eq. (96) that sputtering is necessarily stoichiometric for $\bar{D} = 0$, i.e., if there is no feeding mechanism to compensate for a preferentially sputtered species.

For a nonvanishing diffusion coefficient $\bar{D}$, a closed-form solution can be found in principle but is fairly complex because both Y_i and w depend on fluence via $N_i(0)$. However, in the high-fluence limit, one obtains the appealing result

$$N_i(x) = \mathcal{N}_i + [N_i(0) - \mathcal{N}_i] e^{-x/\beta}, \tag{97}$$

where β is the effective altered-layer thickness, $\beta = \bar{D}/w$, and $N_i(0) = \gamma_i Y_i$ with some species-dependent factor γ_i.

The case of a nonvanishing sputter depth in the absence of transport has been treated recently (Sigmund & Oliva, 1993). Very steep concentration gradients were found to develop near the surface, and the concentrations of all components except the one with the lowest value of $\sigma_i(0)$ (where $\sigma_i(x)$ is the sputter cross section) approached 0 at the surface.

Numerical evaluations of fluence-dependent composition profiles under the influence of sputtering and collisional mixing have been performed by Sigmund et al. (1982), Falcone & Oliva (1984), Oliva et al. (1986), Peinador et al. (1990, 1991), Jiménez-Rodríguez et al. (1992), and Urbassek & Conrad (1992, 1993). The three early papers were based on schematic input. The most important conclusion that emerges from the other three papers — which address overlayer desorption, isotopic mixtures, and an alloy with widely different masses, respectively — is the fact that

the approach to equilibrium appears over a range of fluence that is comparable with that observed experimentally.

Figure 10 illustrates the synergistics of preferential sputtering and Gibbsian segregation for schematic input. It shows the composition profile of a species that sputters preferentially and segregates. The composition spike near the surface is the more pronounced the smaller the ion beam current density.

Rate equations allowing for thermally activated effects as well as cascade mixing in the diffusion picture and preferential sputtering via boundary conditions were solved numerically by a finite-difference scheme (Lam & Wiedersich, 1981). Thermodynamic equilibrium defined the initial state as well as the boundary conditions at $x = \infty$. Since Gibbsian segregation was included via atom exchange between the two upper surface layers, these layers were treated discretely (Lam & Wiedersich, 1982a; Yacout et al., 1989).

Taking into account all the five basic processes in the model requires a large number of physical parameters in the calculations (Lam & Wiedersich 1981, 1987). For binary alloys, three parameters were utilized to determine preferential sputtering, two component sputter yields for the top layer and a sputter fraction for the second atom layer that was assumed to be the same for both components. Displacement mixing was characterized by two parameters, the number of replacements per Frenkel pair and the defect-production efficiency. The damage rate and distribution were calculated by TRIM simulation (Biersack & Haggmark, 1980). Gibbsian segregation was likewise specified by two parameters, the enthalpy and entropy of segregation. These two quantities have been measured for many alloy systems. Quantifying radiation-enhanced diffusion and radiation-induced segregation requires information on diffusivities of vacancies and interstitials and of defect-solute complexes. That is, pre-exponential defect jump frequencies, defect migration energies, and defect-solute binding energies must be provided. In addition, the effective defect formation energies and the concentration of radiation-induced sinks are needed.

The computed time evolution of the concentration profiles in Ni-40 at % Cu and Ni-9.5 at % Si alloys during 3 keV Ne^+ bombardment at 500 C is shown in fig. 15. Both Cu and Si are initially enriched at the surface due to Gibbsian segregation (Lam et al. 1985b, Lam & Hoff 1988). These concentrations decrease gradually as a result of preferential sputtering and finally attain steady-state values. The shapes of the Cu and Si concentration profiles and the thicknesses of altered layers differ noticeably because of different radiation-induced segregation behavior, i.e., Si atoms segregate toward the surface whereas Cu atoms move away from the surface during irradiation (Rehn & Okamoto 1983). This example demonstrates that detailed information about the synergistic effects of pertinent processes on compositional changes can be obtained using this model. The fitting of model

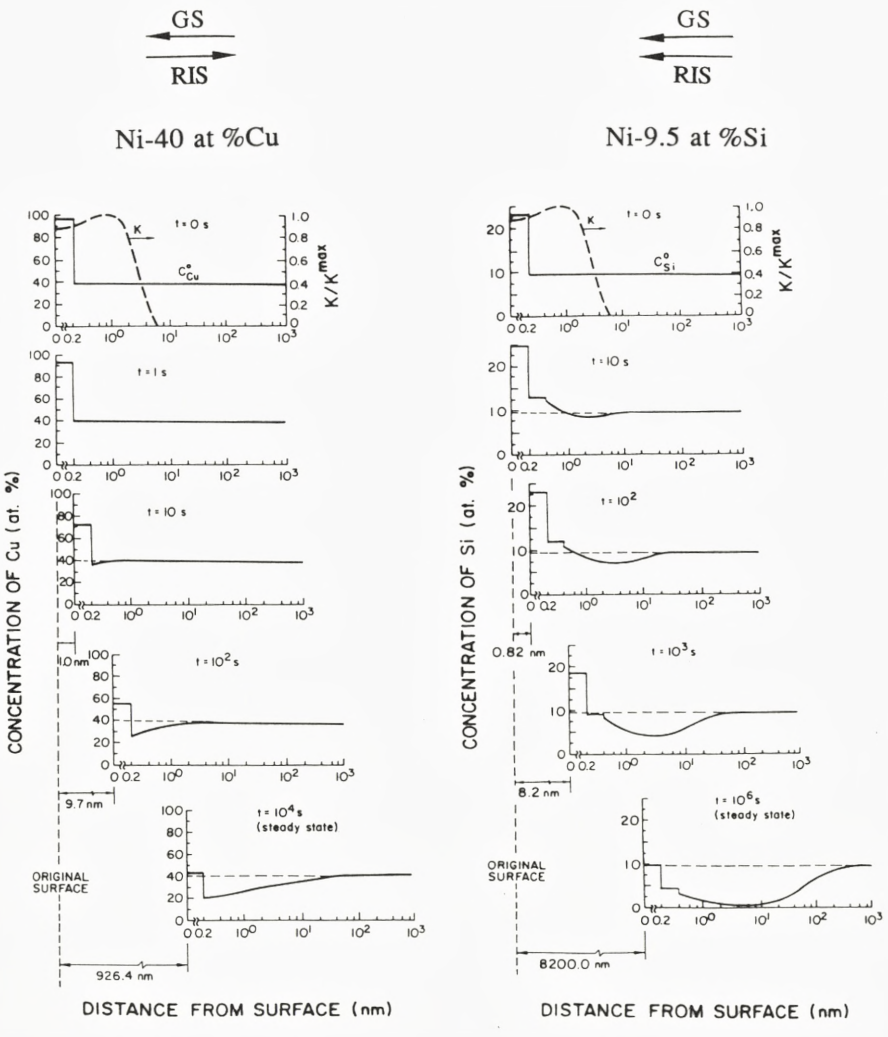

Figure 15. Development of the Cu concentration profile in a Ni-40 at % Cu alloy and of the Si concentration profile in a Ni-9.5 at % Si alloy during 3 keV Ne^+ bombardment at 500 C. The spatially-dependent damage rate K is shown by the dashed curve in the top portions, and the thicknesses of sputtered layers are indicated for various times. From Lam (1990).

calculations to experimental data has provided useful information on properties of point defects and defect-solute interactions in bombarded alloys (Lam & Hoff 1988, Hoff & Lam 1988, Tang & Lam 1989). Similar calculations were performed for near-surface composition modifications in ternary systems (Yacout et al. 1989; Tang et al., 1990).

4.9 Measurements

Bombardment-induced changes in surface composition have been measured in numerous alloy systems. Tabulations may be found in reviews by Betz & Wehner (1983), Andersen (1984), and Shimizu (1987). Mainly data published after 1987 have been summarized in this section. In order to elucidate synergistic effects of the pertinent processes, special emphasis will be laid on temperature-dependent sputtering of alloys.

4.9.1 Experimental Methods

A comprehensive review of various experimental techniques for surface and depth analysis based on sputtering, their principles, advantages and limitations has been given recently by Wittmaack (1991).

Compositional changes have been measured most often by Auger electron spectroscopy (AES). For an extensive survey cf. Betz & Wehner (1983). Because of variations in alloy composition near the surface, Auger transitions of several different energies have usually been employed in the analysis. Low-energy Auger electrons (~100 eV) have mean free paths ~4 Å, while for high-energy electrons (~1 keV), mean free paths lie around 15-20 Å. Low-energy Auger lines thus trace an average composition in the uppermost few surface layers. As a result, low-energy AES can detect the general effect of Gibbsian segregation but is not very suitable to characterize the interplay between this process and preferential sputtering. Recently, Li et al. (1991) showed that detailed composition profiles can be deduced from angle-resolved Auger spectroscopy. X-ray photoelectron spectroscopy (XPS) was also used in several studies (Thomas & Ralph, 1983; Hetzendorf & Varga, 1987; Lawniczak-Jablonska et al., 1989). The depth information is similar to that obtained from high-energy AES. In addition, information regarding phase transformations in the subsurface region may be derived.

Numerous measurements have been made with low-energy ion scattering spectroscopy (ISS). This technique is sensitive to the composition in the uppermost surface layer but does not yield information about the composition and extent of the altered layer. In studies of bombardment-induced composition changes, the same ions that are used to sputter the alloy are also employed to collect the ISS

signals (Swartzfager et al., 1981; Lam et al., 1985a,b).

While SIMS has been used routinely for depth profiling multicomponent materials and for studying preferential sputtering from isotopic mixtures (sect. 3.4), it has not been widely employed to investigate bombardment-induced surface alterations.

SNMS (secondary neutral mass spectrometry) has been applied in the determination of sputter yield and surface composition of binary alloys (Gnaser & Oechsner, 1993). With this technique, problems involving the matrix dependence of ionization/excitation process may be less severe. Since neutral atoms constitute the majority of the sputtered flux, information about compositional modifications at low fluences may be obtained.

Bombardment-induced surface alterations are unavoidable during analyses of the sputtered-flux composition. Furthermore, implantation of beam particles such as O or Cs may give rise to chemically-induced Gibbsian segregation in some alloy systems (Andersen et al., 1983).

Rutherford backscattering spectroscopy (RBS) has also been employed to determine compositional changes and thickness of the altered layer caused by high-energy ion bombardment (Liau et al., 1977, 1978; Affolter et al., 1985) or at elevated temperatures (Harper et al. 1992; Hong & Harper, 1992). Because of relatively poor mass resolution, the technique can only be employed to systems with sizable differences in mass such as metal silicides. Further, the depth resolution of RBS is inadequate for revealing compositional gradients in the near-surface region.

4.9.2 Low Temperatures

Low-energy AES measurements of Li et al. (1982, 1983, 1985) demonstrated the development of a Au spike at the surface and a depleted subsurface layer in Au-Cu alloys during Ar^+ bombardment at temperatures as low as -120 C. These data offered insight into the role of thermodynamic variables in collisional mixing. Although the results have been widely accepted, they did raise a number of concerns. Firstly, the small variations ($1 - 4$ at %) of the alloy composition over a short distance ($\sim$10 Å) from the surface raised a question regarding the experimental accuracy. Shimizu (1987) examined the quantitative correction procedure used by Li et al. under the analysis of the raw data and noted that the accuracy of the reported depth profiles was far beyond that expected on the basis of the experimental data input. Secondly, the dependence of the altered-layer composition on ion current density at -120 C was found difficult to understand (Rehn & Lam, 1987). The size of the observed altered layer indicated that Gibbsian segregation of Au atoms to the surface played an important role. Since normal radiation-enhanced diffusion is negligible in this temperature regime, segregation must be fed by collisional mixing. However, cascade overlap must play a role, since a dependence on

ion current density was observed. Rehn & Lam (1987) estimated that under the experimental conditions, pertinent dynamic events within cascades had to occur over durations of $\sim 10^{-4}$s after the initial knockon event. This is about seven orders of magnitude longer than the lifetime of a cascade.

Koshikawa (1985) measured the effect of 2 keV ion bombardment on the composition of Au-Cu alloy thin films prepared by co-evaporation of the pure metals onto a W substrate. Both low- and high-energy AES were utilized, and no composition changes were found at the surface at -120 C. Noticeable effects (i.e., Au enrichment in the near-surface region) were only observed during bombardment at room temperature. Such an enrichment was reported earlier by Kang et al. (1984) for keV Ar^+ bombardment and ISS analysis.

Qu & Xie (1988) used AES to monitor the time evolution of the near-surface composition of several homogeneous binary alloys (Au-Cu, Au-Ni, Au-Pd, Cu-Ni, and Cu-Pd) during Ar^+ bombardment at different energies. Fresh surfaces were prepared by scraping specimens inside the vacuum chamber before sputtering. Near the surface, the evolution toward steady state, measured by low-energy AES, was found to depend on ion energy. Many profiles showed complex variations in the transients. Qu & Xie attributed these variations to the synergistics of Gibbsian segregation and preferential sputtering. The stationary surface compositions obtained were consistent with component sputter yields $y_i^{(1)}$ equal to the sputter yields of the pure elements. Cu was sputtered preferentially from Cu-Ni and Cu-Pd, and Au was sputtered preferentially from Au-Pd, Au-Cu, and Au-Ni alloys.

Sputtering from Cu-Pd alloys was assessed by ISS (Ackermans et al., 1990b). Their experimental results and conclusion appear conflicting: Preferential sputtering of Cu was said to occur during 2 and 3 keV Ne^+ bombardment, yet the measurements showed virtually no deviations of the Cu concentration in the topmost surface layer from the bulk concentration. These authors stated that it was impossible in these experiments to distinguish between preferential sputtering and radiation-induced segregation. This claim is hardly justified because the steady-state surface composition is only dictated by preferential sputtering. Radiation-induced segregation should affect only the transient behavior of the surface composition and the evolution of the subsurface concentration profile.

Changes in the near-surface composition of a FeSi single crystal under bombardment by Ne^+, Ar^+, and Kr^+ ions in the energy range 0.3 - 3 keV were studied via low-energy AES by Castro & Ballesteros (1988). Si was always sputtered preferentially, and the effect was most pronounced at low ion energies. Ratios of partial sputter yields were similar for all three projectiles below 0.5 keV but became quite different at higher energies. As expected, the steady-state surface composition depended on the type and energy of the bombarding ions at energies above $\sim$1 keV.

Kurokawa & Shimizu (1987) assessed the composition profile of the altered layer formed in an Al-Mg alloy under 3 keV Ar^+ bombardment by ISS, AES and EELS (electron energy loss spectroscopy). Sputtering and radiation-enhanced Gibbsian segregation of Mg resulted in a Mg composition spike at the surface, followed by Mg-depleted layers extending over a depth of ~150 Å. A slight enrichment in Mg of the uppermost atom layer (65 at % compared to 60 at % in the bulk) revealed by ISS may reflect the effect of surface segregation of Mg during post-bombardment ISS analysis with He^+ ions.

Du Plessis et al. (1989b) measured surface and subsurface composition changes in Pd-Pt alloys after 1 keV Ar^+ bombardment by ISS and AES and concluded that during irradiation, Pd segregated to the alloy surface where it was sputtered preferentially. This resulted in a relatively high concentration of Pd on the surface and a strong Pd depletion in subsurface layers. Experimental data were fitted to model calculations to derive the Gibbsian segregation energy and the radiation-enhanced diffusion coefficient.

Lawniczak-Jablonska et al. (1989) used XPS to measure the changes in subsurface composition of Ni-Mo alloys during 1 keV Ar^+ bombardment. The time required to reach steady state in the altered layer and the magnitude of the composition change were found larger for two-phase alloys than for solid solutions. The ratios of the extracted component sputter yields depended strongly on the bulk compositions. Note, however, that sputter yield ratios deduced from XPS or high-energy AES measurements cannot be reliable.

Bombardment-induced compositional changes in Cu-Pt alloys were investigated previously by Andersen et al. (1982, 1983, 1984a). Li et al. (1990) studied this alloy system by means of different Auger transitions. In agreement with the results of Andersen et al., the steady-state Cu profiles could be characterized by the synergistics of radiation-enhanced Gibbsian segregation of Cu to, and preferential sputtering from, the alloy surface during $0.2 - 2$ keV Ar^+ bombardment at room temperature. These profiles were also found consistent with that obtained subsequently by angular-resolved AES for 2.8 keV Ar^+ ions (Li et al., 1991). The latter profile showed more details of changes in the near-surface composition. The observed changes were higher than those created by bombardment at lower energies. Li et al. interpreted this observation in terms of decreasing mass effect with increasing ion energy.

Steady-state enrichment of Cu in the near-surface region of Cu-Zn alloys under 4 keV Ar^+ bombardment was reported by Marchetti et al. (1990), in agreement with earlier observations by Ferron et al. (1983) and Hammer & Shemenski (1984). Marchetti et al. interpreted this as a result of preferentially sputtering Zn. Caution is indicated since composition changes were monitored with high-energy Auger lines.

Preferential sputtering of InP was reviewed and revisited by Malherbe & Barnard (1991). Surfaces of InP wafers bombarded by 0.5 - 5 keV Ar^+ ions were investigated by medium-energy Auger transitions. P was found to be sputtered preferentially, leaving In-enriched surfaces. The steady-state near-surface composition depended on the angle of incidence but was found independent of both ion energy and crystal orientation. The mass difference between In and P was asserted to be the major factor determining preferential sputtering of P while surface binding was thought to be of secondary importance.

Preferential sputtering of Ni leading to Pt enrichment at the surface of Ni-Pt alloys has been observed by several groups (Andersen et al., 1983; de Temmermann et al., 1986, 1987; Weigand et al., 1992; Schmid et al., 1992). ISS measurements revealed that this effect was independent of surface orientation (Weigand et al., 1992), similar to results obtained for InP (Malherbe & Barnard, 1991). The synergistic effect of radiation-enhanced Gibbsian segregation which occurred even at 77 K was reported by Andersen et al. (1983). Surface enrichment in Pt caused an increase in the lattice constant of the upper atom layers. This resulted in the formation of subsurface lattice-mismatch dislocations, which were characterized recently by Schmid et al. (1992) by means of scanning tunneling microscopy.

From AES measurements of composition changes in CdTe, HgTe and HgCdTe during bombardment with 0.6 - 3 keV Ar^+ ions, Stahle & Helms (1992) assessed the sputter preferentiality of alloy components. It was suggested that preferential sputtering from these materials was controlled by the dominant effect of chemical bonding. Sputtering of Cd from CdTe was weakly preferential, whereas Hg sputtering was highly preferential from both HgTe and HgCdTe. The effects of defect-assisted processes appeared unimportant at room temperature because steady state was reached within a very short time.

Van Wyk et al. (1991) bombarded amorphous Cu-Ti alloys of different compositions with 2 keV Ar^+ ions and measured surface and subsurface compositions with ISS and AES. It was found that Cu segregated to the surface where it was sputtered preferentially. The thickness of the altered layer was estimated to be ~40 Å, i.e., equal to the damage depth. By fitting the experimental data with their kinetic model which includes the effects of radiation-enhanced Gibbsian segregation and preferential sputtering, they also derived the segregation energy and the radiation-enhanced diffusion coefficient as functions of alloy composition. The accuracy of these calculated parameters was limited mainly due to the intricate interplay between Gibbsian segregation and preferential sputtering. An excessively large sputter-yield ratio equivalent to $y^{(1)}_{Cu}/y^{(1)}_{Ti} = 6$ was necessary for the best possible fit of the results. Note that point defects are ill-defined in amorphous materials (Adda et al., 1987). Therefore, the concept of radiation-enhanced segregation in these media requires some clarification.

4.9.3 Elevated Temperatures

The first study of bombardment-induced alterations of surface composition at elevated temperatures was carried out on Cu-Ni alloys by Shimizu et al. (1975). Alloys were sputtered at temperatures within the range 100-600 C, and AES analysis of near-surface compositions was performed after samples had been cooled down to room temperature. The interpretation of these measurements was somewhat complicated by effects arising during specimen cooling. Nevertheless, a strong effect of irradiation temperature on near-surface composition changes was observed. Subsurface compositional profiles were not measured. Since sputter yields of metals are insensitive to temperature up to near the melting point, the temperature dependence observed was an indication of the importance of thermally-activated processes in alloy sputtering. A ratio of partial sputter yields was deduced from the composition ratio in steady state. Cu was found to sputter preferentially with a yield ratio ~1.9 at room temperature. Considerably larger yield ratios were found for bombardment at elevated temperatures. This implied bombardment times too short to reach steady state and/or changes in the composition of the sputtered surface during the post-bombardment cooling to ambient temperature.

Simultaneous AES measurements of composition changes in a Cu-40 at % Ni alloy during 5 keV Ar^+ sputtering at temperatures between 50 and 600 C were reported by Rehn et al. (1979, 1980). Two Auger transitions were used for each alloying element: Cu transitions at 106 and 920 eV, and Ni transitions at 102 and 716 eV. Low-energy measurements showed that the Cu concentration in the uppermost atom layers rapidly approached a steady-state value of ~40 at %, and this value was practically independent of temperature over the range investigated. Cu was found to sputter preferentially with a yield ratio ~2. High-energy measurements revealed that above 300 C, Cu depletion in the subsurface region was more pronounced than in the outermost layers, and no steady state was yet reached after 2 hours of bombardment. Indeed, both the time to reach steady state and the degree of Cu depletion in the subsurface region increased with increasing temperature. The extent of compositional change in the subsurface region was also determined by depth profiling of the bombarded specimen after cooling down to room temperature. These measurements demonstrated that Gibbsian segregation and radiation-enhanced diffusion of solute elements played important roles in the formation of the altered layer. Deviations from the bulk composition occurred up to remarkably large depths.

Swartzfager et al. (1981) carried out a similar study on Cu-Ni, Ag-Au and Au-Pd alloys via ISS. Alloys were bombarded by 2 keV Ne^+ ions at temperatures between 200 and 500 C, and compositional changes in the outermost atom layer were probed in situ with the same ions. Sputtering was found to be nonpreferen-

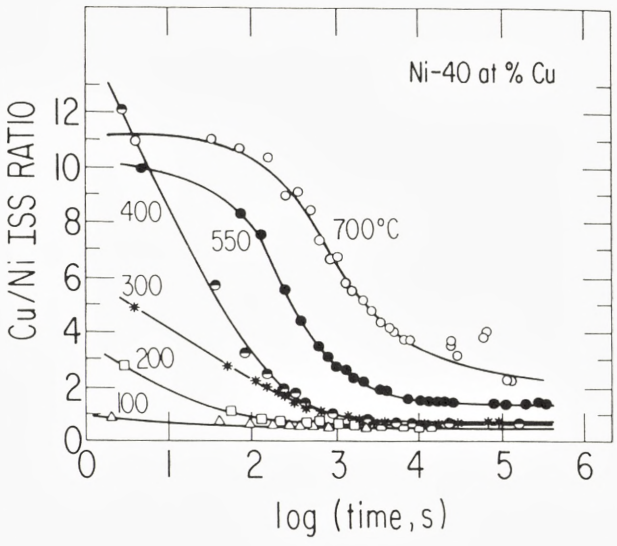

Figure 16. Time dependence of Cu/Ni ISS intensity ratio measured during 3 keV Ne^+ bombardment of a Ni-40 at % Cu alloy with a flux of 3.75 10^{13} ions/cm^{2}s at various temperatures. After Lam et al. (1985b).

tial in Cu-Ni and Ag-Au alloys (in seeming disagreement with AES results), while Pd was sputtered preferentially from Au-Pd. Similar to what was found in AES studies, pronounced alterations of the alloy composition were observed in the near-surface region. These measurements were interpreted in terms of synergistic effects of sputtering, radiation-enhanced diffusion, and Gibbsian segregation. Steady-state concentration profiles were analyzed by means of the model of Ho (1978), eq. (95). This model includes preferential sputtering and radiation-enhanced diffusion and describes the steady-state alloy composition in the altered layer by Ho's equation (97), which indicates that the logarithm of the concentration change in this layer should depend linearly on the distance from the surface with a slope of $-1/\beta$ within the region where radiation-enhanced diffusion dominates. Analyzing their concentration profiles in this way, Swartzfager et al. estimated β and D for several temperatures. The altered-layer thickness was found to be independent of the ion current J_0 and to rise sharply with temperature from ~400 C in Cu-Ni alloys. Extracted diffusion coefficients varied between 10^{-16} and 10^{-15} cm$^2/s$, virtually independent of temperature below ~400 C. This suggests that in this regime, radiation-generated point defects annihilate mainly at extended sinks. Note, however, that segregation was not considered in Ho's model.

ISS measurements on Ni-40 at % Cu alloys by Lam et al. (1985a) confirmed the results of Swartzfager et al.. The data for steady-state surface composition changes during bombardment at room temperature indicated that sputtering of this alloy system was nonpreferential. For bombardment above ~400 C, a noticeable temperature dependence was found (fig. 16). This effect was interpreted in terms of a significant contribution of the second atom layer to the sputtered flux. The same observations were also made on other Ni-based alloys (Lam et al., 1985b; Lam & Hoff, 1988; Hoff & Lam, 1988; Tang & Lam, 1989).

Morita et al. (1981) employed RBS to investigate compositional changes in self-supporting films of Ni-Si and Ni-Au alloys undergoing 5 keV Ar^+ bombardment at elevated temperatures. They found that above ~500 C, overall solute concentrations decreased rapidly with increasing fluence, the depletion being more severe in the near-surface region than deeper inside the specimen. The temperature dependence of solute depletion by sputtering was stronger in Ni-Si than in Ni-Au films.

Compositional changes in Ni-12.7 at % Si alloys bombarded by 5 keV Ar^+ ions at temperatures between 30 and 700 C were also reported by Rehn et al. (1983). Significant loss of Si from the specimen subsurface during bombardment at elevated temperature was detected by AES. This observation was supported by ISS measurements (Lam & Hoff, 1988). In addition, Rehn et al. (1983) found that very near the surface, the composition analyzed by low-energy (~100 eV) Si and Ni Auger signals remained equal to that of the bulk below ~650 C due to near-stoichiometric sputtering.

Li (1988) bombarded Au-Cu alloys by 2 keV Ar^+ ions between 30 and 700 C and performed AES depth profiling at room temperature to investigate the temperature dependence of steady-state redistribution. It was found that depletion of Au near the surface was most pronounced at ~300 C. Above this temperature, the altered layer extended deeper into the bulk and the surface concentration of Au increased steadily. The latter behavior suggested that steady state was not attained during bombardment at the upper end of the temperature range, i.e., above 450 C.

Li (1989) also measured composition changes in Au-Cu alloys during bombardment by 0.2 - 2 keV N^+ ions in the temperature range 25 - 300 C. The results were compared with those obtained for Ar^+ bombardment. There was no difference at 25 C, yet as the temperature increased, bombardment-enhanced Gibbsian segregation became effective, and differences between depth profiles became more apparent. Indeed, the subsurface Au depletion was more pronounced for N^+ bombardment. Li explained this observation in terms of differences in the partial sputter yields and damage depths in the two cases.

Near-surface compositional changes resulting from 2 keV Ar^+ bombardment in Ni-Cr alloys at temperatures between 30 and 600 C were reported by Jeng &

Holloway (1990). In this alloy system, Gibbsian segregation of Ni to the surface was found to be very weak (Jeng et al., 1988). Low-energy Auger measurements revealed that the steady-state Cr/Ni composition ratio increased continuously from 200 to 400 C due to preferential sputtering of Ni atoms transported to the surface by radiation-enhanced Gibbsian segregation. Above 400 C, the same ratio decreased with increasing temperature. This temperature dependence had been measured (Rehn & Wiedersich, 1980) and modeled (Lam & Wiedersich, 1982a) previously for Cu-Ni alloys.

The same behavior was also observed in ternary Fe-18Cr-3Mo alloys during 1 keV Ar^+ bombardment (Schiffman & Polak, 1986). Under steady-state conditions, the Cr/Fe concentration ratios, as monitored by both low- and high-energy Auger lines, showed significant temperature dependence above ~250 C. They reflected significant Fe depletion in the near- and subsurface regions, which increased gradually to maximum values at ~550 C and then decreased. A similar temperature dependence was obtained in phenomenological modeling (Yacout et al., 1989). Schiffman & Polak (1986) also noticed that the presence of small amounts of CO in the target chamber during bombardment caused inversion of this trend. That is, chemically-induced segregation of Cr resulted in surface enrichment of this element, and continuous sputtering of Cr from the surface led to its depletion in the underlying layers.

Chemically-driven segregation can also be triggered by implantation of certain incident-ion species. For example, O^+ bombardment of Ni_5Pd gave rise to surface segregation of Ni (the element with the stronger bond), in contrast to segregation of Pd (the element segregating in thermal equilibrium) during Ar^+ bombardment (Andersen et al., 1983). Similar reversal of segregation trends was also observed in Cu_3Au.

Effects of bulk impurities, such as O and C, on bombardment-induced near-surface composition modifications at elevated temperatures were observed in V-Cr alloys by Dawson & Hu (1985, 1986). Bombardment by Ar^+ ions at ambient temperature depleted the surface in Cr, whereas bombardment at 525 C increased the surface Cr concentration. This Cr enrichment at the alloy surface resulted from co-segregation of V and O or V and C to the surface — this is only possible at high temperature — and simultaneous, preferential removal of V by sputtering.

Compositional changes in binary alloys of heavy and light elements, like Cu-Li and Al-Li, during elevated-temperature sputtering were measured and modeled by Krauss et al. (1984b, 1985, 1988). They found that dilutions of Li in these metals produced surfaces covered with nearly pure Li upon heating. During bombardment above ~300 C, the Li-rich overlayer remained stable; in fact, the surface concentration of Li increased with increasing temperature. Efficient surface segregation processes during irradiation and the low sputter yield of Li play a key role in the

maintenance of the Li overlayer.

Several studies of bombardment-induced compositional changes have been carried out on metal silicides. In general, the development of compositional profiles was found to be controlled by radiation-activated segregation and preferential sputtering of Si. Affolter et al. (1985) bombarded thin films of $CoSi_2$ and $NbSi_2$ on Si substrate by Xe^+ ions in the energy range 200 to 260 keV at different temperatures and analyzed the composition change in the irradiated materials by RBS. Preferential sputtering of Si was demonstrated, and partial sputter yields for the two silicides were shown to be comparable. The amount of sputtered species increased almost linearly with ion fluence until intermixing of the silicide with the underlying Si became appreciable. This occurred at lower fluences during bombardment at temperatures above room temperature. A Si-depleted subsurface layer was observed, the spatial extent of which was found comparable with the Xe range after bombardment at ambient temperature in $CoSi_2$, but significantly smaller after bombardment at 200 C. Marked differences between the results of sputtering at low and high temperature were rationalized in terms of radiation-enhanced diffusion across the silicide film in the presence of an underlying Si substrate.

Compositional modifications of $CrSi_2$ and Cr_3Si induced by 2 to 5 keV Ar^+ sputtering between -80 and 370 C were investigated by Ottaviani & Valeri (1987) using AES. Concentration profiles were measured over a depth of a few nanometers below the surface by simultaneous analysis of low- and high-energy Auger lines. Surface enrichment in Cr was found in both compounds at room temperature, the enrichment being stronger at lower ion energy and in the Si-rich silicide. In addition, elemental concentrations derived from low- and high-energy Auger lines were practically identical, suggesting that the altered layer was formed by preferential sputtering of Si and collisional mixing. Only at temperatures significantly higher than room temperature do thermally-activated processes become dominant in Cr-silicides. In fact, with increasing temperature, a transition to a Si-richer surface composition was observed at ~250 C. During thermal annealing, the same transition occurred at higher temperature. This transition was attributed to the formation of the stable CrSi phase which can be enhanced during bombardment.

Ion beam effects on the near-surface composition of $TaSi_2$ were studied by the same group (Valeri et al., 1991). Steady-state sputtering of this silicide with Ar^+ ions below ~410 C resulted in Si depletion at the surface and, much more severe, in the subsurface region. Preferential sputtering and radiation-enhanced segregation of Si were believed to be responsible for the development of such a compositional profile. Above 410 C, diffusional processes became efficient, progressively reducing the concentration gradients within the altered layer. Furthermore, the subsurface composition measured at room temperature showed a noticeable dependence on ion energy, in agreement with the results reported for other silicides (Wirth et al.,

1984, 1986; Clement et al., 1990).

Recently, Harper et al. (1992) and Hong & Harper (1992) studied the temperature dependence of preferential sputtering of Si by 300 eV Ar^+ ions from $TiSi_2$ and $CoSi_2$, respectively. Compositional changes in the silicide were recorded by RBS and AES. In the case of $TiSi_2$, room-temperature bombardment caused a normal, linear decrease in silicide thickness due to loss of both Ti and Si. As the temperature was increased to 500 - 700 C, the thickness and composition of the silicide remained almost unchanged during bombardment. Since the Ti RBS peak area was almost constant in specimens bombarded at high temperature, this effect was attributed to preferential sputtering of Si being continuously compensated by rapid diffusion of Si from the substrate beneath the silicide layer. Compared with room-temperature values, the partial sputter yield of Ti decreased by a factor of 5 at 500 - 700 C while the yield of Si increased by a factor of 2. This implies that the sputtered flux was close to 100 % Si. Almost the same observations were made on $CoSi_2$ (Hong & Harper, 1992): The sputtering rate of this silicide, when deposited on Si, decreased significantly above 400 C. However, on SiO_2 substrates, the sputtering rate of $CoSi_2$ was nearly constant, independent of bombardment temperature.

4.9.4 Conflicting Characterizations

Some discussion is indicated here of conflicting experimental results published in the literature on preferential sputtering. In the typical case of Cu-Ni alloys, researchers using AES to probe near-surface compositional changes reported preferential sputtering of Cu (Betz & Wehner, 1983, and references therein; Qu & Xie, 1988). Experiments involving ISS led to opposite conclusions. Okutani et al. (1980) studied sputtering of Ni-48 at % Cu alloys by 3 keV Ar^+ ions and found Ni to be sputtered preferentially. Swartzfager et al. (1981) and Lam et al. (1985a) found ISS intensity ratios measured on the sputtered surfaces virtually identical to bulk concentration ratios. This suggested that sputtering of Cu-Ni alloys by Ne^+ ions was nonpreferential. Kamiya et al. (1988) reported that their ISS measurements on dilute Cu-Ni targets showed preferential sputtering of Ni in low-Ni alloys and of Cu in low-Cu alloys - an effect which cannot be understood on the basis of eq. (15). The discrepancy between ISS and AES data can be reconciled in terms of near-surface compositional gradients and the respective depth resolutions of these analysis techniques. The disagreement amongst ISS measurements is, however, difficult to explain; differences in sample preparation, residual gas in the target chamber, and calibration may be important influencing factors.

Discrepancies between AES and ISS measurements should be anticipated for most multicomponent systems, except for some cases where near-surface compo-

sitions remain unchanged during bombardment as a result of near-stoichiometric sputtering and negligible surface segregation. The Ni-Co alloy system is a good example. Several compositional characterizations have been performed on this system over the past decade because of the technological importance of Ni-Co alloy films in the areas of magnetic storage and catalysis. Therefore, a direct comparison of several results can be made.

Tanaka et al. (1983) studied composition changes in these alloys by Auger lines Ni(859 eV) and Co(656 eV) after sputter cleaning with a 5 keV Ar^+ beam. They found that the near-surface concentrations of Ni and Co differed only very slightly from the bulk composition. AES work by Kurokawa et al. (1989b) on Ni-Co alloys under Ar^+ bombardment confirmed these findings. No apparent synergistic effects of preferential sputtering and surface segregation could be detected from both low- and high-energy Auger signals. Since the accuracy of the low-energy Auger signals was rather poor (affected by stray magnetic fields resulting from the ferromagnetic properties of the alloying elements), Kurokawa et al. (1989a) extended their earlier measurements using both ISS and AES. They found that surface and subsurface compositions were the same as in the bulk.

Fujita et al. (1990) and Sethuraman et al. (1990, 1991) used several techniques to characterize Ni-Co films of varying composition. The results of AES depth profiling indicated spatially-uniform film composition, in agreement with previous observations of nonpreferential sputtering from Ni-Co alloys. For this reason, and because of negligibly small corrections for matrix effects, the Ni-Co alloy system has been proposed as a reference material for surface chemical analysis by AES (Fujita et al., 1990).

Among several available analytical techniques, ISS appears to be the most suitable for demonstrating the interplay between Gibbsian segregation and preferential sputtering because it provides, in principle, direct information on the composition in the outermost atom layer. However, since this information comes from the conversion of ISS intensity ratios to compositions, an accurate calibration is required. Most calibrations reported were obtained from sputter-cleaned surfaces and, consequently, affected by preferential sputtering. Reliable calibrations must be performed on fresh surfaces, created in ultrahigh vacuum by, e.g., scraping or fracture (Betz, 1980). Simultaneous analyses with AES (or XPS) and laser-induced fluorescence can be a good complement because the former provides useful information about subsurface composition changes while the latter yields the composition of the sputtered flux (Bay, 1987).

5 Summary and Outlook

Although we have tried to summarize a broad spectrum of problems within the field of alloy and isotope sputtering, we have put emphasis on some aspects and deemphasized others. The primary focus has been on preferential sputtering and related aspects. Information on absolute sputter yields is implicit in much of the discussion but comes rarely to the surface. If pressed to make an explicit statement on the latter point we would have to say that rough estimates can be made by simple reasoning and precise predictions are unavailable.

We tried to focus on precise definitions of those parameters which we believe are important in the understanding of preferential sputter effects, and to stick to a clear and unambiguous notation, flexible enough to accomodate both continuum and discrete descriptions. It is shown that sputter cross sections and component yields are two ways of describing the same physics when combined properly with particle densities and atom fractions, respectively. Explicit introduction of species-dependent atomic volumes allows to incorporate density changes along with compositional changes. Conversely, the assumption of a species-independent atomic volume is equivalent with that of a fixed lattice structure independent of composition. Either description allows inclusion of defects.

During the decade that passed since the appearance of the review by Betz & Wehner (1983), there has been progress in the theory of primary and secondary sputter processes as well as in experiment. Predictions on the dependence of preferential sputtering on mass and surface binding energy have long been available but have been strengthened, clarified, and numerically modified along with increasing experience from numerical simulation. This has led in particular to a fairly clear and consistent theoretical picture of preferential sputtering from isotopic targets. Nevertheless, discrepancies prevail in that area between theoretical predictions and experimental data, and there are also differences between different experimental data on similar systems. Key points are the existence or nonexistence of a pronounced angular variation in the isotopic composition of the sputtered flux and the absolute magnitude of the overall enrichment of this flux at low bombardment fluences. Similar discrepancies are present in alloy sputtering. They are larger in absolute terms, but they tend to receive less attention because of a wider variety of possible disturbing factors.

Much progress has happened in the understanding of secondary effects, namely the role of collisional mixing and thermally-activated processes. This development started little more than a decade ago. The proper mathematical formalism has developed gradually, and numerical results, based on schematic or realistic input, have been emerging with increasing intensity. When starting this project we felt there was an urgent need to reconcile numerous available descriptions of matter

transport in the target during sputtering, developed by different groups at different times and rather independent of each other. With the emergence of our eq. (45) in conjunction with relations like eqs. (42,44), this goal has essentially been achieved. There are still a few open ends, but closing those is not expected to invoke major problems.

The number of uncertain or unknown parameters that govern secondary processes is quite large. Thus, comprehensive quantitative predictions are not likely to emerge in the near future. This does not preclude quantitative predictions with a more limited scope, such as on the fluence dependence of isotope enrichment where the first results have appeared as reported in sect. 3. Moreover, well-planned measurements on alloy sputtering allow to extract pertinent parameters by comparison with numerical simulations on secondary effects. Several examples have been mentioned in sect. 4.

We like to conclude this survey with a list of important problems.

- Absolute measurements on isotope sputtering (composition of target and/or sputtered flux).
- Estimates of energy spectra of sputtered atoms from targets containing strong composition gradients near the surface.
- Quantitative theory of the effect of composition gradients on angular distributions of sputtered particles.
- Quantitative predictions on absolute erosion rates and partial sputter yields.
- Clarification of the role of preferential sputtering and recoil implantation in low-energy alloy and isotope sputtering.
- Experimental studies of preferential sputter depths for materials with widely different constituents.
- Predictions on preferential sputtering from high-density cascades on the basis of a variety of models proposed to describe collision spikes.
- Analytical relationships (scaling laws) describing fluence-dependent preferential sputtering, composition gradients, and altered-layer depths in different regimes of temperature and ion current density. Establishing quantitative criteria for the limits of these regimes.
- Systematic experiments testing scaling laws governing secondary processes.
- Experimental and/or theoretical studies of the interplay between compositional and topographical changes.

Acknowledgements

Our experience in the main topic of this chapter has been acquired over a long time period in cooperation with a number of friends and colleagues, in particular N. Andersen, R. Collins, A. Gras-Marti, K. Johannessen, R. A. Johnson, A. R. Krauss, P. R. Okamoto, A. Oliva, L. E. Rehn, S. J. Rothman, M. W. Sckerl, R. Sizmann, H. Wiedersich, H. F. Winters, and A. Yacout. Numerous aspects have been discussed in the Danish Sputter Club, in particular with H. H. Andersen, F. Besenbacher, J. Bøttiger, J. J. Jiménez-Rodríguez, J. Onsgaard, J. Schou, S. Tougaard, H. M. Urbassek, and M. Vicanek, as well as with D. M. Gruen, R. Kelly, and G. K. Wehner. In addition, H. H. Andersen, R. A. Baragiola, H. M. Urbassek, and M. Vicanek provided useful comments and suggestions on a preliminary manuscript. We wish to express our sincere gratitude to all of them. One of us (PS) would like to acknowledge the hospitality of the Physics Division at Argonne, especially D. S. Gemmell and G. H. Berry, during his tenure of an Argonne Distinguished Fellowship. This work was supported by the U. S. Department of Energy, Office of Basic Energy Sciences, under Contract no. W-31-109-ENG-38 and by a grant from the Danish Natural Science Research Council (SNF).

References

Abramowitz M and Stegun IA, 1964: *Handbook of Mathematical Functions with Formulas, Graphs, and Mathematical Tables* (U.S. Government Printing Office, Washington, D.C.)

Ackermans PAJ, Creuwels MAP, Brongersma HH and Scanlon PJ, 1990a: Surf. Sci. **227**, 361

Ackermans PAJ, Krutzen GCR and Brongersma HH, 1990b: Nucl. Instrum. Methods B **45**, 384

Adda Y, Beyeler M and Brebec G, 1975: Thin Solid Films **25**, 107

Adda Y, Brebec G, Gupta RP and Limoge Y, 1987: Mater. Sci. Forum **15-18**, 349

Affolter K, Hamdi AH and Nicolet MA, 1985: Appl. Phys. A **37**, 19

Almen O and Bruce G, 1961: Nucl. Instrum. Methods **11**, 257

Andersen HH, 1979: Appl. Phys. **18**, 131

Andersen HH, 1980: *The Physics of Ionized Gases (SPIG 1980)*, ed. M. Matic (Boris Kidric Institute of Nuclear Sciences, Beograd) 421

Andersen HH, 1984: *Ion Implantation and Beam Processing*, ed. J. S. Williams and J. M. Poate (Academic Press, Sydney) 127

Andersen HH and Sigmund P, 1965: Riso Report no. **103**

Andersen HH, Chernysh V, Stenum B, Sørensen T and Whitlow HJ, 1982: Surface Sci. **123**, 39

Andersen HH, Stenum B, Sørensen T and Whitlow HJ, 1983: Nucl. Instrum. Methods **209/210**, 487

Andersen HH, Stenum B, Sørensen T and Whitlow HJ, 1984a: Nucl. Instrum. Methods B **2**, 623

Andersen HH, Stenum B, Sørensen T and Whitlow HJ, 1984b: Nucl. Instrum. Methods B **2**, 601

Andersen N and Sigmund P, 1974: Mat. Fys. Medd. Dan Vid. Selsk. **39**, no. 3

Ardell AJ and Janghorban K, 1983: *Phase Transformations during Irradiation*, ed. F.V. Nolfi, Jr. (Applied Science Publishers, London) 291

Asada T and Quasebarth K, 1929: Z. Phys. Chem. A **143**, 435

Averback RS, 1986: Nucl. Instrum. Methods B **15**, 675

Averback RS, Peak D and Thompson LJ, 1986: Appl. Phys. A **39**, 59
Baretzky B and Taglauer E, 1985: Surf. Sci. **162**, 996
Baretzky B, Möller W and Taglauer E, 1987: Nucl. Instrum. Methods B **18**, 496
Baumel LM, Weller MR, Weller RA and Tombrello TA, 1988: Nucl. Instrum. Methods B **34**, 427
Bay HL, 1987: Nucl. Instrum. Methods B **18**, 430
Betz G, 1980: Surface Sci. **92**, 283
Betz G and Wehner GK, 1983: *Sputtering by Particle Bombardment II.* Top. Appl. Phys. **52**, ed. R. Behrisch.(Springer-Verlag, Berlin) 11
Biersack JP, 1987: Nucl. Instrum. Methods B **27**, 21
Biersack JP and Eckstein W, 1984: Appl. Phys. A **34**, 73
Biersack JP and Haggmark LG, 1980: Nucl. Instrum. Methods **174**, 257
Brongersma HH, Sparnaay MJ and Buck TM, 1978: Surface Sci. **71**, 657
Burnett JW, Biersack JP, Gruen DM, Jørgensen B, Krauss AR, Pellin MJ, Schweitzer EL, Yates JT and Young CE, 1988: J. Vac. Sci. Technol. A **6**, 2064
Carter G, Navinsek B and Whitton JL, 1983: *Sputtering by Particle Bombardment II*, Top. Appl. Phys. **52**, ed. R. Behrisch (Springer-Verlag, Berlin) 231
Castro GR and Ballesteros A, 1988: Surf. Sci. **204**, 415
Chen I-W, 1983: J. Nucl. Mater. **116**, 249
Cheng YT, 1990: Mater. Sci. Repts. **5**, 45
Cheng YT, Van Rossum M, Nicolet MA and Johnson WL, 1984: Appl. Phys. Lett. **45**, 185
Cheng YT, Dow AA and Clemens BM, 1988: Appl. Phys. Lett. **53**, 1346
Cheng YT, Simko SJ, Militello MC, Dow AA, Auner GW, Alkaisi MH and Padmanabhan KR, 1992: Nucl. Instrum. Methods B **64**, 38
Chou NJ and Shafer MW, 1980: Surf. Sci. **92**, 601
Clement M, Sanz JM and Martinez-Duart JM, 1990: Surf. Interf. Anal. **15**, 440
Collins R, 1978: Rad. Effects **37**, 13
Collins R and Jiménez-Rodríguez JJ, 1982: Radiat. Eff. Lett. **68**, 19
Collins R and Sigmund P, 1992: J. Appl. Phys. **72**, 1993
Collins R, Jiménez-Rodríguez JJ, Wadsworth M and Badheka R, 1988: J. Appl. Phys. **64**, 1120
Conrad U and Urbassek HM, 1991: Nucl. Instrum. Methods B **61**, 295
Conrad U and Urbassek HM, 1992: Surf. Sci. **278**, 414
Conrad U and Urbassek HM, 1993: Nucl. Instrum. Methods B, submitted
Damask AC and Dienes GJ, 1963: *Point Defects in Metals* (Gordon and Breach, New York)
d'Heurle F, Baglin JEE and Clarke GJ, 1985: J. Appl. Phys. **57**, 1426
Dawson PT and Hu MP, 1985: Surf. Sci. **163**, 198
Dawson PT and Hu MP, 1986: J. Nucl. Mater. **139**, 198
de Temmermann L, Creemers C, van Hove H, Neyens A, Bertolini JC and Massardier J, 1986: Surf. Sci. **178**, 888
de Temmermann L, Creemers C, van Hove H and Neyens A, 1987: Surf. Sci. **183**, 565
Diaz de la Rubia T, Averback RS, Benedek R and King WE, 1987: Phys. Rev. Lett. **59**, 1930
Dienes GJ and Damask AC, 1958: J. Appl. Phys. **29**, 1713
Dienes GJ and Vineyard GH, 1957: *Radiation Effects in Solids* (Interscience Publishers, New York) 138
Dumke MF, Tombrello TA, Weller RA, Housley RM and Cirlin EH, 1983: Surf. Sci. **124**, 407
du Plessis J, 1990: Solid State Phenomena **11**, 1
du Plessis J and van Wyk GN, 1989a: J. Phys. Chem. Solids **50**, 237
du Plessis J, van Wyk GN and Taglauer E, 1989b: Surf. Sci. **220**, 381
Eckstein W and Biersack JP, 1985: Appl. Phys. A **37**, 95
Eckstein W and Möller W, 1985: Nucl. Instrum. Methods B **7/8**, 727

Falcone G, 1991: Phys. Lett. A **160**, 189
Falcone G and Oliva A, 1984: Appl. Phys. A **33**, 175
Falcone G and Sigmund P, 1981: Appl. Phys. **25**, 307
Falcone G, Aiello D, Forlano L, Piperno F, 1991: Phys. Lett. A **160**, 189
Ferron J, De Bernardez LS, Goldberg EC and Buitrago RH, 1983: Appl. Surf. Sci. **17**, 241
Fine J, Andreadis TD and Davarya F. 1983: Nucl. Instrum. Methods **209/210**, 521
Fluit JM, Friedman L, Boerboom AJH and Kistemaker J, 1961: J. Chem. Phys. **35**, 1143
Foiles SM, 1985: Phys. Rev. B **32**, 7685
Foiles SM, 1992: personal communication
Foreman AJE, 1972: Radiat. Eff. **14**, 175
Fujita D, Tanaka A, Goto K and Homma T, 1990: Surf. Interf. Anal. **16**, 183
Gao F & Bacon DJ, 1993: Phil. Mag. A **67**, 289
Gibson JB, Goland AN, Milgram M and Vineyard GH, 1961: Phys. Rev. **120**, 1229
Gnaser H and Hutcheon ID, 1988: Surf. Sci. **195**, 499
Gnaser H and Oechsner H, 1989: Phys. Rev. Lett. **63**, 2673
Gnaser H and Oechsner H, 1990: Nucl. Instrum. Methods B **48**, 544
Gnaser H and Oechsner H, 1993: Phys. Rev. B **47**, 14093
Goktepe OF, Andreadis TD, Rosen M, Mueller GP and Roush ML, 1986: Nucl. Instrum. Methods B **13**, 434
Gruen DM, Pellin MJ, Young CE, Mendelsohn MH and DeWald AB, 1983: Phys. Scr. **T6**, 42
Gschneidner KA, 1964: Solid State Physics **16**, 275
Gupta RP and Lam NQ, 1979: Scripta Metall. **13**, 1005
Haff PK, 1977: Appl. Phys. Lett. **31**, 259
Haff PK and Switkowski ZE, 1976: Appl. Phys. Lett. **29**, 549
Haff PK, Watson CC and Tombrello TA, 1981: J. Geophys. Res. **86**, 9553
Hammer GE and Shemenski RM, 1984: J. Vac. Sci. Technol. A **2**, 1132
Harper JME, Motakef S and Moy D, 1992: Appl. Phys. Lett. **60**, 1196
Harrison DE, 1983: Rad. Effects **70**, 1
Hetzendorf G and Varga P, 1987: Nucl. Instrum. Methods B **18**, 501
Ho PS, 1978: Surf. Sci. **72**, 253
Hofer WO, 1991: *Sputtering by Particle Bombardment III*, Top. Appl. Phys. **64**, ed. R. Behrisch and K. Wittmaack (Springer-Verlag, Heidelberg) 15
Hofer WO and Littmark U, 1979: Phys. Lett. **71A**, 457
Hoff HA and Lam NQ, 1988: Surf. Sci. **204**, 233
Hofmann S, 1990: *Surface Segregation Phenomena*, ed. P.A. Dowben and A. Miller (CRC Press, Boca Raton, Florida) 107
Hong QZ and Harper JME, 1992: J. Appl. Phys. **71**, 4527
Hubbard KM, Weller RA, Weathers DL and Tombrello TA, 1989a: Nucl. Instrum. Methods B **36**, 395
Hubbard KM, Weller RA, Weathers DL and Tombrello TA, 1989b: Nucl. Instrum. Methods B **40/41**, 278
Husinsky W, Wurz P, Strehl B and Betz G, 1987: Nucl. Instrum. Methods B **18**, 452
Ichimura S, Shimizu H, Murakami H and Ishida Y, 1984: J. Nucl. Mater. **128 & 129**, 601
Itoh N and Morita K, 1984: Rad. Effects **80**, 163
Jeng SP and Holloway PH, 1990: Surf. Sci. **227**, 273
Jeng SP, Batich CD and Holloway PH, 1988: Surf. Sci. **193**, L63
Jiménez-Rodríguez JJ, Conrad U, Urbassek HM, Abril I and Gras-Marti A, 1992: Nucl. Instrum. Methods B **67**, 527
Johnson RA and Lam NQ, 1976: Phys. Rev. B **13**, 4364
Johnson RA and Lam NQ, 1978: J. Nucl. Mater. **69 & 70**, 424-433

Johnson RE and Schou J, 1993: Mat. Fys. Medd. Dan. Vid. Selsk., Mat. Fys. Medd. Dan. Vid. Selsk. **43**, 403
Kamiya I, Buck TM, Sakurai T and Patterson CH, 1988: Nucl. Instrum. Methods B **33**, 479
Kang HJ, Shimizu R and Okutani T, 1982: Surf. Sci. **116**, L173
Kang HJ, Matsuda Y and Shimizu R, 1983: Surf. Sci. **127**, L179
Kang HJ, Kawatoh E and Shimizu R, 1984: Surf. Sci. **144**, 541
Kelly R, 1978: Nucl. Instrum. Methods **149**, 553
Kelly R, 1980: Surf. Sci. **100**, 85
Kelly R, 1985: Surf. Interf. Anal. **7**, 1
Kelly R, 1989a: Mater. Sci. Eng. A **115**, 11
Kelly R, 1989b: Nucl. Instrum. Methods B **39**, 43
Kelly R and Harrison DE, 1985: Mater. Sci. Eng. **69**, 449
Kelly R and Miotello A, 1991: Nucl. Instrum. Methods B **59/60**, 517
Kelly R and Miotello A, 1992: Surf. and Coatings Technol. **51**, 343
Kelly R and Oliva A, 1986a: Nucl. Instrum. Methods B **13**, 283
Kelly R and Oliva A, 1986b: *Erosion and Growth of Solids Stimulated by Atom and Ion Beams*, ed. G. Kiriakidis et al., NATO ASI Series, no. **112** (Nijhoff, Dordrecht) 41
Kelly R and Sanders JB, 1976: Surf. Sci. **57**, 143
Kelly R and Sanders JB, 1976b: Nucl. Instrum. Methods **132**, 335
Kim SJ, Nicolet MA, Averback RS and Baldo P, 1985: Appl. Phys. Lett. **46**, 154
King WE and Benedek R, 1983: J. Nucl. Mater. **117**, 26
Kirk MA and Blewitt TH, 1982: J. Nucl. Mater. **108/109**, 124
Konoplev V and Gras-Marti A, 1992: Phys. Rev. B **46**, 13713
Koponen I, 1991: Nucl. Instrum. Methods B **59/60**, 41
Koponen I and Hautala M, 1992: Nucl. Instrum. Methods B **69**, 182
Koshikawa T, 1985: Appl. Surf. Sci. **22/23**, 1985
Koshikawa T and Goto K, 1987: Nucl. Instrum. Methods B **18**, 504
Krauss AR, Gruen DM and DeWald AB, 1984a: J. Nucl. Mater. **121**, 398
Krauss AR, Gruen DM, Lam NQ and DeWald AB, 1984b: J. Nucl. Mater. **128 & 129**, 570
Krauss AR, DeWald AB, Gruen DM and Lam NQ, 1985: Rad. Effects **89**, 129
Krauss AR, Gruen DM, Lam NQ, DeWald AB, Valentine MG, Sagara A and Kamada K, 1988: J. Scanning Microscopy **2**, 1365
Kurokawa A and Shimizu R, 1989: Surf. Sci. **207**, 460
Kurokawa A, Shimizu R, Kubota Y and Kang HJ, 1989a: Surf. Interf. Anal. **14**, 388
Kurokawa A, Tezuka M, Takegoshi K, Kudo M and Shimizu R, 1989b: Nucl. Instrum. Methods B **39**, 57
Lam NQ, 1975: J. Nucl. Mater. **56**, 125
Lam NQ, 1990: Scanning Microscopy Supplement **4**, 311
Lam NQ and Hoff HA, 1988: Surf. Sci. **193**, 353
Lam NQ and Johanessen K, 1992: Nucl. Instrum. Methods B **71**, 371
Lam NQ and Leaf GK, 1986: J. Mater. Res. **1**, 251
Lam NQ and Rothman SJ, 1976: *Radiation Damage in Metals*, ed. N.L. Peterson and S.D. Harkness (American Society for Metals, Metals Park, Ohio) 125
Lam NQ and Wiedersich H, 1981: J. Nucl. Mater. **103/104**, 433
Lam NQ and Wiedersich H, 1982a: Mater. Res. Soc. Symp. Proc. **7**, 35
Lam NQ and Wiedersich H, 1982b: Rad. Effects Lett. **67**, 107
Lam NQ and Wiedersich H, 1987: Nucl. Instrum. Methods B **18**, 471
Lam NQ, Rothman SJ and Sizmann R, 1974: Rad. Effects **23**, 53
Lam NQ, Okamoto PR and Johnson RA, 1978a: J. Nucl. Mater. **78**, 408
Lam NQ, Okamoto PR and Wiedersich H, 1978b: J. Nucl. Mater. **74**, 101

Lam NQ, Leaf GK and Wiedersich H, 1980: J. Nucl. Mater. **88**, 289
Lam NQ, Kumar A and Wiedersich H, 1982: *Effects of Radiation on Materials - 11th Conference, ASTM STP782*, ed. H.R. Brager and J.S. Perrin (American Society for Testing and Materials, Philadelphia) 985
Lam NQ, Hoff HA and Régnier PG, 1985a: J. Vac. Sci. Technol. **A3**, 2152
Lam NQ, Hoff HA, Wiedersich H and Rehn LE, 1985b: Surf. Sci. **149**, 517
Lawniczak-Jablonska K, Heinonen M and Sulyok A, 1989: Surf. Sci. **222**, 129
Li RS, 1988: Surf. Sci. **193**, 373
Li RS, 1989: Appl. Surf. Sci. **35**, 409
Li RS and Koshikawa T, 1985: Surf. Sci. **151**, 459
Li RS, Koshikawa T and Goto K, 1982: Surf. Sci. **121**, L561
Li RS, Koshikawa T and Goto K, 1983: Surf. Sci. **129**, 192
Li RS, Li CF and Zhang WL, 1990: Appl. Phys. A **50**, 169
Li RS, Li CF, Liu G, Zhang XS and Bao DS, 1991: J. Appl. Phys. **70**, 5351
Liau ZL, Brown WL, Homer R and Poate JM, 1977: Appl. Phys. Lett. **30**, 626
Liau ZL, Mayer JW, Brown WL and Poate JM, 1978: J. Appl. Phys. **49**, 5295
Lindhard J, Scharff M and Schiøtt HE, 1963: Mat. Fys. Medd. Dan. Vid. Selsk. **33**, no. 14
Lindhard J, Nielsen V and Scharff M, 1968: Mat. Fys. Medd. Dan. Vid. Selsk. **36**, no. 10
Littmark U and Hofer WO, 1980: Nucl. Instrum. Methods **168**, 329
Littmark U and Hofer WO, 1984: *Thin Film and Depth Profile Analysis*, Top. Appl. Phys. **37**, ed. H. Oechsner (Springer-Verlag, Berlin) 159
Lo DY, Tombrello TA and Shapiro MH, 1989: Nucl. Instrum. Methods B **40/41**, 270
Lomer WM, 1954: UKAEA Report AERE T/R **1540**
Ma E, 1991: Nucl. Instrum. Methods B **58**, 194
Malherbe JB and Barnard WO, 1991: Surf. Sci. **255**, 309
Manning JR, 1968: *Diffusion Kinetics for Atoms in Crystals* (van Nostrand, Princeton)
Manning JR, 1981: *Phase Stability during Irradiation*, ed. JR. Holland et al. (The Metallurgical Society of AIME, New York) 3
Marchetti F, Dapor M, Girardi S, Cipparrone M and Tiscione P, 1990: Vacuum **41**, 1706
Martin G, Cauvin R and Barbu A, 1983: *Phase Transformations during Irradiation*, ed. F.V. Nolfi, Jr. (Applied Science Publishers, London) 47
Marton D, Fine J and Chambers GP, 1988: Phys. Rev. Lett. **61**, 2697
Marton D, Fine J and Chambers GP, 1989: Mater. Sci. Eng.. **A115**, 223
Marwick AD, Piller RC and Sivell PM, 1979: J. Nucl. Mater. **83**, 35
Matteson S and Nicolet MA, 1983: Ann. Rev. Mater. Sci. **13**, 339
Matteson S, Paine BM and Nicolet MA, 1981: Nucl. Instrum. Methods **182/183**, 53
Mayer JW and Lau SS, 1983: *Surface Modification and Alloying*, ed. J.M. Poate et al. (Plenum, New York) 241
Mazurowski J and Dowben PA, 1990: *Surface Segregation Phenomena*, ed. P.A. Dowben and A. Miller (CRC Press, Boca Raton, Florida) 365
Möller W and Eckstein W, 1984: Nucl. Instrum. Methods B **2**, 814
Möller W and Eckstein W, 1985: Nucl. Instrum. Methods B **7/8**, 645
Möller W, Eckstein W and Biersack JP, 1988: Comp. Phys. Commun. **51**, 355
Morita K, Nakamura H, Hayashibara M and Itoh N, 1981: J. Nucl. Mater. **103 & 104**, 1373
Morita K, Tsuchiya T, Hayashibara M and Itoh N, 1983: J. Nucl. Mater. **116**, 63
Morita K, Ohno H, Hayashibara M and Itoh N, 1984: Nucl. Instrum. Methods B **2**, 596
Ng YS, Tsong TT and McLane SB, 1979: Phys. Rev. Lett. **42**, 588
Nieminen R, 1993: Mat. Fys. Medd. Dan. Vid. Selsk. **43**, 81
Oechsner H and Bartella J, 1981: *Proc. 7th Intern. Conf. on Atomic Collisions in Solids*, 1977, Moscow (Moscow State University Publishing House, USSR) **2**, 55

Okamoto PR and Rehn LE, 1979: J. Nucl. Mater. **83**, 2
Okano J, Ochiai T and Nishimura H, 1985: Appl. Surf. Sci. **22/23**, 72
Okutani T, Shikata M and Shimizu R, 1980: Surf. Sci. **99**, L410
Oliva A, Kelly R and Falcone G, 1986: Surf. Sci. **166**, 403
Olson RR and Wehner GK, 1977: J. Vac. Sci. Technol. **14**, 319
Olson RR, King ME and Wehner GK, 1979: J. Appl. Phys. **50**, 3677
Onderdelinden D, 1968: Can. J. Phys. **46**, 739
Ottaviani G and Valeri S, 1987: Nucl. Instrum. Methods. B **19/20**, 97
Paine BM and Averback RS, 1985: Nucl. Instrum. Methods B **7/8**, 666
Paine BM and Nicolet MA, 1983: Nucl. Instrum. Methods **209/210**, 173
Peinador JA, Abril I, Jiménez-Rodríguez JJ and Gras-Marti A, 1990: Nucl. Instrum. Methods B **48**, 589
Peinador JA, Abril I, Jiménez-Rodríguez JJ and Gras-Marti A, 1991: Phys. Rev. B **44**, 2061
Peiner E and Kopitzki K, 1988: Nucl. Instrum. Methods B **34**, 173
Pellin MJ, Young CE, Gruen DM, Aratono Y and DeWald AB, 1985: Surf. Sci. **151**, 477
Peterson NL, 1975: *Diffusion in Solids - Recent Developments* (Academic Press, New York) 115
Peterson NL, Barr LW and Le Claire AD, 1973: J. Phys. C **6**, 2020
Pickering HW, 1976: J. Vac. Sci. Technol. **13**, 618
Piller RC and Marwick AD, 1978: J. Nucl. Mater. **71**, 309
Qu Z and Xie TS, 1988: Surf. Sci. **194**, L127
Rehn LE, 1982: Mat. Res. Soc. Symp. Proc. **7**, 17
Rehn LE and Lam NQ, 1987: J. Mater. Eng. **9**, 209
Rehn LE and Okamoto PR, 1983: *Phase Transformations during Irradiation*, ed. F.V. Nolfi, Jr. (Applied Science Publishers, London) 247
Rehn LE and Okamoto PR, 1987: Mater. Sci. Forum **15-18**, 985
Rehn LE and Wiedersich H, 1980: Thin Solid Films **73**, 139
Rehn LE, Danyluk S and Wiedersich H, 1979: Phys. Rev. Lett. **43**, 1764
Rehn LE, Boccio VT and Wiedersich H, 1983: Surf. Sci. **128**, 37-50
Rehn LE, Lam NQ and Wiedersich H, 1985: Nucl. Instrum. Methods B **7/8**, 764
Rehn LE, Hoff HA and Lam NQ, 1986: Phys. Rev. Lett. **57**, 780
Robinson MT, 1983: J. Appl. Phys. **54**, 2650
Robinson MT, 1993: Mat. Fys. Medd. Dan. Vid. Selsk. **43**, 27
Robrock KH, 1983: *Phase Transformations during Irradiation* ed. FV. Nolfi, Jr. (Applied Science Publishers, London) 115
Rosen M and Bassel RH, 1984: Nucl. Instrum. Methods B **2**, 592
Rosen M, Mueller GP and Fraser WA, 1983: Nucl. Instrum. Methods **209/210**, 63
Rothman SJ, 1983: *Phase Transformations during Irradiation*, ed. F.V. Nolfi, Jr. (Applied Science Publishers, London) 189
Rothman SJ, Lam NQ, Sizmann R and Bisswanger H, 1973: Radiat. Eff. **20**, 223
Roush ML, Andreadis TD and Goktepe OF, 1981: Radiat. Effects **55**, 119
Roush ML, Goktepe OF, Andreadis TD and Davarya F, 1982: Nucl. Instrum. Methods **194**, 611
Roush ML, Davarya F, Goktepe OF and Andreadis TD, 1983: Nucl. Instrum. Methods **209/210**, 67
Russell WA, Papanastassiou DA and Tombrello TA, 1980: Radiat. Eff. **52**, 5
Sarholt-Kristensen L, Andreev A, Johansen A, Andersen HH and Johnson E, 1992: Nucl. Instrum. Methods B **68**, 258
Schiffman B and Polak M, 1986: Surf. Interf. Anal. **9**, 151
Schmid M, Biedermann A, Stadler H, Slama C and Varga P, 1992: Appl. Phys. A **55**, 468
Schorn RP, Zaki Ewiss MA and Hintz E, 1988: Appl. Phys. A **46**, 291
Schou J, 1992: Dr. Sci. Thesis, Odense University

Seeger A, 1975: Phys. Stat. Sol. A **28**, 157
Sethuraman AR, 1991: Nucl. Instr. and Meth. B **54**, 513
Sethuraman AR, Reucroft PJ, De Angelis RJ, Kim DK and Okazaki K, 1990: J. Vac. Sci. Technol. A **8**, 2255
Shapiro MH, Haff PK, Tombrello TA and Harrison DA, 1985: Nucl. Instrum. Methods B **12**, 137
Shapiro MH, Tombrello TA and Harrison DE, 1988: Nucl. Instrum. Methods B **30**, 152
Sharp JV, 1969: UKAEA Report AERE-R **6267**
Shewmon PG, 1963: *Diffusion in Solids* (McGraw-Hill, New York)
Shimizu H, Ono M and Nakayama K, 1975: J. Appl. Phys. **46**, 460
Shimizu N and Hart SR, 1982: J. Appl. Phys. **53**, 1303
Shimizu R, 1987: Nucl. Instrum. Methods B **18**, 486
Sigmund P, 1969a: Phys. Rev. **184**, 383; **187**, 768
Sigmund P, 1969b: Appl. Phys. Lett. **14**, 114
Sigmund P, 1969c: Rad. Effects **1**, 15
Sigmund P, 1979: J. Appl. Phys. **50**, 7261
Sigmund P, 1980: J. Vac. Sci. Technol. **17**, 396
Sigmund P, 1981: *Sputtering by Particle Bombardment I*, Top. Appl. Phys. **47**, ed. R. Behrisch (Springer-Verlag, Heidelberg) 9
Sigmund P, 1987a: Nucl. Instrum. Methods B **18**, 375
Sigmund P, 1987b: Nucl. Instrum. Methods B **27**, 1
Sigmund P, 1988: Nucl. Instrum. Methods B **34**, 15
Sigmund P, 1993a: *Ionization by Heavy Charged Particles*, ed. R.A. Baragiola, NATO ASI Series (Plenum Press, New York) 59
Sigmund P, 1993b: Nucl. Instrum. Methods B, **82**, 192
Sigmund P and Claussen C, 1981: J. Appl. Phys. **52**, 990
Sigmund P and Gras-Marti A, 1980: Nucl. Instrum. Methods **168**, 389
Sigmund P and Gras-Marti A, 1981: Nucl. Instrum. Methods **182/183**, 25
Sigmund P and Oliva A, 1993: Nucl. Instrum. Methods B **82**, 242
Sigmund P and Sckerl MW, 1993: Nucl. Instrum. Methods B **82**, 269
Sigmund P, Oliva A and Falcone G, 1982: Nucl. Instrum. Methods **194**, 541; B **9** (1985) 354
Sigmund P, Robinson MT, Baskes MI, Hautala M, Cui FZ, Eckstein W, Yamamura Y, Hosaka S, Ishitani T, Shulga VI, Harrison DE, Chakarov IR, Karpuzov DS, Kawatoh E, Shimizu R, Valkealahti S, Nieminen RM, Betz G, Husinsky W, Shapiro MH, Vicanek M and Urbassek HM, 1989: Nucl. Instrum. Methods B **36**, 110
Sizmann R, 1978: J. Nucl. Mater. **69 & 70**, 386
Stahle CM and Helms CR, 1992: J. Vac. Sci. Technol. A **10**, 3239
Swalin RA, 1962: *Thermodynamics of Solids* (Wiley, New York), ch. 9
Swartzfager DG, Ziemecki SB and Kelley MJ, 1981: J. Vac. Sci. Technol. **19**, 185
Szymonski M, 1980: Appl. Phys. **23**, 89
Szymonski M, Bhattacharya RS, Overeijnder H and de Vries AE, 1978: J. Phys. D **11**, 751
Taglauer E, 1982: Appl. Surf. Sci. **13**, 80
Taglauer E and Heiland W, 1978: Appl. Phys. Lett. **33**, 950
Tanaka A, Takemori M and Homma T, 1983: J. Elect. Spect. Rel. Phen. **32**, 277
Tang S and Lam NQ, 1989: Surf. Sci. **223**, 179
Tang S, Lam NQ and Yacout A, 1990: Surf. Sci. **231**, 253
Thomas MP and Ralph B, 1983: Surf. Sci. **124**, 129
Thompson M, 1968: Phil. Mag. **18**, 377
Titov VV, 1979: Zh. Tekh. Fiz. **49**, 844 (Sov. Phys. J. Tech. Phys. **24**, 488)
Urbassek HM and Conrad U, 1992: Nucl. Instrum. Methods B **69**, 413

Urbassek HM and Conrad U, 1993: Nucl. Instrum. Methods B **73**, 151
Urbassek HM and Vicanek M, 1988: Phys. Rev. B **37**, 7256
Valeri S, di Bona A, Ottaviani G and Procop M, 1991: Nucl. Instrum. Methods. B **59/60**, 98
van Wyk GN, du Plessis J and Taglauer E, 1991: Surf. Sci. **254**, 73
Varga P and Taglauer E, 1981: J. Nucl. Mater. **111/112**, 726
Vicanek M and Sigmund P, 1994: To be published
Vicanek M and Urbassek HM, 1988: Nucl. Instrum. Methods B **30**, 507
Vicanek M, Jiménez-Rodríguez JJ and Sigmund P, 1989: Nucl. Instrum. Methods B **36**, 124
Vicanek M, Conrad U and Urbassek HM, 1993: Phys. Rev. B **47**, 617
Wadsworth M, Armour DG, Badheka R and Collins R, 1990: Int. J. Numerical Modelling **3**, 157
Wagner W, Rehn LE and Wiedersich H, 1982: Philos. Mag. A **45**, 957
Wagner W, Rehn LE, Wiedersich H and Naundorf V, 1983: Phys. Rev. B **28**, 6780
Waite TR, 1957: Phys. Rev. **107**, 463
Watson CC and Haff PK, 1980: J. Appl. Phys. **51**, 691
Weathers DL, Spicklemire SJ, Tombrello TA, Hutcheon ID and Gnaser H, 1993: Nucl. Instrum. Methods B **73**, 135
Webb R, Carter G and Collins R, 1978: Rad. Effects **39**, 129
Wehner GK, 1955: J. Appl. Phys. **26**, 1056
Wehner GK, 1977: Appl. Phys. Lett. **30**, 185
Weigand P, Novacek P, van Husen G, Neidhart T, Mezey LZ, Hofer W and Varga P, 1992: Nucl. Instrum. Methods B **64**, 93
Wiedersich H, 1972: Radiat. Eff. **12**, 111
Wiedersich H, 1983: *Surface Modification and Alloying*, ed. J.M.Poate et al. (Plenum, New York) 261
Wiedersich H, 1985: Nucl. Instrum. Methods B **7/8**, 1
Wiedersich H and Lam NQ, 1983: *Phase Transformations during Irradiation*, ed. F.V. Nolfi, Jr. (Applied Science Publishers, London) 1
Wiedersich H, Okamoto PR and Lam NQ, 1979: J. Nucl. Mater. **83**, 98
Winterbon KB, Sigmund P and Sanders JB, 1970: Mat. Fys. Medd. Dan. Vid. Selsk. **37**, no. 14
Winters HF and Sigmund P, 1974: J. Appl. Phys. **45**, 4760
Winters HF and Taglauer E, 1987: Phys. Rev. B **35**, 2174
Wirth Th, Atzrodt V and Lange H, 1984: phys. stat. sol. A **82**, 459
Wirth Th, Procop M and Lange H, 1986: Vacuum **36**, 433
Wittmaack K, 1991: *Sputtering by Particle Bombardment III*, Top. Appl. Phys. **64**, ed. R. Behrisch and K. Wittmaack (Springer, Heidelberg) 161
Wollenberger HJ, 1970: *Vacancies and Interstitials in Metals*, ed. A Seeger et al, (North-Holland, Amsterdam) 215
Wollenberger HJ, 1987: Mater. Sci. Forum **15-18**, 1363
Wucher A and Reuter W, 1988: J. Vac. Sci. Technol. A **6**, 2316
Wynblatt P and Ku RC, 1979: *Interfacial Segregation*, ed. W. C. Johnson and J. M. Blakeley (American Society for Metals, Metals Park, Ohio) 115
Yacout AM, Lam NQ and Stubbins JF, 1989: Nucl. Instrum. Methods B **42**, 49
Yamamura Y and Muraoka K, 1989: Nucl. Instrum. Methods B **42**, 175
Zee RH, Guinan MW and Kulcinski GL, 1983: J. Nucl. Mater. **114**, 190
Zhu H, Lam NQ, Devanathan R and Sabochick MJ, 1992: Mat. Res. Soc. Symp. Proc. **235**, 533; and to be published
Ziegler JF, Biersack JP and Littmark U, 1985: *The Stopping and Range of Ions in Solids* (Pergamon, New York)